AFHRL-TR-84-27

AIR FORCE HUMAN RESOURCES LABORATORY

AD-A149 641

DTIC FILE COPY

20000804101

WIDE-FIELD-OF-VIEW, HELMET-MOUNTED INFINITY DISPLAY SYSTEM DEVELOPMENT

CAE Electronics Ltd.
P.O. Box 1800, Saint-Laurent
Montreal, Quebec
Canada H4L 4X-

OPERATIONS TRAINING DIVISION
Williams Air Force Base, Arizona 85240-6457

December 1984
Interim Report for Period June 1981 - October 1983

AIR FORCE SYSTEMS COMMAND
BROOKS AIR FORCE BASE, TEXAS 78235-5000

NOTICE

When Government drawings, specifications, or other data are used for any purpose other than in connection with a definitely Government-related procurement, the United States Government incurs no responsibility or any obligation whatsoever. The fact that the Government may have formulated or in any way supplied the said drawings, specifications, or other data, is not to be regarded by implication, or otherwise in any manner construed, as licensing the holder, or any other person or corporation; or as conveying any rights or permission to manufacture, use, or sell any patented invention that may in any way be related thereto.

The Public Affairs Office has reviewed this report, and it is releasable to the National Technical Information Service, where it will be available to the general public, including foreign nationals.

This report has been reviewed and is approved for publication.

MILTON E. WOOD, Technical Director
Operations Training Division

ANTHONY F. BRONZO, JR., Colonel, USAF
Commander

Unclassified

SECURITY CLASSIFICATION OF THIS PAGE

AD-A149641

REPORT DOCUMENTATION PAGE

1a REPORT SECURITY CLASSIFICATION	1b RESTRICTIVE MARKINGS
2a SECURITY CLASSIFICATION AUTHORITY	3 DISTRIBUTION/AVAILABILITY OF REPORT: Approved for public release; distribution unlimited.
2b DECLASSIFICATION/DOWNGRADING SCHEDULE	
4 PERFORMING ORGANIZATION REPORT NUMBER(S)	5 MONITORING ORGANIZATION REPORT NUMBER(S): AFHRL-TR-84-27
6a NAME OF PERFORMING ORGANIZATION: CAE Electronics Ltd., P.O. Box 1800	6b OFFICE SYMBOL (If applicable)
7a NAME OF MONITORING ORGANIZATION: Operations Training Division, Air Force Human Resources Laboratory	
6c ADDRESS (City, State and ZIP Code): Saint-Laurent, Montreal, Quebec, Canada H4L 4X4	7b ADDRESS (City, State and ZIP Code): Williams Air Force Base, Arizona 85224-5000
8a NAME OF FUNDING/SPONSORING ORGANIZATION: Air Force Human Resources Laboratory	8b OFFICE SYMBOL (If applicable): HQ AFHRL
9 PROCUREMENT INSTRUMENT IDENTIFICATION NUMBER: F33615-81-C0012	
8c ADDRESS (City, State and ZIP Code): Brooks Air Force Base, Texas 78235-5000	10 SOURCE OF FUNDING NOS

PROGRAM ELEMENT NO	PROJECT NO	TASK NO	WORK UNIT NO
63227F	2743	00	01

11 TITLE (Include Security Classification): Wide-Field-of-View, Helmet-Mounted Infinity Display System Development

12 PERSONAL AUTHOR(S)

13a TYPE OF REPORT	13b TIME COVERED	14 DATE OF REPORT (Yr., Mo., Day)	15 PAGE COUNT
Interim	FROM Jun 81 TO Oct 83	December 1984	114

16 SUPPLEMENTARY NOTATION: A cost-shared program under the Canada/US Defense Development Sharing Agreement. Contract 14SU 70C3-81-R-0012.

17 COSATI CODES		
FIELD	GROUP	SUB GR

18 SUBJECT TERMS (Continue on reverse if necessary and identify by block number)

computer-generated imagery; helmet-position sensing; eye slaving; infinity display; fiber optics; visual simulation

19 ABSTRACT (Continue on reverse if necessary and identify by block number)

This report details the development of a fiber-optic-coupled helmet-mounted display. A working breadboard model has been developed. A computer-generated image projected from a light valve is relayed to the input of a large format coherent fiber-optic bundle. The fiber-optic bundle transfers the image to a set of helmet-mounted optics which display the imagery via two in-line, wide-angle infinity displays. The helmet position and attitude are sensed and used to control the image content. Studies were also conducted on requirement for eye-slaved control of image content.

20 DISTRIBUTION/AVAILABILITY OF ABSTRACT	21 ABSTRACT SECURITY CLASSIFICATION
UNCLASSIFIED/UNLIMITED [X] SAME AS RPT [ ] DTIC USERS [ ]	Unclassified

22a NAME OF RESPONSIBLE INDIVIDUAL	22b TELEPHONE NUMBER (Including Area Code)	22c OFFICE SYMBOL
Nancy A. Perrigo, Chief, STINFO Office	(512) 536-3877	AFHRL/TSR

DD FORM 1473, 83 APR — EDITION OF 1 JAN 73 IS OBSOLETE

Unclassified

SECURITY CLASSIFICATION OF THIS PAGE

SUMMARY

Current military requirements for visual systems include a very large field of view as being almost mandatory. Unfortunately, in order to obtain these large fields of view at a reasonable cost, resolution and image detail have to be sacrificed.

The traditional solution is the dome visual display employing head-slaved area of interest.

This approach is economical in terms of channels and display devices required for a large FOV, but suffers from the technical difficulty of rapidly slewing pictures about a dome screen to follow the head and the requirement for large facilities to accommodate 40-ft-diameter domes.

The basis of the helmet-mounted display (HMD) is the area-of-interest technique. Mounting the display directly on the pilot's helmet (and, hence, his head) immediately eliminates any requirement to slew display devices; all that slews is the easily controllable video image. Furthermore, bu using wide-field infinity optics for the helmet display, the image can have the clarity, brightness, contrast and comfortable viewing relationship of the classical infinity display. The demands upon the computer image generator are reduced, especially if the display is further refined to incorporate an eye-slaved area of interest.

This report details the initial stage of the development of an eye-slaved, wide-field, fiber-optic-coupled helmet-mounted display. Details of the design and development work leading to the delivered, working breadboard system are provided. The subjects covered include:

- Optical design of helmet and relay optics
- Fiber-optic cable design and development
- Color and dynamic multiplexing techniques
- Mechanical structure and helmet counterbalancing technique
- Helmet position sensing systems
- Mechanisms to reduce latency in the image
- Accelerometer prediction of head position
- Video projector considerations
- Helmet design.

A research apparatus developed to study aspects of eye-slaved area of interest is also described.

The system delivered has successfully demonstrated the viability of the approach and further development is continuing.

PREFACE

This report represents the initial development phase of a research and development (R&D) program on which the objective is to provide a compact, portable, efficient, high brightness, full color, wide-angle display for use in combat mission training of Air Force pilots. The R&D is being supported under the Canada/US Defense Development Sharing Agreement and is being conducted under the administration of the Operations Training Division of the Air Force Human Resources Laboratory by CAE Electronics; with Farrand Optical Co. and AO Reichert Scientific Instruments as principal subcontractors. Mr. Brian Welch is the project scientist for CAE, with Mr. Marty Shenker and Mr. Paul Weissman of Farrand acting as optical designers and Dr. Walter Siegmund of AO Reichert providing fiber-optic cable design. For the Air Force, the program has been administered by Lt Col Peter Cook, project manager, Capt Caroline Hanson, assistant project manager, Mr. Bruce McCreary, project engineer, and Dr. Tom Longridge, project scientist.

The authors would like to express their appreciation to many colleagues whose assistance was invaluable; specifically to Mr. Uwe List, exchange scientist (Federal Office for Military Technology and Procurement, West Germany) for his contributions on the use of accelerometers for head motion prediction, Dr. Yehoshua Zeevi (Technion Institute, Haifa) for his assistance in resolving problems related to the visual psychophysiology, and to Singer personnel on-site at AFHRL for their constant assistance in making things work.

TABLE OF CONTENTS

TABLE OF CONTENTS (Cont'd)

TABLE OF CONTENTS (Cont'd)

TABLE OF CONTENTS (Cont'd)

LIST OF ILLUSTRATIONS

LIST OF ILLUSTRATIONS (Cont'd)

LIST OF TABLES

1. INTRODUCTION

1.1 Scope. This report describes the first phase of a research and development (R&D) program to make an advanced visual system utilizing the eye tracking principle and a helmet-mounted display (HMD).

Current military requirements for visual systems include a very large field of view as being almost mandatory. Unfortunately, in order to obtain these large fields of view at a reasonable cost, resolution and image detail have to be sacrificed. Many training tasks do not require high resolution and high image detail although the training effectiveness of the simulator would probably be improved if these parameters could be improved.

There is one group of training tasks, however, which is attaining a significant importance in simulation and requires both high resolution and high image detail, coupled with a very large field of view. This group of tasks pertains to the close air support (CAS) role. High resolution and high image detail are required for the prime task of air-to-ground weapons delivery and for the task of air-to-air combat at low altitude. The tasks of navigation and flying at very low altitude also require these parameters, although to a lesser extent.

The conventional approach to this problem is to try to duplicate the real world; however, the normal human visual system has a field of view of approximately 200 degrees by 150 degrees and, of this, only the central foveal region has high acuity. If the simulated visual scene could be matched to the acuity of the eye, tremendous savings in system bandwidth could be obtained. K. Friedrich Kraiss and Ernst Schubert[1], in a paper presented at the 1977 Society for Information Display (SID) symposium, described an experiment in which image resolution was matched to eye resolution. It is relevant to quote part of the conclusion; "It may be concluded from this preliminary result that matched resolution may be applied without loss in picture quality, be it to save bandwidth or to enlarge the field of view for a given bandwidth" (p. 44).

The design concept described, when applied to a computer-generated image (CGI) visual system, provides almost two orders of magnitude increase in image detail for a given system capacity and allows image resolution approaching that of the eye.

The R&D program reported here consists of three phases:

(a) Breadboard fiber-optic helmet-mounted display (FOHMD) development and evaluation.

---

[1] Kraiss, K.F., & Schubert, E. Matching Image Resolution to the Eye Resolution. Society for Information Display Symposium, 1977, Volume VIII.

(b) Prototype FOHMD (incorporating design improvements following evaluation of the breadboard) and experimentation phase.

(c) Enhanced prototype incorporating eye-slaved area-of-interest results of experimentation phase.

This report describes phase (a) of the program.

1.2 System Description

1.2.1 Description. The breadboard HMD is shown schematically in Figure 1. It consists of a modified helmet on which are mounted two Pancake Window™ displays. The video imagery is transferred to the head via four high-resolution fiber-optic cables employing color multiplexing to reduce individual fiber speckle effects. A mechanical arm is attached on top of the helmet to provide reference head position information, while an accelerometer package mounted at the back provides information for accurate head movement lead prediction. Any excess weight (beyond that of a normal helmet) is compensated for by a constant-force spring from which the helmet is suspended on a sliding, gimballed mechanism.

The video imagery for the helmet display originates in four high-resolution, high-brightness light valve projectors.

1.2.2 Display Optics. The display optics consist of four basic items:

(a) Relay/combining optics

(b) Fiber-optic cable

(c) Optical multiplexer

(d) Helmet display.

The optics transform the input from four high-resolution, high-brightness television projectors to a display at the pilot's eye. Two projectors provide overlapping 80-degree, low-resolution images, and the remaining two provide an input for an overlapping high-resolution inset which can be selected between 25 degrees and 40 degrees.

1.2.3 Relay/Combining Optics. The relay and combining optics serve to relay the images produced by the light valve to the input of the fiber-optic cables. They provide correction for size and scale of the image, and mapping to match the helmet display optics.

1.2.4 Fiber-Optic Cable. The fiber-optic cables consist of series of multi-fiber bundles arranged into a large-diameter, coherent optical cable. The size of the individual fibers within the cable is 10 microns, with cores of approximately 8 microns in diameter. The cable format is basically 8 x 10 mm (13 mm diameter). The standard cables are 6 feet in length; however, lengths up to 9 feet can be achieved. The cable is sheathed with a light, flexible, stainless steel covering for protection.

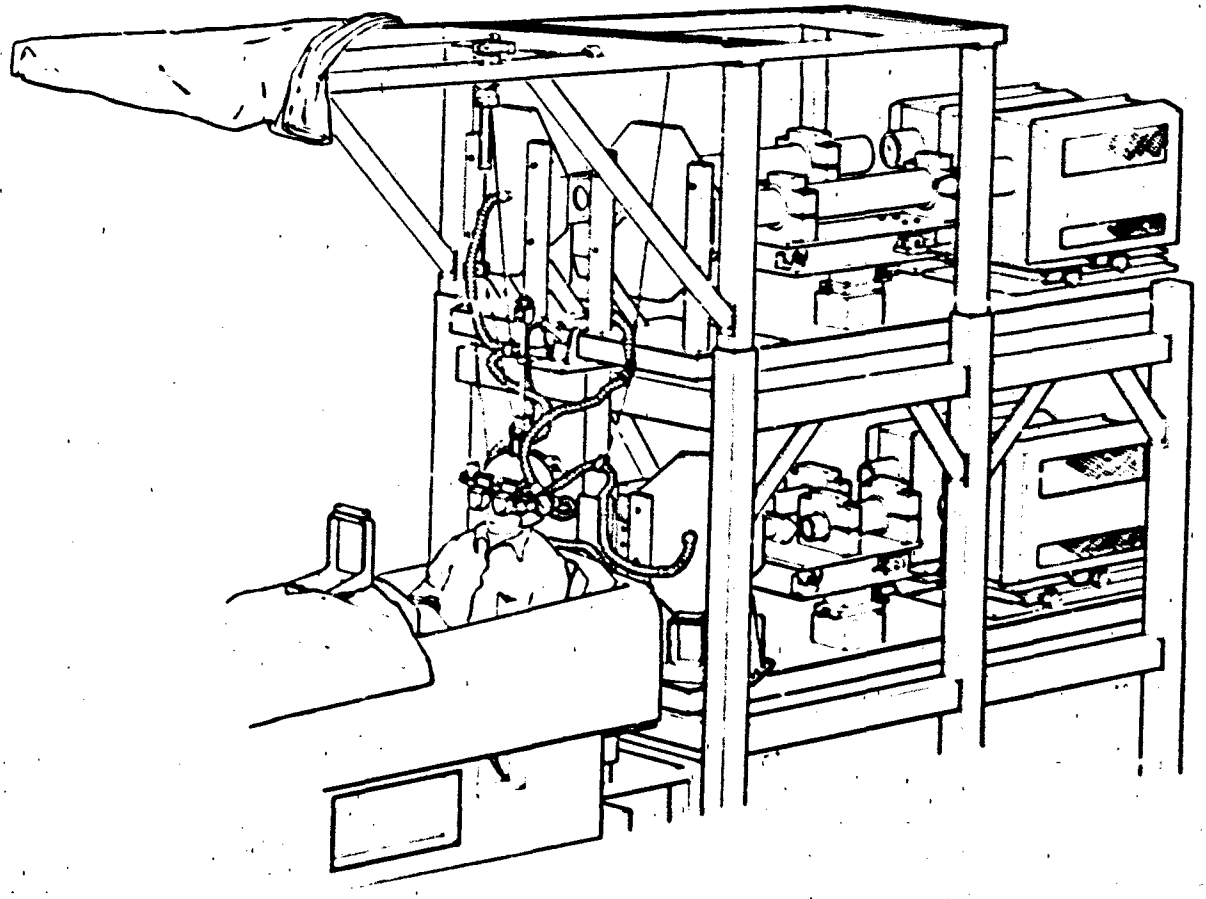

Figure 1. Breadboard FOHMD.

1.2.5 Optical Multiplexer. The resolution of the fiber-optic cable is determined by the dimension of the smallest transmission element, which is equivalent to the diameter of the fiber core. Some loss of information can occur due to image detail falling in the space between fiber cores (2 x cladding thickness), and due to the occasional broken fiber. This effect can be substantially reduced by use of optical multiplexing. The optical multiplexing device provides multiple images of the video output at the input to the fiber-optic cable, varying in position across the transmitting region. The output from the fiber cable is demultiplexed using an identical device, synchronized with the input multiplexing. In this way, individual elements of the scene, which would not have been "sampled" by the fiber cores, are sampled and displayed to the viewer. Two methods are available to accomplish this (color multiplexing and dynamic multiplexing).

1.2.6 Color Multiplexing. Placing a glass wedge at the fiber cable input causes a one-dimensional smear of colored images due to the prismatic effect. A prism at the opposite end of the cable restores a single sharp full color image. This technique is cheap, simple, lightweight and requires no moving parts, power or control lines to the helmet. However, it only eliminates structure effectively in one dimension.

1.2.7 Dynamic Multiplexing. Dynamic multiplexing "wobbles" the image in time at the input to the fiber cable. A perfectly synchronized motor provides a counter-wobble at the other end of the cable. The "wobble" is created by rotating an off-axis glass plate in the optical path. This system requires synchronized motors at both ends of the fiber cable and is bulkier and more complex than color multiplexing. However, it offers optimum performance as the structure is removed in all axes.

1.2.8 Helmet Display. The helmet display consists of two 3-inch-diameter Pancake Windows™ mounted in front of the eyes, with an optical interface to the fiber-optic cables and optical multiplexers which provides the correctly mapped input. The Pancake Window™ is a compact, in-line, wide field (80 degrees), reflective infinity display which provides overlapping full-color images to each eye. The Pancake Windows™ are semi-transparent (about 10 percent transmission), permitting cockpit controls and indicators to be viewed normally through the display with the video blanked. The exit pupil is large to minimize the adjustment needed when putting on the HMD. The eye relief is sufficient to allow the use of aviator glasses by the wearer. The overlapping displays provide an instantaneous field of view of 60 degrees vertically by 135 degrees horizontally, including a high-resolution inset field selectable between 25 and 40 degrees. The optics, built by the Farrand Optical Company, are of very high quality and are rigidly packaged to maintain alignment under all normal simulator operations.

1.2.9 Helmet Position Sensing. The position of the helmet (and hence, the head) must be accurately known to permit accurate, rapid control of the video CGI position/orientation. Mechanical links to the helmet are capable of this control, but restrict pilot head movement and add extra drag and weight. The optical and electromagnetic systems presently in use in military aircraft

suffer limitations of accuracy, field of view, and in particular, response. To control the video CGI accurately under rapid head motion requires a minimum of 60-Hz output from the head position sensor. To accommodate this, CAE, in conjunction with Concordia University in Montreal, has designed and built an optical helmet-position sensing system.

1.2.10 Accelerometer Prediction of Head Position. To reduce the CIG image response time on the HMD, it is necessary to predict the position of the head movement. The approach chosen was to integrate an acceleration signal to predict position. To this end, an angular accelerometer package is installed on the helmet and sampled by the head-tracking computer. A predictor scheme calculates the extrapolated head position based on the present position plus the estimated velocity. The estimated velocity is derived from the actual velocity plus an acceleration term. To eliminate overshoots, the estimated velocity is limited to a reasonable value.

1.2.11 Helmet Suspension System. To create the feel of an ordinary aircrew helmet, it is necessary to match the weight, balance, and inertia of the HMD as closely as possible to those of a conventional helmet. This is done in several ways.

(a) The optics are mounted as close to the head as possible to reduce the angular inertia of the HMD.

(b) The fiber-optic cables are supported from behind the helmet to eliminate their weight.

(c) To compensate for any residual weight and balance discrepancies, a helmet suspension system is provided. A cable attached at suitable points on the helmet is suspended from a constant force spring mounted on fore/aft sliding tracks above the pilot's head. This system has proved very successful on the breadboard HMD, where no other attempt was made to reduce weight.

1.2.12 Projection System. The video input to the system is provided by four GE PJ 5855 Talaria large-screen television projectors, two for each eye. The PJ 5855 is a high-resolution, high-brightness device providing an 875-line picture at 1000 lumens in full color.

The projectors are mounted on vibration-damping optical tables behind each crew seat and are coupled to the HMD via the previously described relay optics and fiber-optic cable.

1.2.13 Computer Image Generation Requirements. The HMD imposes some restrictions on image generator performance.

1.2.13.1 Update Rate/Throughput Delay. To minimize lag effects under rapid head motion the image generator must operate at a true 60-Hz update rate. That is, each field of the 875-line/60-Hz video image must be computed from a new position input from the head position sensor processor. The data

stream from the helmet-position sensor processor to the CIG host must be synchronized to the field update and optimized to reduce signal delays. The CIG throughput delay should be less than 67 ms for best performance.

1.2.13.2 Channel/Viewpoint Capacity. The basic HMD requires four channels, two for the 80-degrees low-resolution background fields and two for the 25- or 40-degree high-resolution inset fields.

1.2.13.3 Cockpit Mapping. To blank out helmet video when the pilot looks at his instruments, a cockpit mask is required. This is defined by a black moving model fixed in space relative to the pilot position. No special display mapping is required by the light valve, as mapping corrections are done in the optics.

1.3 Program Status. The breadboard HMD system, integrated with an AFHRL cockpit, computer system, and CIG visual system, has been demonstrated to AFHRL personnel.

The breadboard system consists of the following:

(a) Helmet and helmet support system

(b) HMD optical system

(c) Fiber-optic cables (4)

(d) Mechanical head-tracking system

(e) Optical cable driving systems (4)

(f) Support structure for system components

(g) Light valve projectors (4) supplied by the AFHRL.

The demonstration showed operation of all components, in particular, the display optics and fiber-optic cables in conjunction with light valve projectors.

A concurrent demonstration was given of an experimental eye-tracking/slaved projection system developed as part of the current program.

Further activities covered by the current program are support of the system during demonstration and evaluation activities at the Air Force Human Resources Laboratory (AFHRL) and the carrying out of experiments (in conjunction with the AFHRL) to determine parameters for the engineering prototype system.

2. OPTICS

2.1 Introduction. The optical system proposed for the HMD was based on a previous program performed by Farrand for the Aerospace Medical Research Laboratory (AMRL) on what is called the Visually Coupled Airborne Systems Simulation (VCASS) Program. The system proposed originally for the AFHRL HMD is shown in Figure 2. It was based on using two separate relays within the helmet-mounted display to utilize two fiber-optic cables of the same diameter. The relays would have different magnifications and thus the overall angular subtenses and also the resolution capabilities of the fiber-optic cables would differ by the ratio of the relay magnifications. It was expected that the relay images would be combined by beamsplitters on the long conjugate end of the relays.

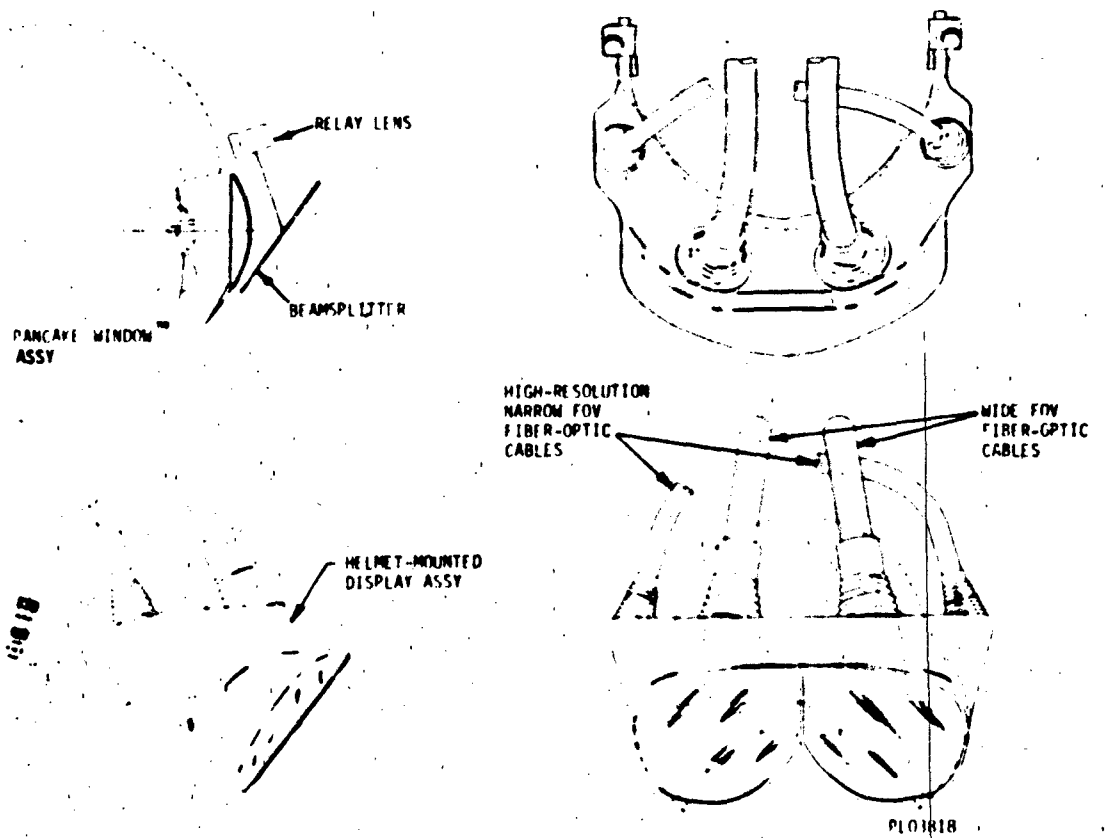

Figure 2. Original Helmet-Mounted Display Concept.

2.2 System Arrangement. The system arrangement that evolved from this effort is shown schematically in Figure 3.

A single relay is utilized to combine two inputs: one is 30 mm in diameter corresponding to an 80-degree, high-resolution-background field of view (FOV) and the other is a 15-mm input corresponding to a 40-degree, high-resolution section of the 80-degree FOV. These inputs are combined by the beamsplitter cube.

The 30-mm background is brought through a 10-mm fiber-optic cable and expanded to 30 mm by a 3X fiber-optic expander. The 15-mm high-resolution input is brought directly through the 15-mm fiber-optic cable.

The arrangement of the system was to include a vertical fold following the Pancake Window™ eyepiece. However, this was subsequently changed to a system with a horizontal fold that significantly reduced the moment of inertia with elevation head motion.

Work was performed to fold this breadboard system as close as possible to the head without cutting into the helmet. At one time, this design permitted the use of a single combiner for the two eyes, permitting a constant see-through illumination over the total horizontal field. This was implemented but found to add significant weight and inertia. Individual combiners having dimensions in accordance with the displayed field and permitting increased see-through transmission beyond this dimension were then used. This has proved satisfactory thus far, with no reports of problems caused by the discontinuities in the see-through transmission.

The arrangement of the delivered breadboard system is as shown in Figure 4.

The optical characteristics of this system are as follows:

(a) Effective focal length (EFL) ≈ 21.2 mm

(b) Exit pupil = 15 mm

(c) Individual horizontal field = 80 deg = 30 mm

(d) Vertical field = 60 deg ≈ 22.5 mm

(e) Overlap, variable between 25 deg and 40 deg

(f) Total horizontal field is variable between 135 deg and 120 deg

(g) Eye relief = 39.5 mm

(h) Mapping = Fθ.

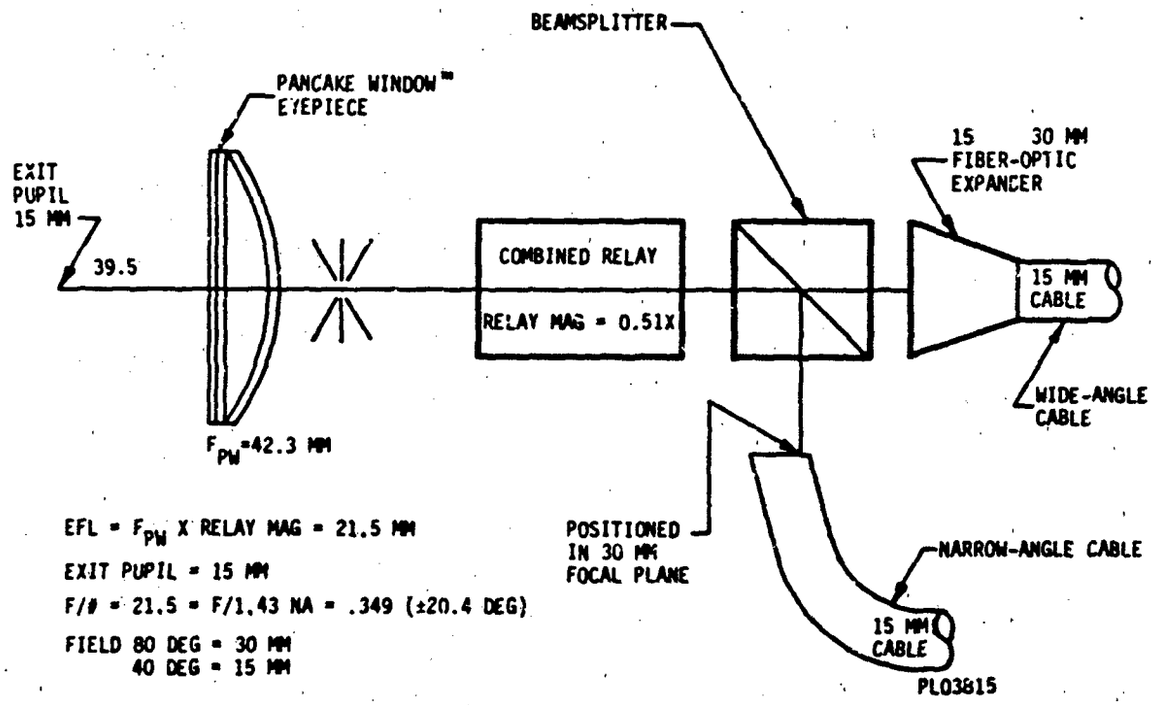

Figure 3. Study Result Proposed System.

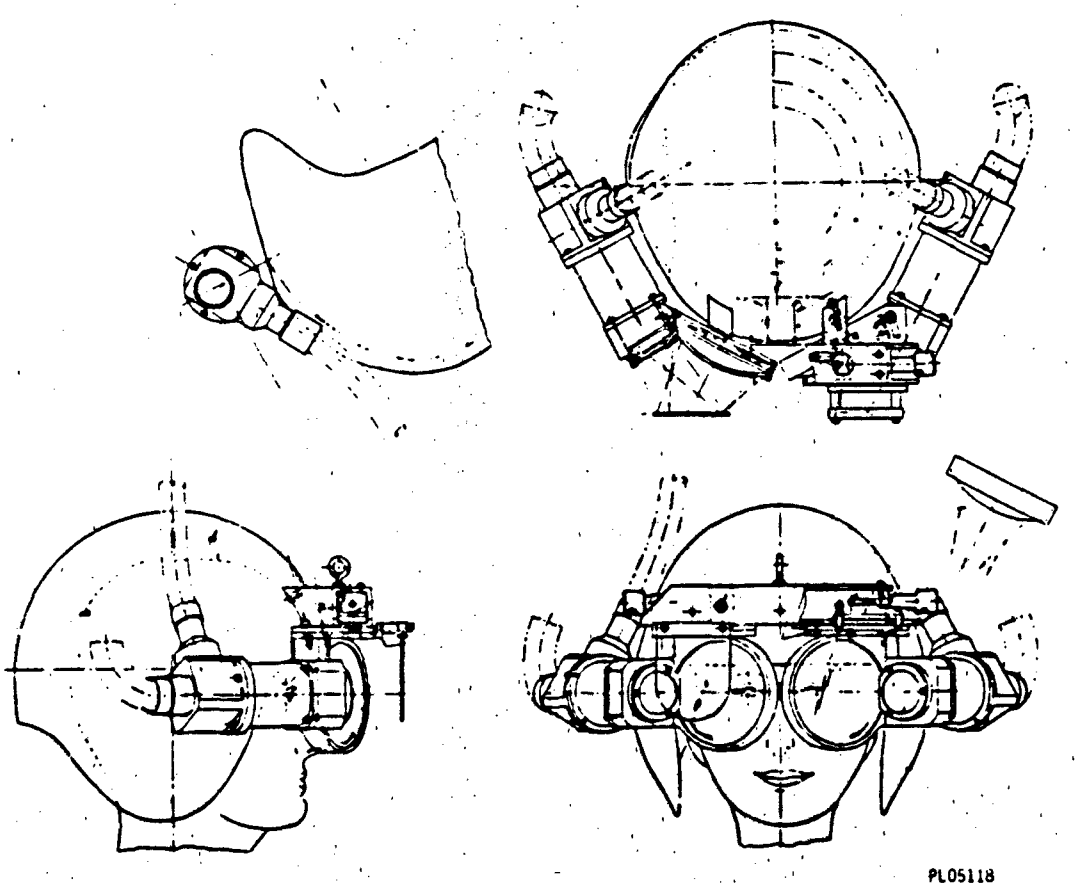

Figure 4. Delivered Breadboard System Arrangement.

2.3 Input Fields of View. The input fields of view for the display system are shown in Figure 5 for the case with the 25-degree overlap with the individual 40-degree fields of view. The angular definitions for these fields of view are shown in Figure 5. The light valve format has linear dimensions (i.e., is rectangular).

2.3.1 Background FOV. The background light valve input dimension scales as 1.1 inch = ±40-degree field. Stating that this input has F tan θ mapping, this input is defined as having a focal length of 0.655 in (16.65 mm).

The output display is defined as having a focal length of 0.835 inch (21.20 mm) with F θ mapping so that 80 degrees = 30 mm.

This means that the optical system that images the wide-field light valve (LV) format to the display system must have a magnification of

$$\frac{\text{EFL Display}}{\text{EFL Light Valve Format}} = \frac{21.20}{16.65} = 1.273\text{X at the center of the field}$$

and a magnification of

$$\frac{\text{Semi-Diam. Display}}{\text{Semi-Diam. Horizontal LV Input}} = \frac{15}{13.97} = 1.073\text{X at the edge of the field}$$

with a proper gradient of magnification between them.

Another way to describe this is that 18.6-percent barrel distortion must be introduced in the wide-angle input relay system.

The interface for the background field with the light valve system utilizes the light valve T6E objective lens interfacing with the exit pupil of the 83.1-mm focal length relay lens.

Thus, the EFL of the system to be added to the T6E is 105.79 mm.

The nominal optical design data for the T6E were available, and it was decided not to attempt any aberrational compensation between the added system and the T6E other than to include the 2.5-percent distortion present in the T6E in the total system distortion correction.

2.3.2 High-Resolution Inset FOV. While the background system has its optical axis normal to both the light valve focal plane and the display input focal plane, this is not the case in the insertion of the high-resolution input.

The background systems are centered on the displays, and the axes of the background displays are turned outward by significant angles.

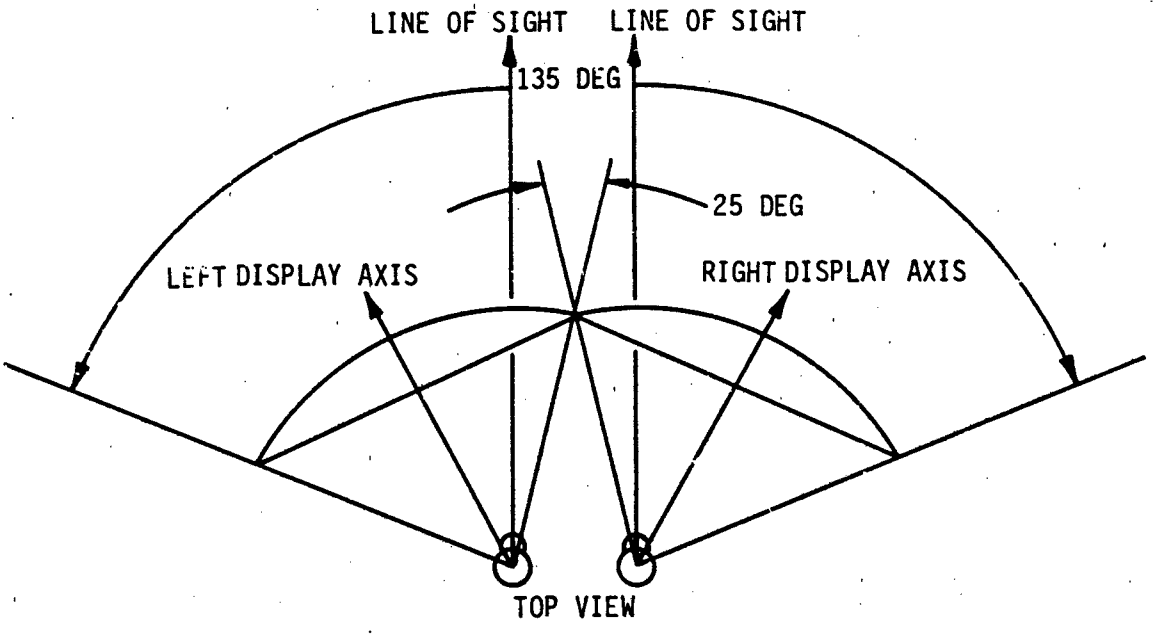

80 DEG HORIZ. FIELD (EACH EYE)
12-1/2 DEG OVERLAP (EACH EYE)
25 DEG OVERLAP

FIELDS OF VIEW

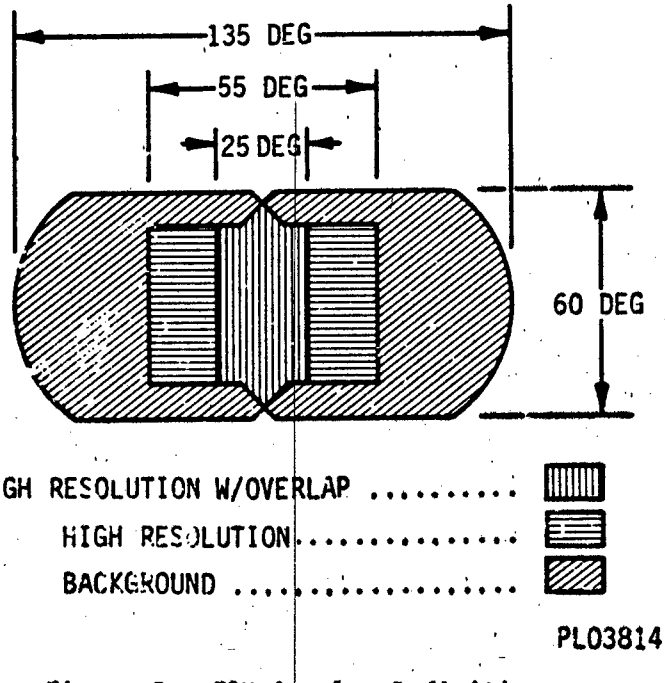

Figure 5. FOV Angular Definitions.

The high-resolution inputs are to be positioned on-axis relative to the observer. Therefore, they are off-axis relative to the wide-field inputs. They must accurately match the wide-field inputs in terms of details so that there is no obvious, abrupt change in the image of an object as it crosses this border. The magnification and distortion characteristics of the high-resolution input must match those of the background.

For the 40-degree, high-resolution input (the 25-degree is a subset of the 40-degree), the scale of the input at the light valve image plane is:

$$\frac{0.55 \text{ in}}{\tan 20 \text{ deg}} = 1.511 \text{ in } (38.38 \text{ mm})$$

The focal length of the T6F objective supplied with the light valve projector used for the inset is 84.7 mm. A 2.207X telescopic system was added to the T6F to provide a system with the required EFL of 38.38 mm (the corresponding numbers for the 25-degree input are 63.01 mm EFL and a 1.344X telescope). The telescope assembly is shown in Figure 6.

Farrand has the data for the nominal T6F objective but has not corrected the aberrations of the T6F other than the approximately 1.5-degree, distortion so that the telescope plus the T6F have F tan θ mapping.

The total optical system is called the 40-degree, high-resolution collimating lens assembly.

This optical system has an external exit pupil to be positioned at the entrance pupil of the next portion of the optical train, which is the high-resolution projection lens system. The light between the two optical assemblies is collimated and, since this is in true angular space, it is perfectly accurate to rotate the whole high-resolution collimating lens system around its exit pupil so that its axis is at a significant angle to the high-resolution projection lens axis. In the case of the high-resolution input, this rotational angle is similar to the angle through which the display axes have been turned outward, approximately 20 to 27.5 degrees.

NOTE: If full overlap between the two high-resolution images is desired, the angle off-axis of the input into the high-resolution projection lens is made equal to the angular turnout of the display systems.

The high-resolution projection lens has focal length (21.2 mm) and mapping characteristics (F θ) identical to those of the display system.

2.4 Problems of Pupil Diffusion. The use of the pupil in the light valve as a real exit pupil in a pupil-forming visual display is precluded for several reasons:

(a) The xenon arc lamp used with a reflecting condensing system produces a pupil with a central obscuration.

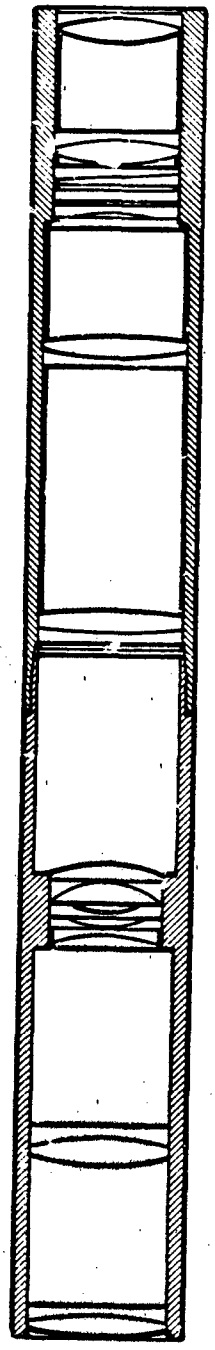

Figure 6. Telescope Assembly.

(b) The Schlieren bars at the exit pupil of the light valve reproduce their image at subsequent pupils.

(c) In the color light valve system, the pupil is not chromatically uniform.

A test was performed at Farrand utilizing a light valve, reimaging lens, fiber-optic cable and a Pancake Window™. The general arrangement was the same as the AFHRL Helmet-Mounted Display, with one exception (no see-through to the outside world). It was learned from this mockup that the fiber-optic cables would not diffuse the pupil of the light valve and that eye movement in a pupil, formed by these combinations of optics, resulted in darkening and hot spots. A suitable diffusing surface had to be found to interface the light valve images to the HMD.

An evaluation of rear surface projection screen material with a low gain was begun. This ended when it was realized that the materials used for rear screen projection are colloidal and a few thousandths of an inch thick. All of the above materials would significantly reduce the resolution of the relatively small projected image used by the HMD. Utilizing a large intermediate focal plane to make screen materials usable would have caused a large light loss in the display.

Until this time, ground surfaces were not considered because past experience with ground glass surfaces provided very non-uniform diffusion. However, because the fiber-optic cables slightly altered the pupil, it was decided to try ground fiber-optic surfaces. Samples of the fiber-optic material were surface ground with 30-micron abrasives. The results were satisfactory in terms of diffusion. Subsequent samples were ground with finer abrasives.

It was determined that grinding one end of a fiber-optic cable with a 5-micron abrasive will diffuse the pupil of a light valve without significantly reducing the resolution in the HMD. Consequently, all fiber-optic output surfaces in the HMD have been ground with this abrasive.

2.5 Fiber-Optic Expanders. As the HMD concept changed from four optical relays per HMD (two per eye) to two relays per HMD, fiber-optic expanders were investigated. Although their use made the display possible with presently available fiber-optic cables, they also presented several problems. A brief description of an expander is necessary to understand their problems and some solutions.

The expanders are made of solid, fused, fiber-optic material. In the HMD, the material is approximately 30-mm-diameter rod with an individual fiber size of 10 microns. An appropriate length of the stock rod is cut off and held at each end. The center of the length of the rod is heated and then the rod is drawn. As the ends are drawn apart, the center becomes

2.5 Fiber-Optic Expanders (Cont'd)

thinner. When the ratio of the width of the end section to the center section equals the desired magnification, the drawing is stopped. After cooling, the rod is saw-cut in the center. This produces two fiber-optic expanders. Length from the small to the large end is approximately 40 mm (a transitional zone). The tendency seems to be to slightly overdraw and remove material from the small end of the transitional zone until the magnification is correct.

During the initial stages of the design, use of an expander at only one end of the cable (the helmet end) was proposed. Distortion from the manufacture of individual expanders made this impossible. However, using both halves of the drawn rod (matched pairs), with the correct phasing, cancelled out local distortions of the center section of the rod. Matched pairs of expanders are now being used, one at each of the fiber-optic cable. The faces of the large ends of the expanders are marked during assmbly of the cable-expander combination so that phasing is maintained during the cementing operation.

During the first cementing, another peculiarity was noticed; the geometric center of the small end was not connected to the geometric center of the large end. A dot placed in the geometric center of the small end was a few millimeters off the center of the larger end. The cementing was a few millimeters off the center of the larger end. The cementing was discontinued and the expanders were returned to the manufacturer. This problem, called frame runout, results from a lack of parallelism between tre large and small ends of the expander. A frame runout tolerance of 0.5 mm was established. One set of expanders was found to be correctable; the other set was remanufactured. When the expanders were returned, cementing to the cables was completed.

3. FIBER-OPTIC CABLES

3.1 Breadboard HMD Cables. The resolution goal for the HMD was 2 to 3 arc minutes per line pair. Such high resolution was required only in that part of the field of view where foveal vision would normally be used. The area outside this region could be allowed to degrade progressively without affecting the observer's perception of the displayed image. Although a number of approaches were suggested at the beginning of the project for obtaining the required resolution using one fiber-optic cable for each eye, it was decided that the lowest-risk approach for the breadboard design would be two cables for each eye. One cable would be used to provide relatively low-resolution imagery outside of the central region and the other would provide high-resolution imagery in the center of the overall FOV. This approach allowed the use of conventional fiber-optic cables and, at the same time, allowed exploratory work on cables having more desirable characteristics to proceed as a parallel development.

The minimum length of cable which would allow adequate head movement was determined to be 6 feet. The cross-sectional area was chosen such that the weight would not be excessive but would still allow the cable to have a sufficient modulation transfer function (MTF) to have a minimal effect on the MTF of the light valve being used as an image source. The MTFs of each component are discussed in section 9. This criterion led to the selection of an 8-mm x 10-mm cable for the background fields. The high-resolution fields had the same resolution requirements, but the cable had to be considerably larger to allow the inset FOV to be changed from 25 degrees to 40 degrees during the evaluation of the HMD. The optical steering mechanism (described in section 6) also added an extra requirement for cable size. Given weight considerations, it was decided that a 15-mm x 15-mm cable was the largest that could be tolerated. The specific density of the glass being used was 1.5, giving a weight of 0.5 pound per foot for the cable plus a certain amount for the cover. Although most of the cable would be supported by the external frame, at least 1 foot would be directly supported by the head. It was considered that if the total weight of fiber-optic cables supported by the head exceeded 2 pounds, a meaningful evaluation of the HMD would be difficult and the feasibility of the concept would be jeopardized.

Although the 15-mm x 15-mm cable was considerably larger than absolutely necessary from the standpoint of resolution, it would allow some flexibility to decide the optimum size and position of the inset FOV without adjusting or modifying the helmet optics. This was an obvious advantage in a breadboard design. A further consideration was the plan to attach the eye-slaved projector (see section 13) to the HMD. The two 15-mm x 15-mm cables would provide a high-resolution central field of 40 degrees vertical by 55 degrees horizontal assuming a 25-degree overlap. This would be sufficient to allow an eye-slaved, 15-degree inset to be moved ±20 degrees horizontally and ±12.5 degrees vertically.

An important parameter for the fiber-optic cables is the numerical aperture. This is equal to the sine of the acceptance angle. The numerical aperture of the cables produced by American Optical at the time of ordering the cables was 0.55, which corresponds to an acceptance angle of 33 degrees. Any light ray angle greater than 33 degrees to the normal on the fiber-optic face is lost. The magnification of the relay optics between the light valve and the fiber-optic cable effectively controls the angle of the cone of light incident on the fibers. Due to the non-uniform nature of the exit pupil in the light valve, an acceptance angle smaller than the half-angle of this cone will not only reduce the light transmitted through the fibers but will also cause a change in color. Because of this, a numerical aperture of 0.55 is barely adequate for the present design and higher numerical aperture fibers will be used in the future. Exploratory work is being carried out to determine whether a numerical aperture of 0.8, giving an acceptance angle of 53 degrees, is feasible.

Several different types of covers for the fiber-optic cables were investigated before a satisfactory solution was found. Available covers ranged from soft neoprene rubber to heavy flexible metal hoses. Although production versions of an HMD would probably not require fiber-optic cables with a great deal of protection, it was decided that the breadboard device would need a more substantial cover than the soft neoprene rubber. Eventually a flexible metal hose made of 0.01-inch stainless steel was obtained for the 8-mm x 10-mm cables. This cover not only offered good protection to the fibers but was extremely flexible and weighed 0.16 pound per foot compared to the fiber weight of 0.2 pound per foot. The cover procured for the 15-mm x 15-mm cable was, unfortunately, much heavier and considerably less flexible. Since covers having almost identical characteristics to the former type can be procured in a larger diameter, future cables will use this type of cover.

Records are being kept of the broken fibers in each cable on the breadboard HMD to assist in the selection of cover materials.

3.2 Image Enhancement in Fiber-Optic Cables. The quality of an image transmitted through a fiber-optic bundle can be seriously degraded by the structure of the fiber bundle. The image falling on a single fiber is averaged in both color and luminance to form a single pixel at the output image. The spacing of the fibers, therefore, determines the limiting resolution and the MTF of the cable. As this is a quantizing process, aliasing effects will also occur. The main degradation occurs due to the fixed-pattern noise produced by the multifiber structure. The current manufacturing process in the USA for large coherent bundles first produces a 5 x 5 array of single fibers, which is then wound onto a drum to form continuous ribbons of the desired width. These ribbons are stacked together to form a rectangular block of the required size which is then impregnated with epoxy and cut to obtain a single coherent bundle. The array or multifiber structure is very visible. A further small degradation is due to the slight non-coherence caused by minor variations in the spacing of the multifiber and the removal of a portion of the fibers during the cutting and polishing procedure.

The effect on image quality of these manufacturing characteristics can be reduced considerably by the use of either color or dynamic multiplexing. Both techniques, although quite different in implementation, cause each image element to be transmitted by many individual fibers. Upon recombination at the output end of the cable, the structure of the fibers is suppressed and the image quality is considerably enhanced. Both techniques were tried and are described in the following paragraphs.

3.2.1 Color Multiplexing. This approach uses a prism at the input end of the cable to spread each pixel of the image into a linear spectrum covering several multifibers. An identical prism is used at the output end to correct the color dispersion. If the spectral dispersion is large enough, broken multifibers appear as faintly colored streaks. If the dispersion is equivalent to only two or three multifibers, this becomes a fairly bright colored defect. Tests with a light valve showed that a dispersion of 0.5 mm between blue and red was necessary to reduce the effect of a broken multifiber to negligible proportions. The color multiplexing technique was actually used in the breadboard design but other optical design considerations prevented more than 0.2 mm of dispersion being used. Although the overall image quality in the 25-degree inset is quite high, the fixed pattern noise and broken fibers are still visible. The effect of this residual fiber structure will be evaluated on the breadboard system. It now seems possible to use a greater amount of spectral dispersion and, if the engineering prototype retains this image enhancement technique, the dispersion should be at least equivalent to 10 multifibers.

The effect on resolution of color multiplexing is shown in Figure 7. The resolution characteristics are determined by the diameter of the single-fiber core rather than the spacing of the fibers. The limiting resolution of a standard cable is increased by slightly more than a factor of two, due to the fact that a 10-micron fiber has an 8-micron core. The color multiplexing technique can be used only in a single linear direction. Due perhaps to non-uniformity in the fiber structure, however, an increase in resolution is also obtained in a direction perpendicular to the dispersion. The MTF curve in Figure 8 is only for the direction parallel to the dispersion.

3.2.2 Dynamic Multiplexing. The alternative approach for image enhancement is dynamic multiplexing. The input image is physically scanned across several multifibers in either a circular or random manner. When the output image is scanned in a synchronous fashion, the fiber structure is eliminated and the resolution is improved considerably. The theory is described in some detail by Kapany[2]. The size and mass of the equipment needed to add this feature on the helmet made it impractical for the breadboard, and the color multiplexing approach was adopted. Nevertheless, it was generally accepted that the image quality was superior using the dynamic multiplexing technique, and work is continuing to find a way of incorporating this technique into the engineering prototype.

---

[2] Kapany, N.S. Fiber Optics Principles and Applications. New York, New York: Academic Press, 1967.

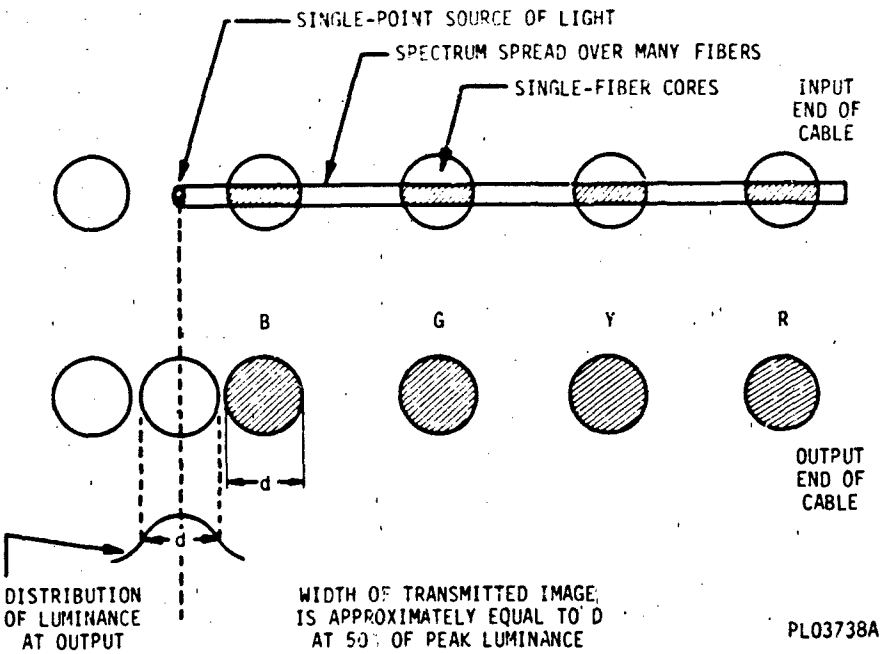

Figure 7. Effect of Color Multiplexing on Spread Function of Point Light Source.

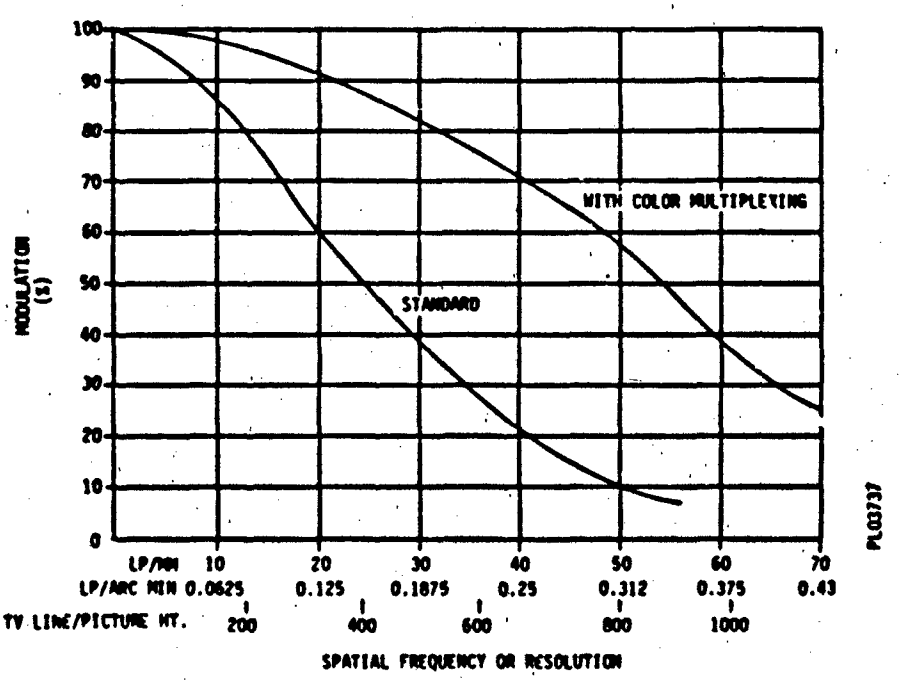

NOTE: STANDARD FIBER-OPTIC CABLE HAS AN 8-MM BY 10-MM IMAGE FORMAT, 10-MM FIBERS AND IS 4-FEET LONG.

Figure 8. Standard Fiber-Optic Cable MTF.

3.3 High-Resolution Cables. The image enhancement techniques just described offer a method of making much higher resolution cables with the same conventional area as standard cables. The resolution of cables using either technique is governed by the diameter of the fiber core. If a cable is made using fibers with the standard 10-micron cladding diameter but 3-micron cores instead of the usual 8 microns, an increase in limiting resolution of 8/3 (i.e., 2.7) can be expected.

A single 12-mm cable used for the entire 80-degree FOV of each eyepiece would provide angular resolution similar to that of the 15-mm bundle used for the inset field in the breadboard.

Accordingly, a small-diameter cable (4 mm x 4 mm) was built to determine the feasibility of this approach. The cable had the expected increase in resolution, and no severe manufacturing difficulties were encountered. Handling of the fibers proved easier than expected because the multifibers were considerably less fragile, reducing breakage in the assembled bundle. Full-size cables using 3-micron cores and 6-micron cladding are currently being produced for evaluation in the breadboard. The transmission of these cables will be reduced in proportion to the relative cross-sectional area of the fiber core to the overall area of the fiber. In effect, this technique trades image luminance for resolution.

3.4 Variable Resolution Cables. As explained (paragraph 3.1), two cables are used for each eyepiece to give higher resolution in the central region of the visual field. A single cable having the required resolution would have been far too large using conventional construction techniques. The approach described in paragraph 3.3 will give the required resolution in a reasonable-size cable at the expense of reduced transmission. If, however, the spatial density of the fiber could be varied across the cable so that the lower resolution resulting from fewer fibers per unit area matched the acuity of the eye, a smaller number of fibers could be used without loss of visual performance.

Conventional fiber-optic manufacturing techniques preclude investigations in this area, but it was realized that, if the magnification of the input image could be varied across the FOV and corrected in the helmet optics, a similar effect could be obtained. Figure 9 shows how the tan θ mapping function of the computer-generated imagery system would be modified by a variable-magnification relay lens to form a new image on the fiber-optic cable. The magnification varies from one in the central 20 degrees to eight at the extreme periphery. The area of the output image is approximately one-third that of the input image.

A company specializing in aspheric optics was asked to give a quote to study this concept. After a certain amount of investigation, the company concluded that, although there was a good chance of making a lens with the required characteristics at the input end, there was only a 20-percent chance of success in making a lens with the opposite function at the helmet end. This area of research has been dropped for the engineering prototype phase.

3.4 Variable Resolution Cables (Cont'd)

The leached bundle technique, however, may allow fiber-optic cables having variable resolution to be manufactured. Once the exploratory work on leached bundles has been completed, this area will be re-examined.

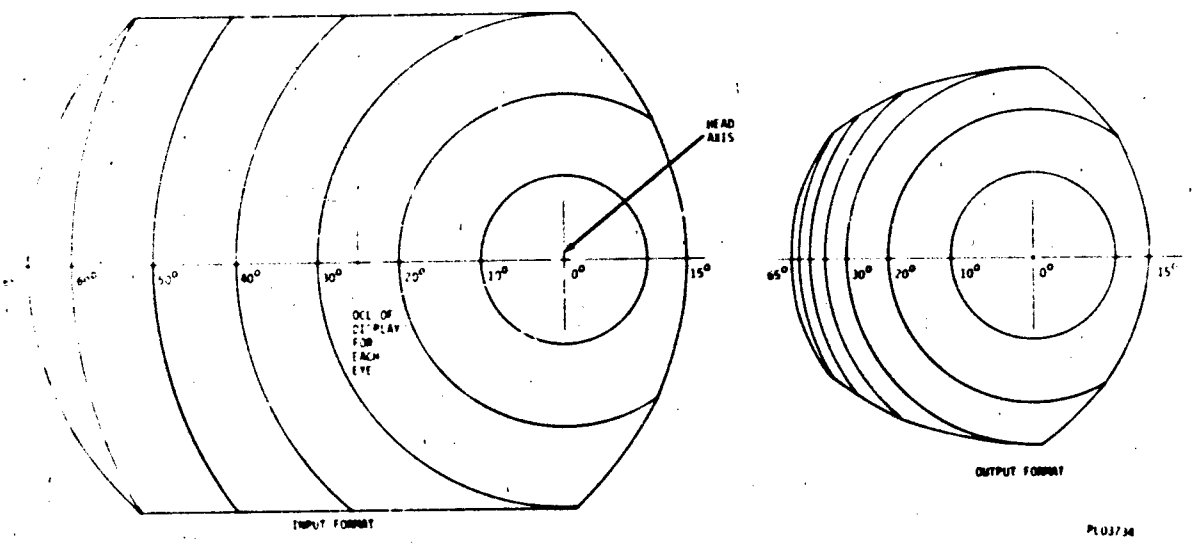

Figure 9. Mapping Function for Relay Lens.

4. MECHANICAL SUPPORT STRUCTURE

4.1 Mechanical Structure and Modules. The mechanical structure of the HMD system consists of a steel frame structure supporting four individually vibration-isolated modules (see Figure 10). The top two modules (one of which is shown in Figure 11) contain the projectors, relay optics, and optical steering for the low-resolution or wide FOV, while the bottom two modules (one of which is shown in Figure 12) contain the projectors, relay optics and optical steering for the high-resolution or narrow FOV.

4.1.1 Wide Field of View Modules. Each of the wide FOV modules (refer to Figure 11) contains the following: (Letters in circles on figure correspond to letters in parentheses in the following list.)

(a) Light valve projector;

(b) The projector alignment assembly, which is capable of moving the projector in five directions: ±0.30 inches in vertical, ±0.75 inches in lateral, ±1.50 inches in longitudinal, ±1 degree in pitch and ±3 degrees in yaw (see Figure 13);

(c) The low-resolution relay optics, 80-degree afocal telescope (see section 2);

(d) The angular alignment assembly, which is capable of ±1.6 degrees in pitch and ±4 degrees in yaw (see Figure 14);

(e) The vertical alignment stage, manufactured by Optikon Corp. Ltd., Part Number MV.80 (see Figure 15). A micrometer reading of one unit corresponds to a vertical displacement of 5 microns (0.0002 inch);

(f) The longitudinal and lateral alignment stages, manufactured by Optikon Comp. Ltd., Part Number MRT.120.40 (see Figure 16);

(g) The 80-degree telescope base, a welded aluminum construction;

(h) The fiber-optic cable (see section 3);

(j) The optical steering assembly (see section 6);

(k) The optical steering support frame;

(m) Laminated steel honeycomb optical table, manufactured by Ealing Corp., Part Number 24-5142. The tables offer the advantages of low weight, rigidity, internal dampening, and a high natural frequency important in obtaining low displacements due to dynamics; and

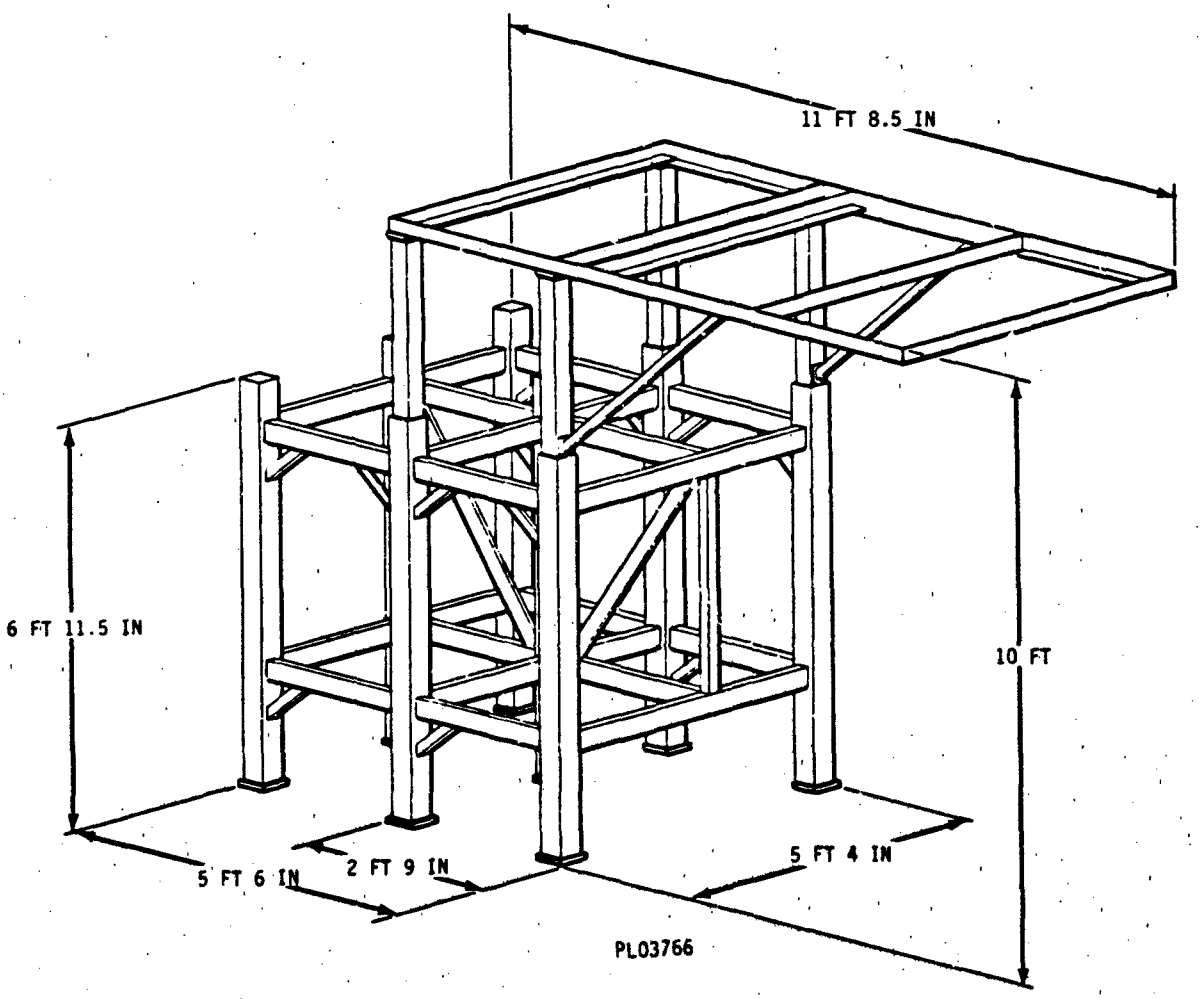

Figure 10. HMD Main Frame.

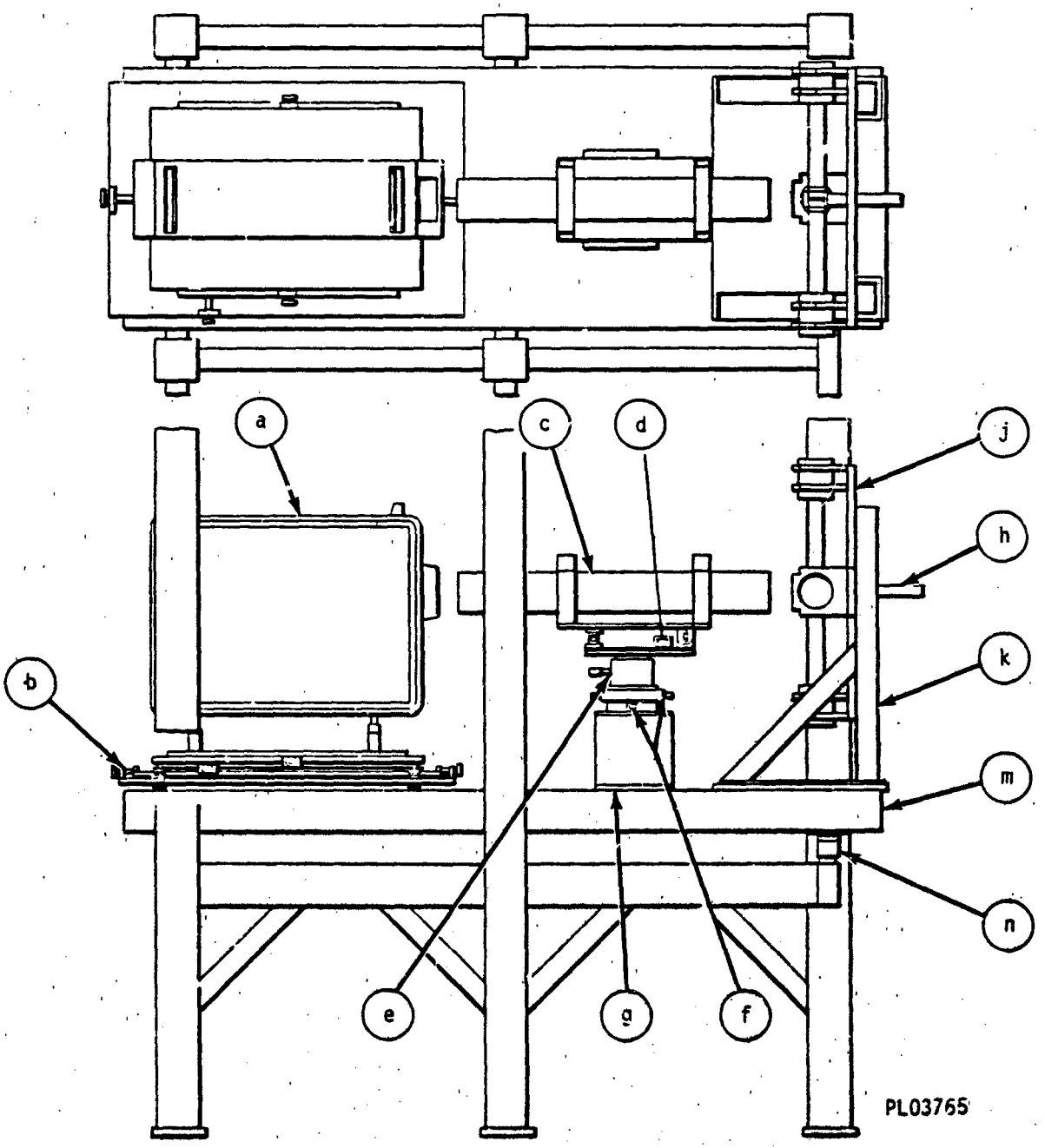

Figure 11. Wide-FOV (Low-Resolution) Module.

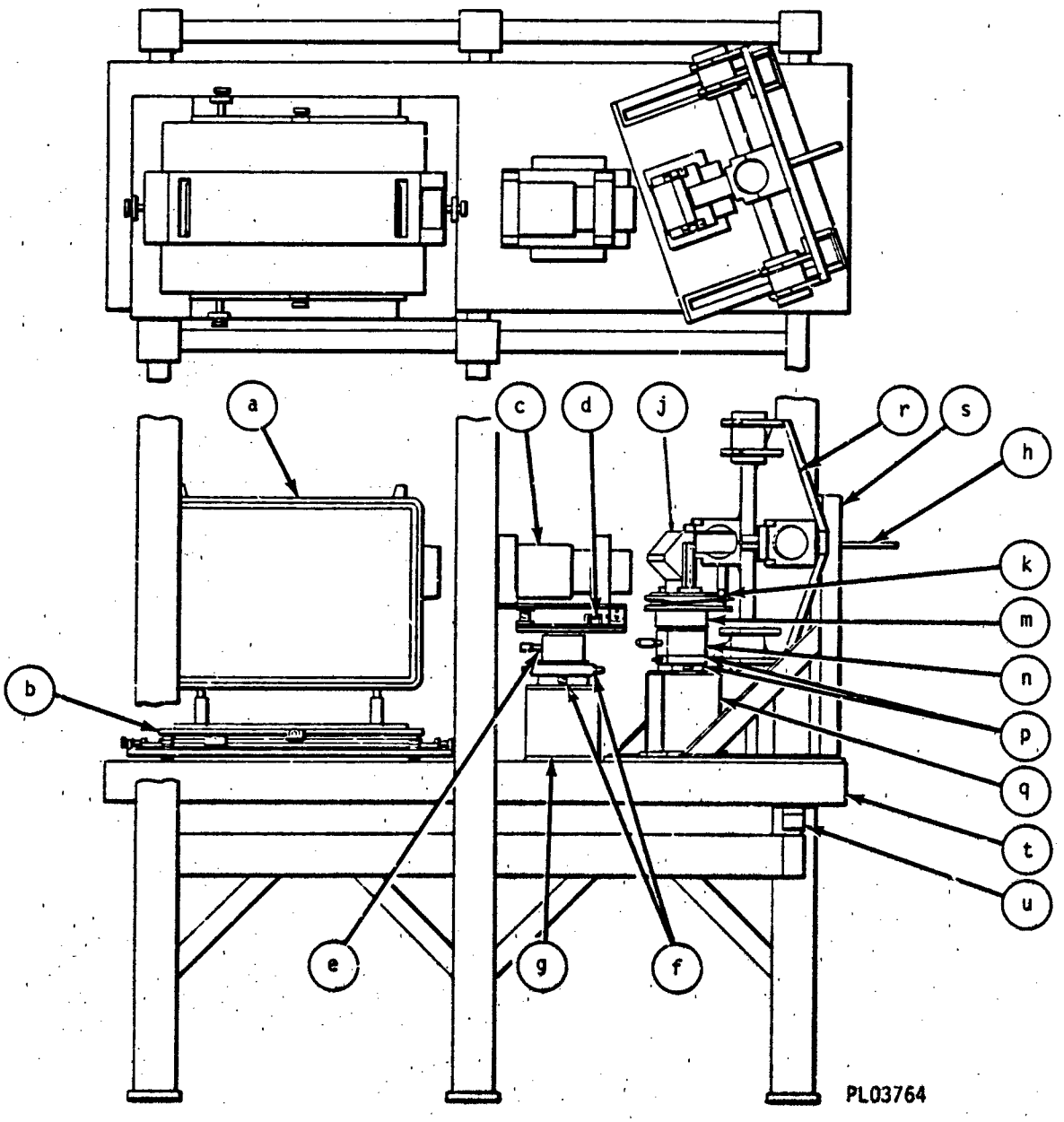

Figure 12. Narrow-FOV (High-Resolution) Module.

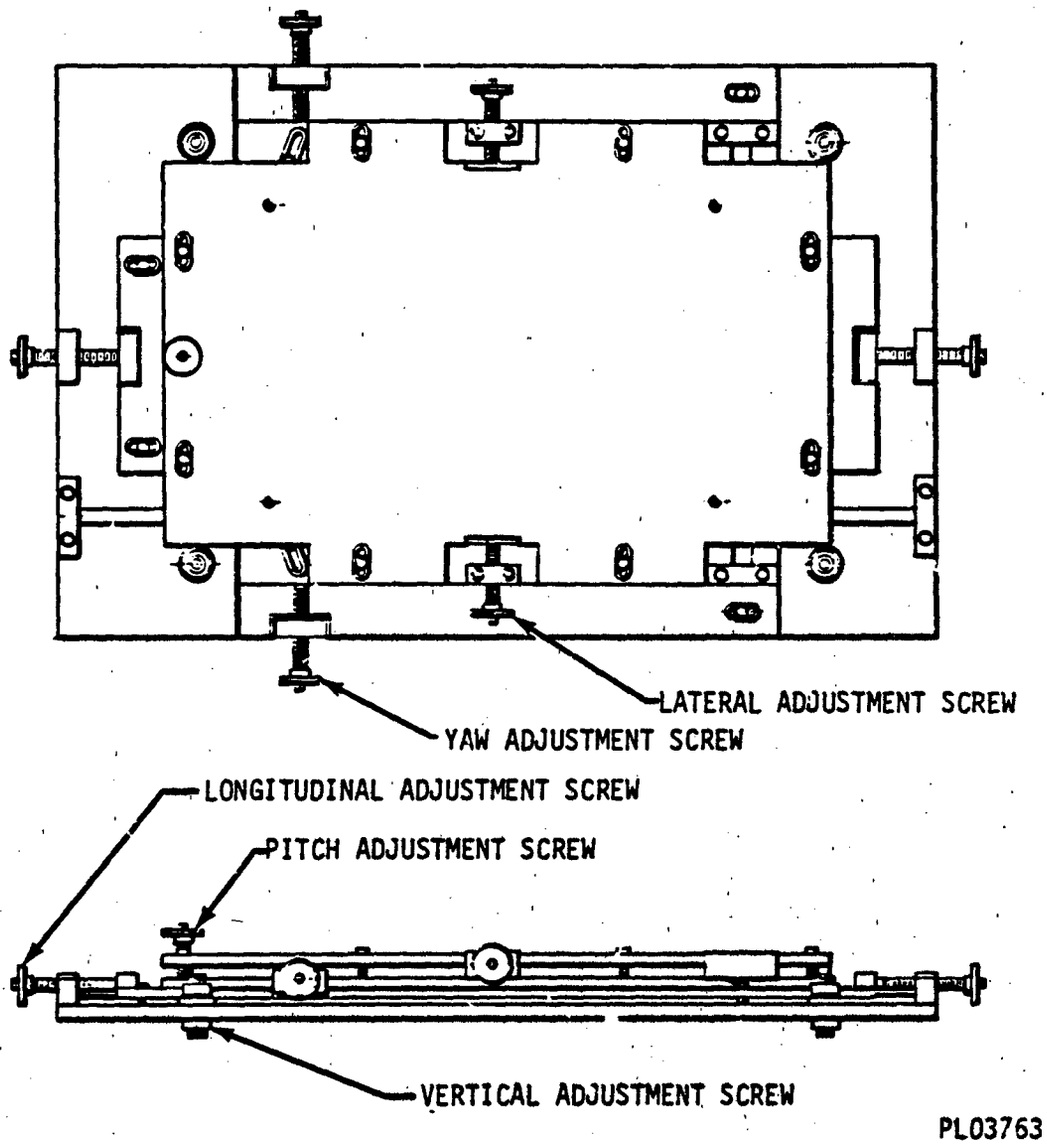

Figure 13. Light Valve Projector Alignment Assembly.

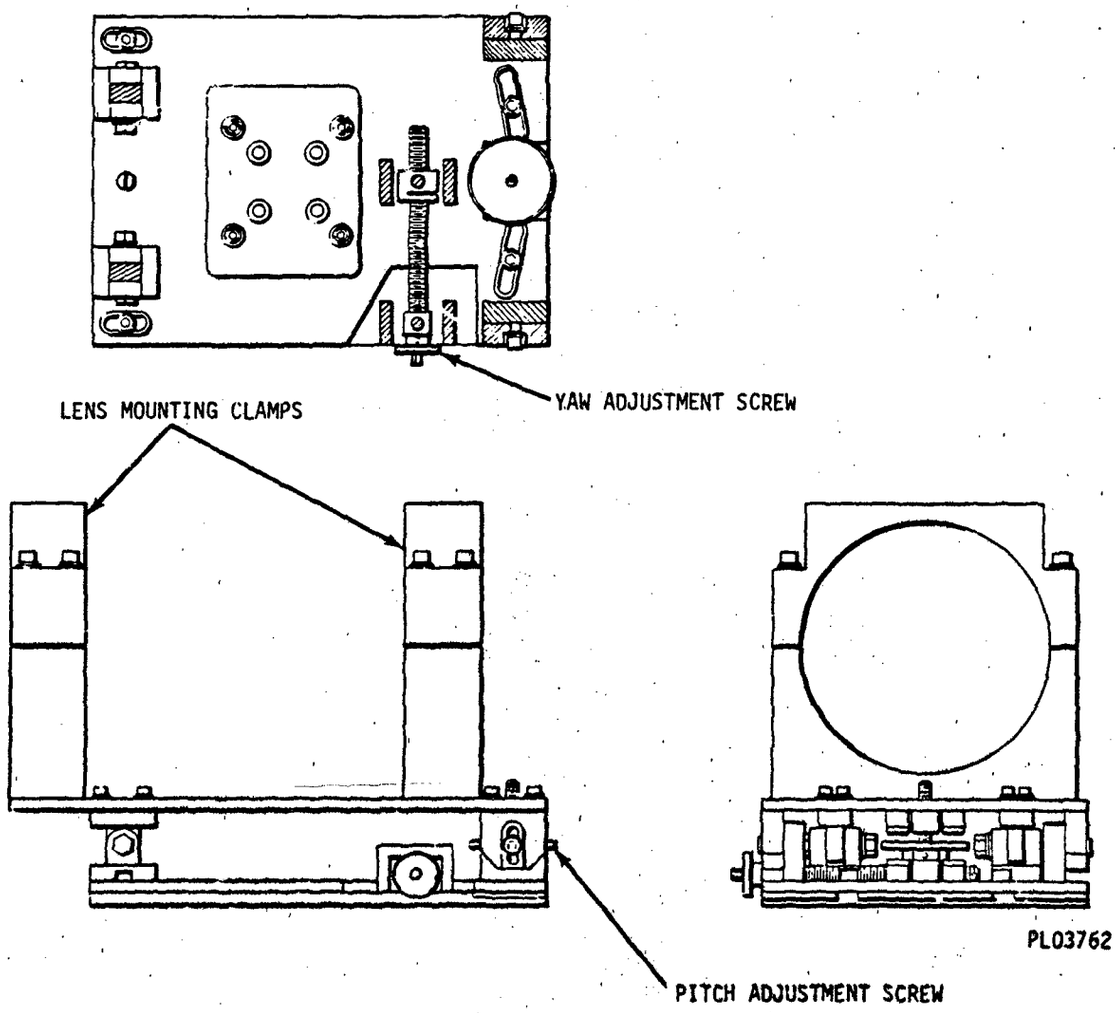

Figure 14. Afocal Telescope Angular Alignment Assembly.

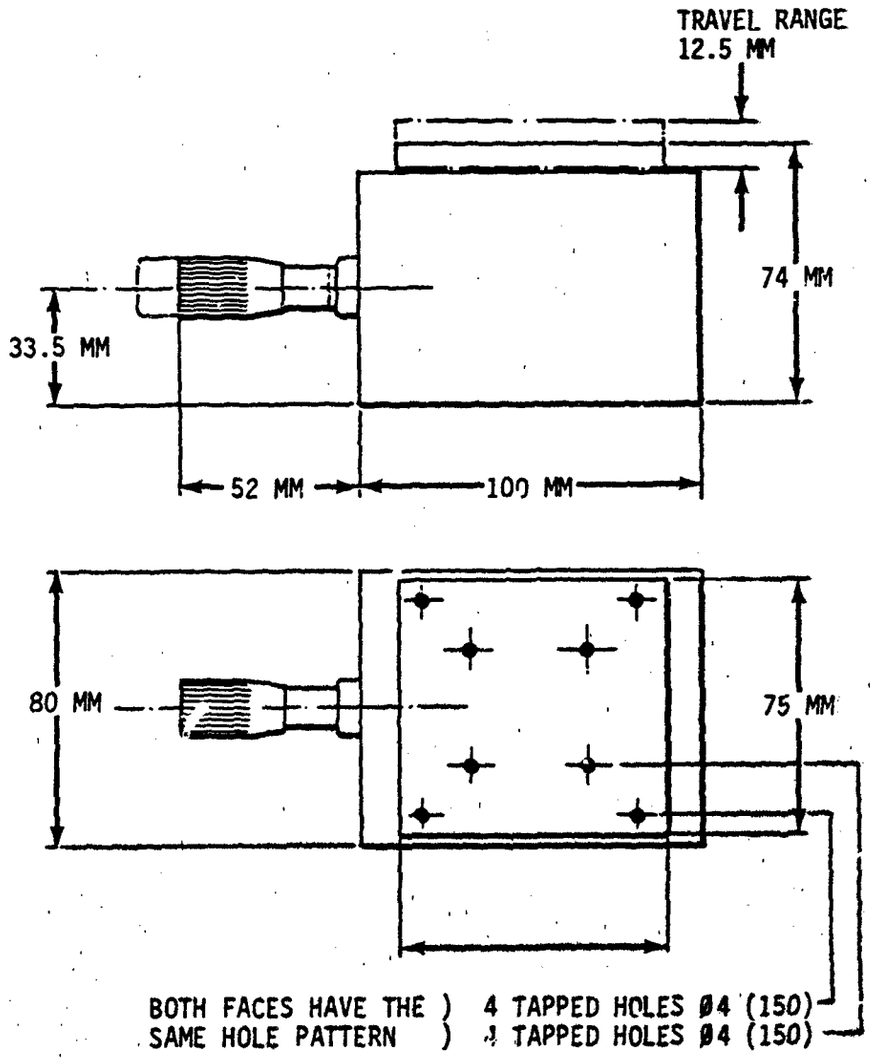

Figure 15. Vertical Alignment Stage.

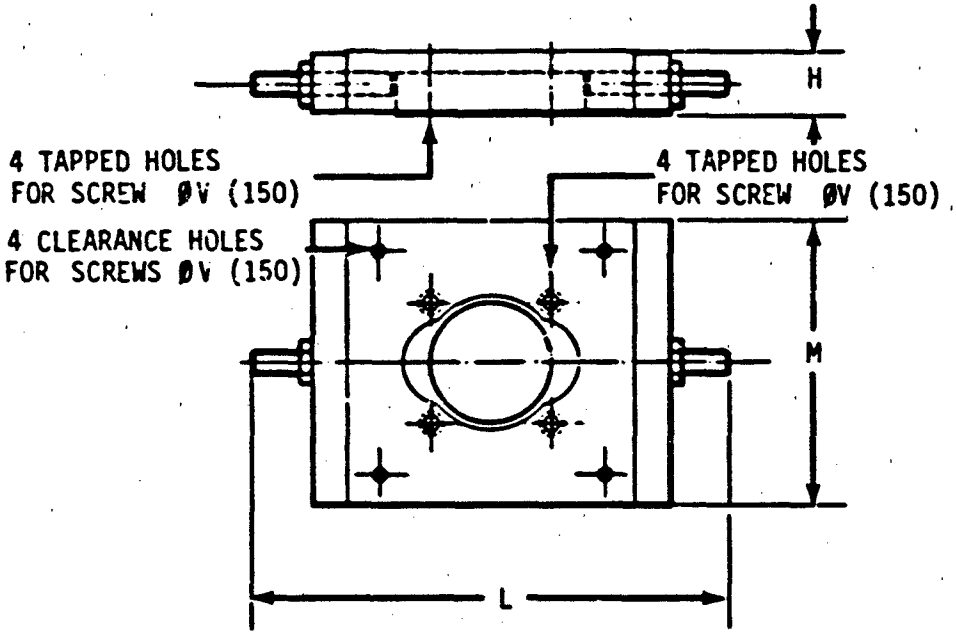

PART NO.	RANGE	H	L	M	V
MRT.80.25	25	18	133	80	4
MRT.120.40	40	26	198	120	5

PL03760

ALL DIMENSIONS ARE IN MILLIMETERS.

Figure 16. Longitudinal and Lateral Alignment Stage.

(n) Low-profile, low-frequency elastomeric noise and vibration isolators, manufactured by Barry Controls, Part Number 633A-130. The mounts effectively isolate disturbing frequencies as low as 15 Hz.

4.1.2 Narrow Field of View Modules. Each of the narrow-FOV modules (refer to Figure 12) contains the following:

(a) Light valve projector;

(b) Projector alignment assembly (see Figure 13);

(c) The high-resolution relay optics, 25- or 40-degree afocal telescope (see section 2);

(d) The angular alignment assembly (see Figure 14);

(e) The vertical alignment stage (see Figure 15);

(f) The longitudinal and lateral alignment stages (see Figure 16);

(g) The 25- or 40-degree afocal telescope base, a welded aluminum construction;

(h) The fiber-optic cable (see section 3);

(j) The high-resolution projection lens (see Section 13);

(k) The inclination stage, for pitch alignment, manufactured by Optikon Corp. Ltd., Part Number TG.120 (see Figure 17). The inclination stage is capable of ±2-degree 30-minute tilt;

(m) The rotational stage, for yaw alignment, manufactured by Optikon Corp. Ltd., Part number TR.120 (see Figure 18);

(n) The vertical alignment stage (see Figure 15);

(p) The longitudinal and lateral alignment stages, manufactured by Optikon Corp. Ltd., Part Number MRT.80.25 (see Figure 16);

(q) The high-resolution projection lens base, a welded aluminum construction;

(r) The optical steering assembly (see section 6);

(s) The optical steering support frame. This support frame is capable of rotating about a pivot (which coincides with the exit pupil of the afocal telescope and the entrance pupil of the projection lens) in order to accommodate the two different insets (25 and 40 degrees). The alignment procedure is described in paragraph 4.3;

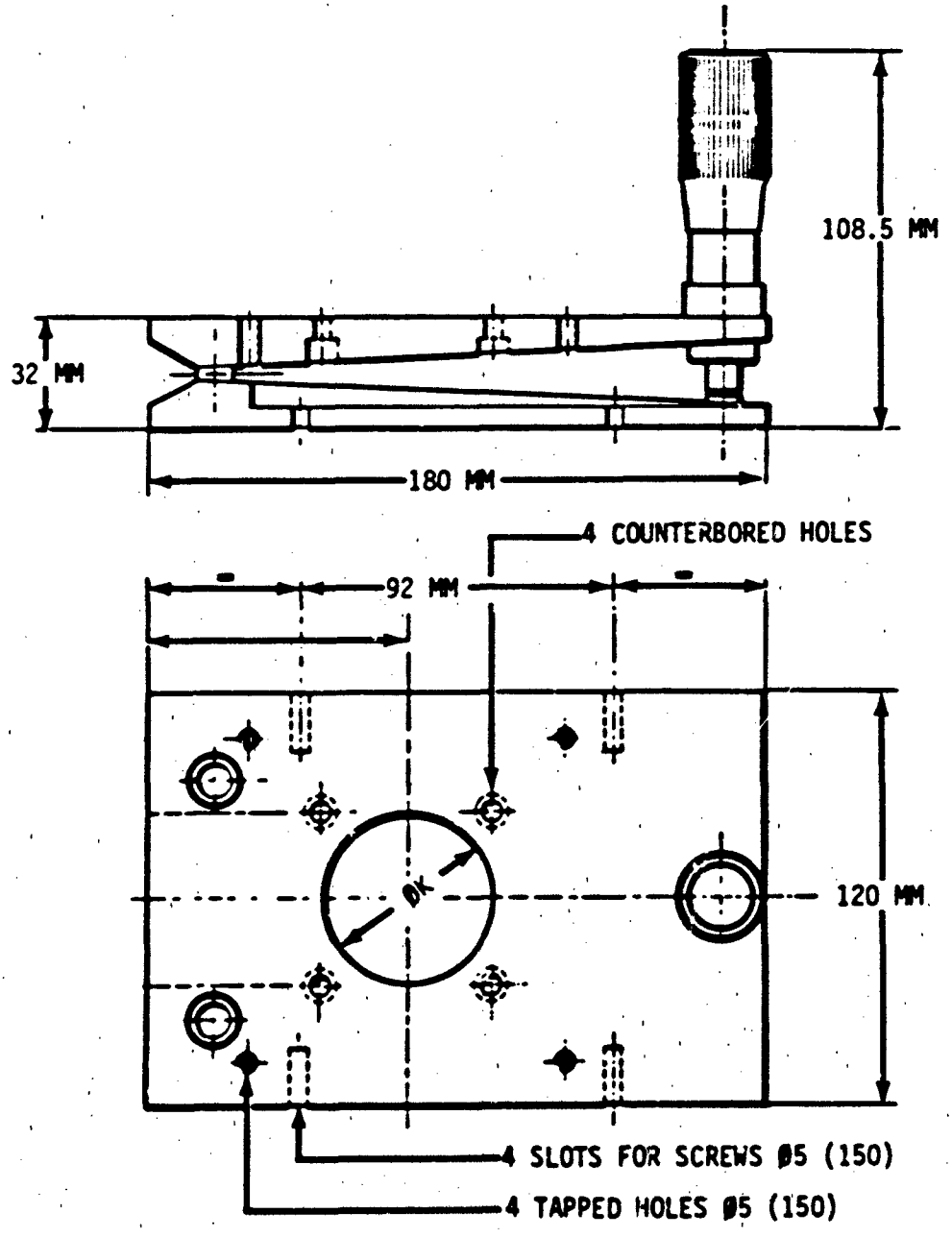

Figure 17. Inclination Stage.

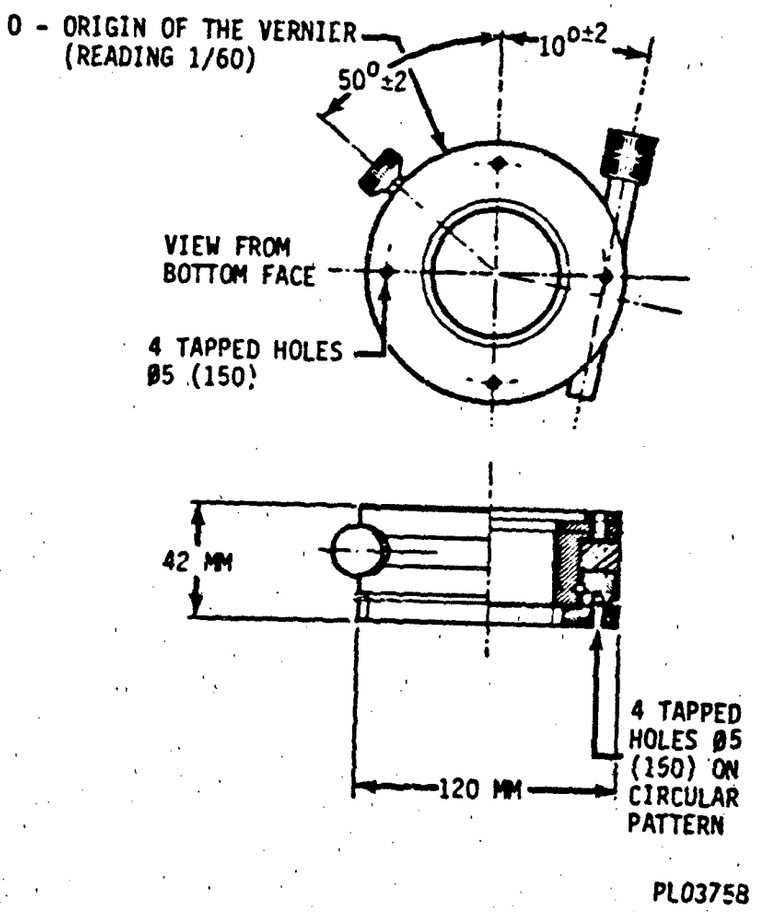

Figure 18. Rotational Stage.

(t) Laminated steel honeycomb optical table; and

(u) Low-profile, low-frequency elastomeric noise and vibration isolators.

4.2 Counterbalance Mechanism. The purpose of this assembly is to nullify the moments produced by

(a) The weight of the helmet-mounted optics about the head's pivot point, and

(b) The weight of the fiber-optic cables.

The assembly, as shown in Figure 19, consists of three subassemblies which are all similar in design. Each assembly is made up of a pair of constant-force springs wound on two freely rotating drums all suspended on a hardened-steel rod through a linear bearing. On the assembly supporting the helmet optics, the constant-force springs are connected to the helmet through a single pulley. (This reduces the moments produced by the optics in the roll axis as well.)

4.3 Alignment of the High-Resolution Input

4.3.1 Basic Alignment Principles. In terms of a general overview, the system is aligned as an in-line optical system. The axis of the system is in a plane parallel to the optical table. The optical table is in plane that is level to the ground; therefore, the optical axis will be parallel to the ground. The complete input has one moving part: the high-resolution projection lens/fiber-optic cable assembly (see Figure 20). This part pivots at an axis which intersects the axis of the optical system at a location where the exit pupil of the afocal telescope and the entrance pupil of the high-resolution projection lens coincide.

There are several optical mechanical deviations that must be considered in the basic alignment. The high-resolution inset is not centered in the displayed field of each eye and is, therefore, not centered geometrically on the high-resolution axis. The fiber-optic cable is displaced by 7.5 mm. This brings one edge of the cable to the axis of the high-resolution input. The cable edge would appear as a vertical line bisected by the optical axis. The direction of displacement of the cable is toward the right, on the horizontal axis, for the right eye input and toward the left for the left eye input (see Figure 21). The high-resolution projection lens includes a spherical mirror beamsplitter and folding mirror. This combination displaces the optical axis by 75 mm (nominal) in the vertical direction. As mentioned, the high-resolution projection lens/ fiber-optic cable assembly is pivoted about the exit pupil of the afocal telescope. This angle locates the image from the light valve (projector) at the correct place on the high-resolution fiber-optic cable. This is done without further adjustment of the cable location after the initial alignment.

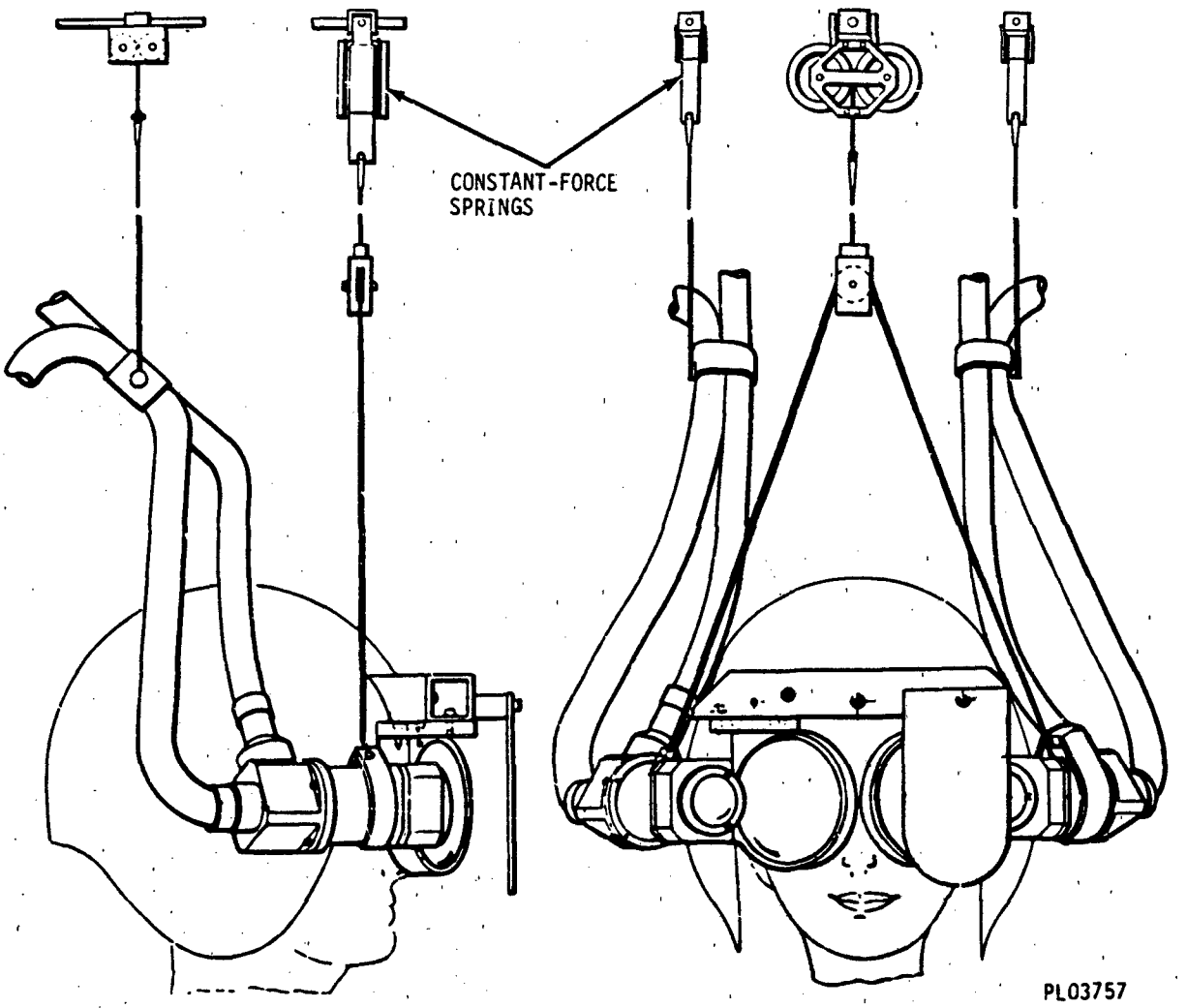

Figure 19. Helmet Optics Counterbalance Mechanism.

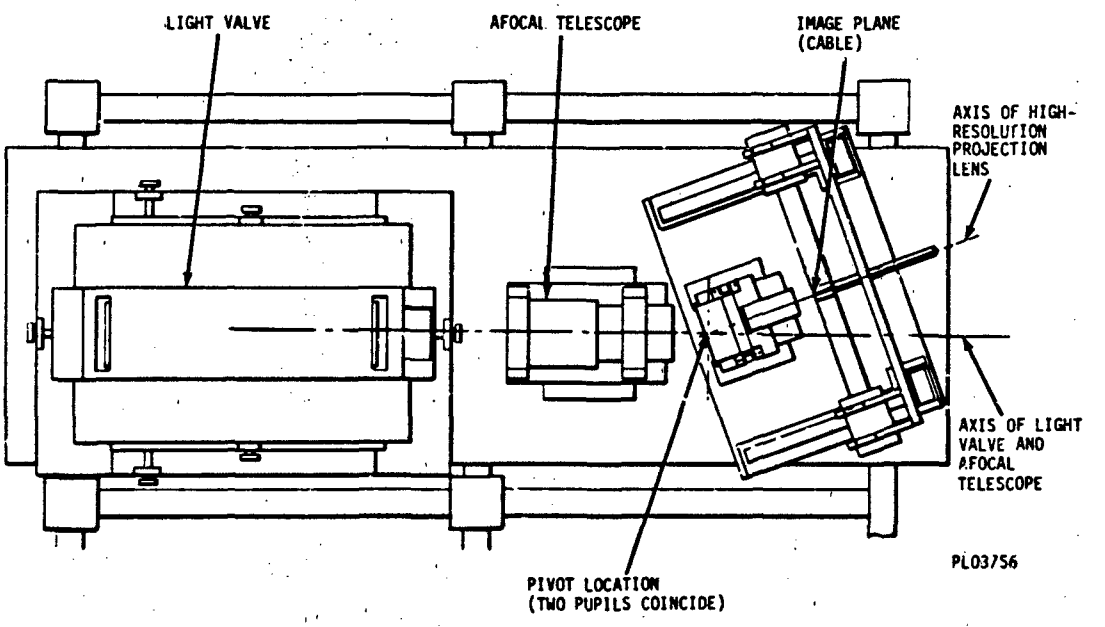

Figure 20. Position of High-Resolution Cable Input.

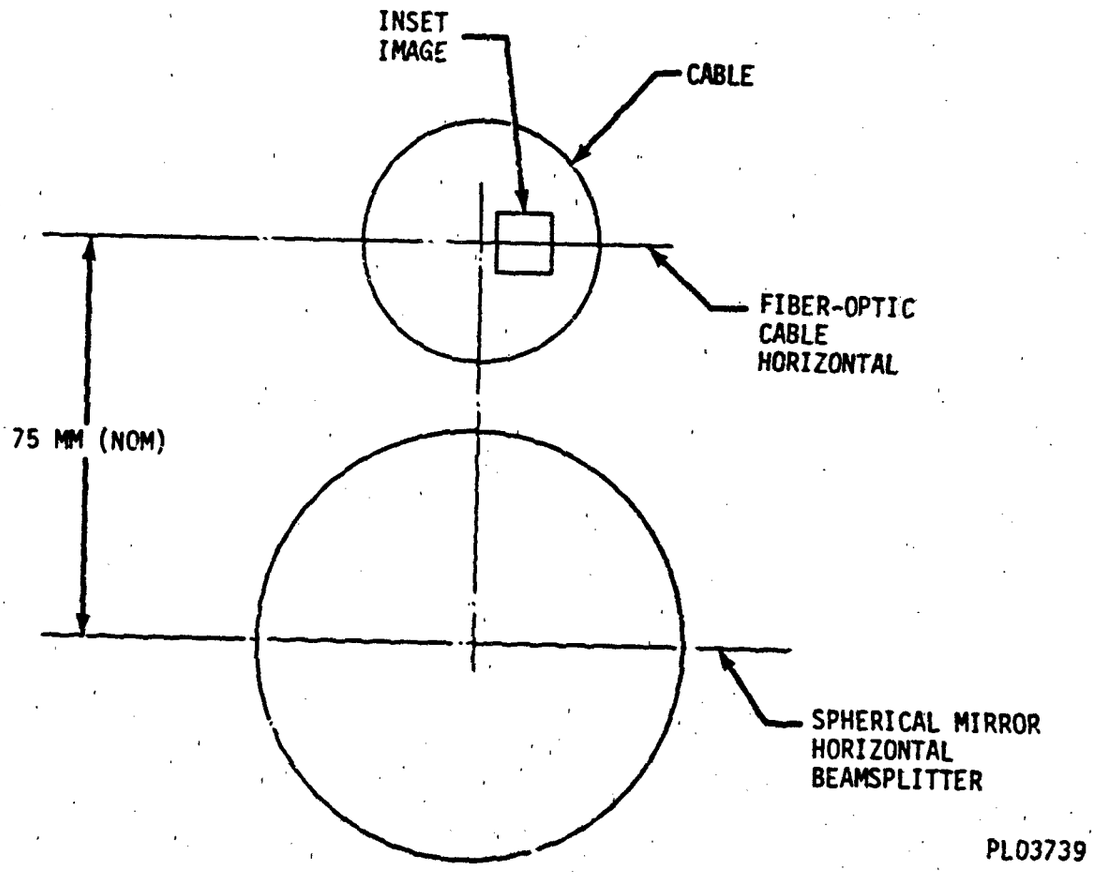

Figure 21. Right Eye Input Viewed from Light Valve Direction.

4.3.2 Alignment of the Fiber-Optic Cable. A cross-hair reticle is placed on the fiber-optic cable end which is toward the display. The reticle is cemented to a fixture which pivots on the ferrule of the fiber-optic cable. The reticle is rotated until one reticle line bisects the cable in the horizontal direction. The optical table is leveled to the ground to within 0.5 degree. An alignment telescope is attached to the optical table at the end furthest from the optical steering assembly. Using the bisected edge of the fiber-optic cable and a flat parallel mirror placed against the fiber-optic cable end (which is in the optical steering assembly), an optical axis is established. Adequate adjustment of the alignment telescope in the vertical direction is provided to account for the vertical displacement of the optical axis.

4.3.3 Alignment of the Projection Lens. The high-resolution projection lens is attached to the standoff by four 4-40 screws going through L brackets into the sides of the main body housing. An alignment mirror is attached to the main body housing by the two tapped holes in the front of the housing (facing the light valve). Using a height gauge set to the image of the reticle on the fiber-optic cable, the high-resolution projection lens is adjusted to approximately its proper height using the scribed lines on the lens barrel as a reference. The correct back focus is set between the fiber-optic cable and the lens. The alignment telescope is then used to look at the alignment mirror on the projection lens, and the projection is brought into angular alignment (pitch and yaw) by use of the two angular adjustments provided on the standoff. The alignment telescope is then moved down to the predetermined new height. Angular adjustment is rechecked.

The high-resolution projection lens is then adjusted in the vertical direction until the reticle is centered in the alignment telescope. The projection lens is then moved horizontally until the vertical edge of the fiber bundle is centered in the alignment telescope. The angular adjustment is rechecked and adjusted if necessary.

After alignment of the projection lens, a check is made to verify that the entrance pupil of the projection lens is in line with the pivot. A cone-shaped point will be placed on top of the pivot to locate the pivot.

On the side of the main housing of the projection lens, a mark will be provided that locates the longitudinal position of the pupil. A transit will be angularly aligned to the side of the housing using an auto-collimating eyepiece through the transit by moving the transit in horizontal and vertical directions. At the same time, the indicator mark for the pupil is kept in the field of view. After the transit is aligned, the vertical angle of the transit is changed and the point which locates the center of the pivot is located. The deviation is recorded. If the deviation is greater than 0.010 inch, the fiber-optic cable is adjusted longitudinally accordingly. The alignment is then rechecked.

4.3.4 25-Degree Telescope Alignment. The 25-degree telescope is initially aligned along the axis of the high-resolution projection lens. A cardboard template supplied with the 25-degree telescope will, when placed on the end of the telescope, locate the exit pupil of the telescope. The telescope is placed on the standoffs. Using the alignment telescope, a flat parallel mirror is placed on the end of the 25-degree telescope toward the alignment telescope.

The 25-degree telescope is brought into angular alignment using the two angular adjustments on the standoffs. The 25-degree telescope is then adjusted for position. The transit is used to locate the longitudinal position of the exit pupil via the template. Vertical and horizontal alignment is accomplished by use of the fiber-optic cable reticle and the alignment telescope. The vertical and horizontal adjustments on the standoffs are used to bring the fiber-optic reticle and the edge of the fiber-optic bundle to the center of the alignment telescope field. The 25-degree telescope is then rechecked for angular alignment. If angular alignment must be re-adjusted, then the 25-degree telescope must be reset horizontally and vertically.

After alignment of the 25-degree telescope, the alignment telescope can be removed, as well as the reticle on the fiber-optic cable end.

4.3.5 Light Valve Alignment. The light valve projector is focused for an infinite conjugate. The light valve is placed on the table and brought to the proper distance from the 25-degree telescope. A central spot should be generated in the light valve format. This spot can be viewed on the face of the fiber-optic cable end that will be placed in the helmet display through a neutral density filter. The spot should be in focus and on the edge of the cable. The reticle may be relocated at this time, for centering, on the cable edge. After centering, a grid pattern is generated on the light valve and focus can be accomplished on the fiber-optic cable end of the high-resolution projection lens.

The last task on the input end is to set the angle of the optical steering assembly about the pivot point. A transit is set up, using the auto-collimating eyepiece, perpendicular to the high-projection lens. A long mirror placed along the standoffs reflects the image of the eyepiece. The transit will be at a close distance to the projection lens. This angle is set to zero. The required angle is set on the transit (27.5 degrees). The optical steering assembly is then rotated about the pivot until the auto-collimated image is again seen through the eyepiece and the transit.

5. HELMET-POSITION SENSING SYSTEM

5.1 Introduction. In order for the computer-generated image to appear stationary as the pilot moves his head, the position of the pilot's helmet must be known relative to the simulator's fixed axes. This position is defined by three translation parameters (X, Y, Z) and three rotation parameters (Euler angles). This information must also be known in order to align the CGI with the frame of the windscreen.

A fundamental part of this development project is, therefore, the helmet-position sensing system. Several sensing systems are presently available and are described in this section. The design of a mechanical system is presented. Alternative solutions, based on the state of the art in noncontact position sensing, are also discussed.

Paragraph 5.2 outlines the requirements for the helmet-position sensing system and serves as a guide in the evaluation of the various approaches described in paragraph 5.3.

5.2 Specifications

5.2.1 Range and Accuracy. Head movement within a simulator is restricted by the geometry of the cockpit and by the physical limitations of the pilot. In most cockpits, the position of the pilot's helmet never exceeds the envelope defined by the following:

(a) Yaw: +150 degrees to -150 degrees

(b) Roll: +45 degrees to -45 degrees

(c) Pitch: +90 degrees to -45 degrees

(d) Max longitudinal travel: +24 inches to 0 inches

(e) Max lateral travel: +6 inches to -6 inches

(f) Max travel along Z-axis: +6 inches to -6 inches.

These values define the required effective range of the helmet-position sensing system. Any measurement taken within this range should not be in error by more than a specified amount. Although there is no bound on the systematic error, the random error (i.e., repeatability) should be better than 0.1 degree for rotation or 0.1 inch for translation.

5.2.2 Weight and Size. Because combat aircraft normally undergo high rates of acceleration, there is a real need to minimize the helmet weight. In simulator applications, g-loading is not a problem but the helmet weight must be kept realistic. The helmet-mounted visual display, together with the position sensing system, must not significantly increase the weight of the helmet. Increasing the size of the helmet is also unacceptable in the limited area of the cockpit.

In military aircraft, the primary function of the flight helmet is protection. Since this is not the case in simulators, there are fewer constraints on mounting additional hardware or modifying the helmet in order to reduce the weight.

5.2.3 Calibration. The accuracy and repeatability of the helmet-position sensing system should be assessed in a realistic, working environment where conditions are generally less favorable than in the laboratory. Some of the available systems are particularly sensitive to interfering or modifying inputs. These systems provide significantly better results in a "clean" environment. The magnetic systems, for example, are susceptible to the noise generated by a variety of electrical devices, especially switching power supplies. Such systems require a lengthy, in situ calibration procedure that must be performed regularly and with specialized equipment.

The ideal helmet-position sensing system would not require a tedious calibration, only an initial alignment within the cockpit. Moreover, it would be insensitive to all interfering and modifying inputs.

5.2.4 Response. Most digital image generators designed for simulator applications operate at a maximum frame rate of 60 Hz. Transportation delays of two or more frames are common. Delays of this kind can be compensated for by implementing algorithms which predict helmet-position and orientation across the appropriate number of frames. These predict-ahead algorithms are usually based on both helmet-position and velocity. Helmet velocity can be determined by taking the difference between two successive position readings and dividing by the interval of time between them. The helmet-position sensing system must, therefore, be capable of providing position data at a minimum rate of 120 readings per second in all six degrees of freedom.

Conceivably, some tracking systems may introduce a significant time delay even if operating at 120 Hz. Therefore, the measured position of the pilot's helmet must not lag the actual position by more than one period. The magnetic systems are particularly poor in this respect. They require a settling time of three or more iterations following a step change in helmet-position.

5.3 Available Systems

5.3.1 System A. This system utilizes a three-dimensional magnetic field produced by an orthogonal set of radiating coils. These coils are fixed to the airframe at a point on the longitudinal axis just above and behind the pilot's head (see Figure 22). The radiating coils excite the windings of a second set of sensor coils located on the pilot's helmet. The output of the sensing coils can be used to calculate the position of the pilot's head relative to the fixed axes of the radiator (see Figure 23).

Two such systems employ the same basic hardware but differ significantly in their approach to the problem of interference. One relies on a map of the ambient magnetic field within the cockpit. This map is unique to each installation and is determined experimentally. The test rig required to develop the map consists of a magnetic sensor mounted on an X-Y table. The table is placed inside the cockpit and measurements are taken at 2-inch intervals throughout the X-Y plane. During normal operation, the ambient magnetic field can be determined by interpolation and a correction factor can be applied to the position data.

In the other, it is assumed that the ambient magnetic field emanates from a number of parasitic dipoles on or in the vicinity of the helmet. These dipoles are scaled such that they fit the magnetic map of the cockpit. This approach provides a closed-form solution for the ambient magnetic field. Furthermore, the parasitic dipoles can be treated in much the same way as the radiating coils, thus simplifying the algorithm.

System A is extremely sensitive to electromagnetic interference. The addition or removal of metal from the cockpit will usually necessitate the development of a new magnetic map. Metal components which mount directly on the helmet are particularly difficult to deal with, especially if they obstruct the data link between sensor and radiator. The use of certain devices which must be helmet-mounted (i.e., the display hardware) could preclude the use of this system.

The system requires high-performance data acquisition and processing capabilities. The analog signals from the sensing coils are amplified and converted to digital form via a high-speed, 12-bit analog-to-digital (A/D) converter. Arithmetic and logical functions such as the coordinate transformations are performed by four cascaded 2901-bit-sliced processors. The overall system performance is summarized in Table 1. It should be noted that the system was evaluated in a clean environment. Special nonmetallic fixtures were developed to hold and position the sensor during testing.

A modified version of this system has been developed specifically for simulator applications. It uses a PDP 11/60 computer with a 14-bit A/D converter. Despite the increased data acquisition and processing capabilities, the performance is only marginally improved, indicating that the magnetic transducers are the limiting factor.

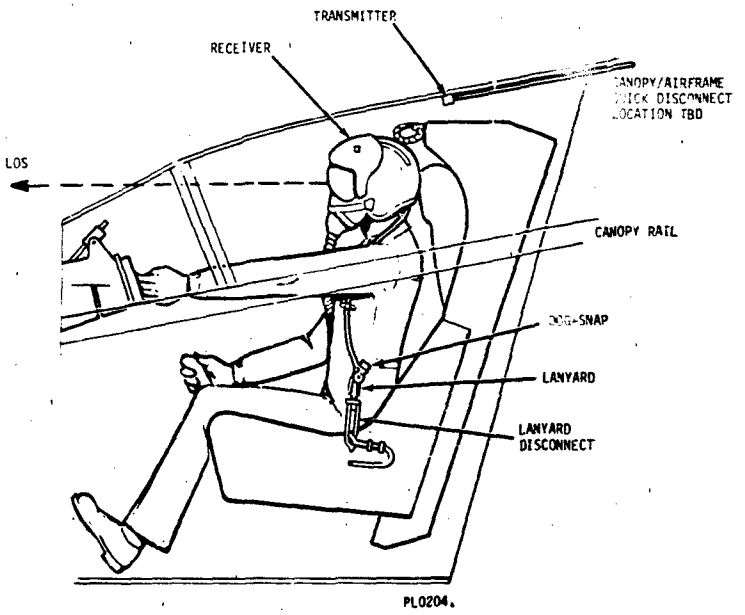

Figure 22. Installation Detail for System A.

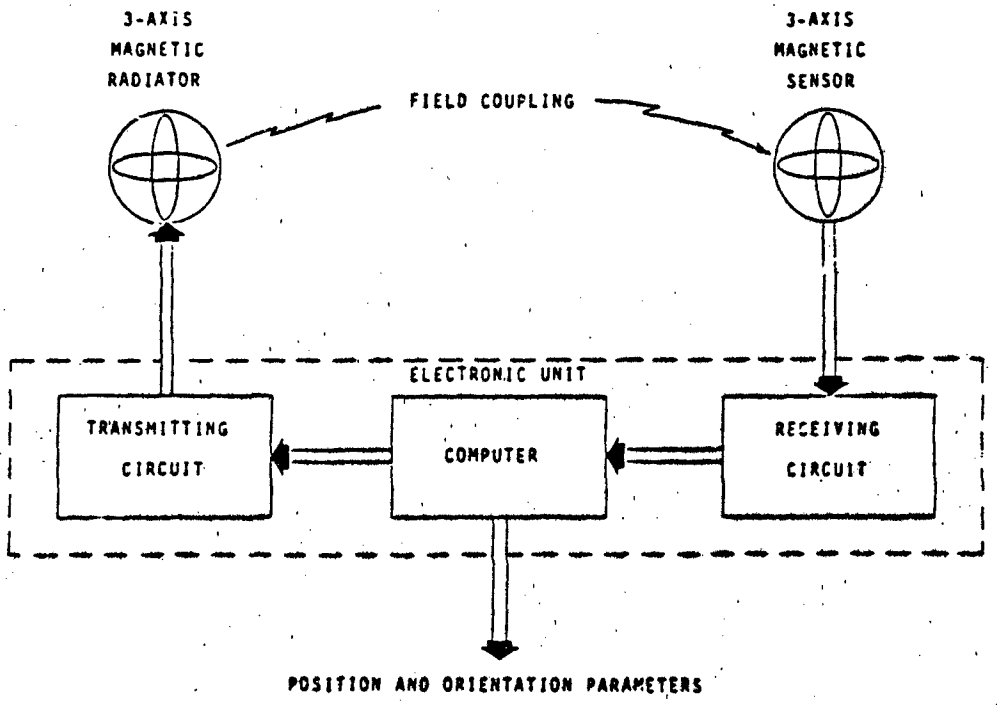

Figure 23. Block Diagram of System A.

Table 1. Performance Summary of Existing Systems.

EFFECTIVE RANGE	CAE SPEC	SYSTEM A	SYSTEM B
-YAW (deg)	-150 +150	-135 +135	-180 +180
-ROLL (deg)	-45 +45	-30 +30	-20 +20
-PITCH (deg)	-45 +90	-70 +80	-70 +70
-FORE/AFT (in)	0 +24	0 +16	-6 +6
-LATERAL (in)	-6 +6	-10 +10	-4 +4
-Z AXIS (in)	-6 +6	-6 +6	N/A
ACCURACY: -ROTATION (deg)	0.1	0.3	0.5
-TRANSLATION (in)	0.1	0.35	N/A
ITERATION RATE (Hz)	120	50	30 to 50

5.3.2 System B. System B takes advantage of recent advancements in electro-optical technology. Central to the system is the cockpit-mounted V-slit camera. This camera is directed at a triad of infrared light-emitting diodes (LEDs) which are fixed to the side of the pilot's helmet (see Figure 24). When one of the three LEDs is flashed on, infrared light enters the camera through a narrow 0.008-inch V-slit and creates an image across a high-resolution linear charge-coupled device (CCD) (see Figure 25). This device consists of 1728 discrete photosensitive elements. The analog signals from these elements are transferred out of the CCD serially at a rate of 2.5 MHz. The resulting output waveform consists of a series of pulses which are amplitude modulated with the optical information. It takes approximately 0.7 millisecond for one complete scan of all the elements in the array.

The position of an LED can be determined in both the horizontal and vertical planes from the two points where the V-image intersects the CCD. Lateral translation of the LED causes the two points to move across the CCD without changing their separation. The separation changes when the LED is moved longitudinally. The intersection points correspond to peaks in the CCD output waveform.

In order to determine the helmet-position and orientation, the V-slit camera first samples and stores the background illumination with the helmet LEDs switched off. The LEDs are then flashed on in sequence and the CCD output waveform is subtracted from the background illumination. This is done to improve the definition of the LED peaks. By using the corrected waveform to gate counters, the location of each peak is determined. The raw

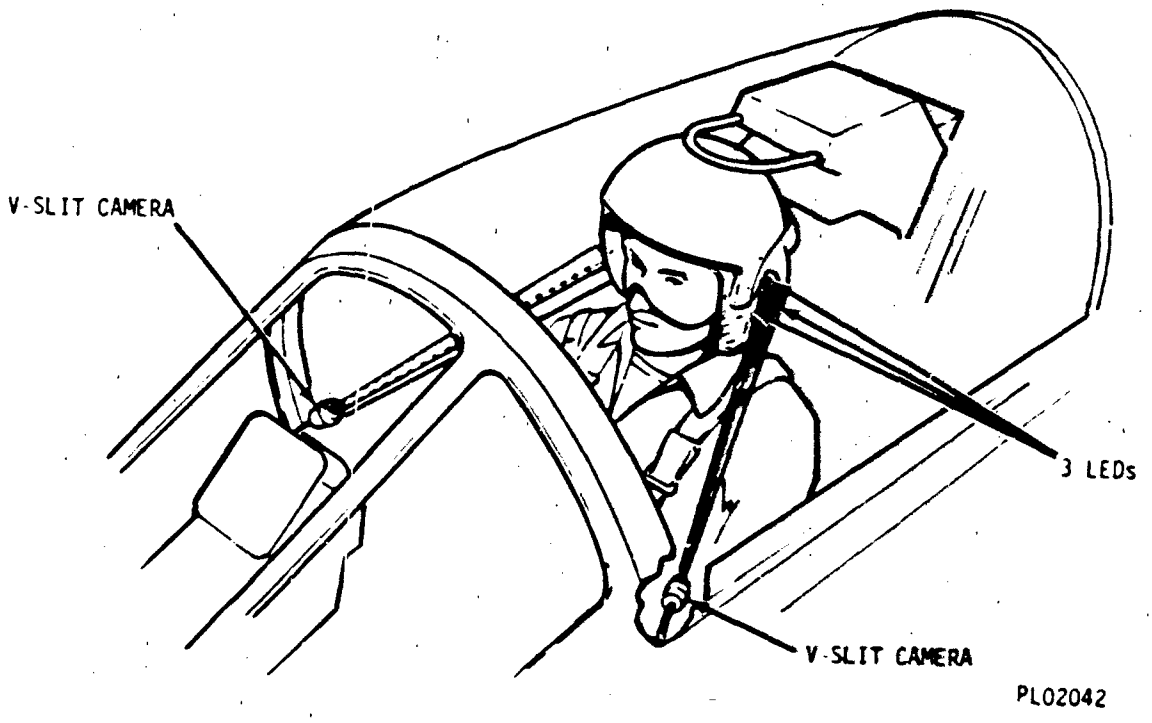

Figure 24. Installation Detail for System B.

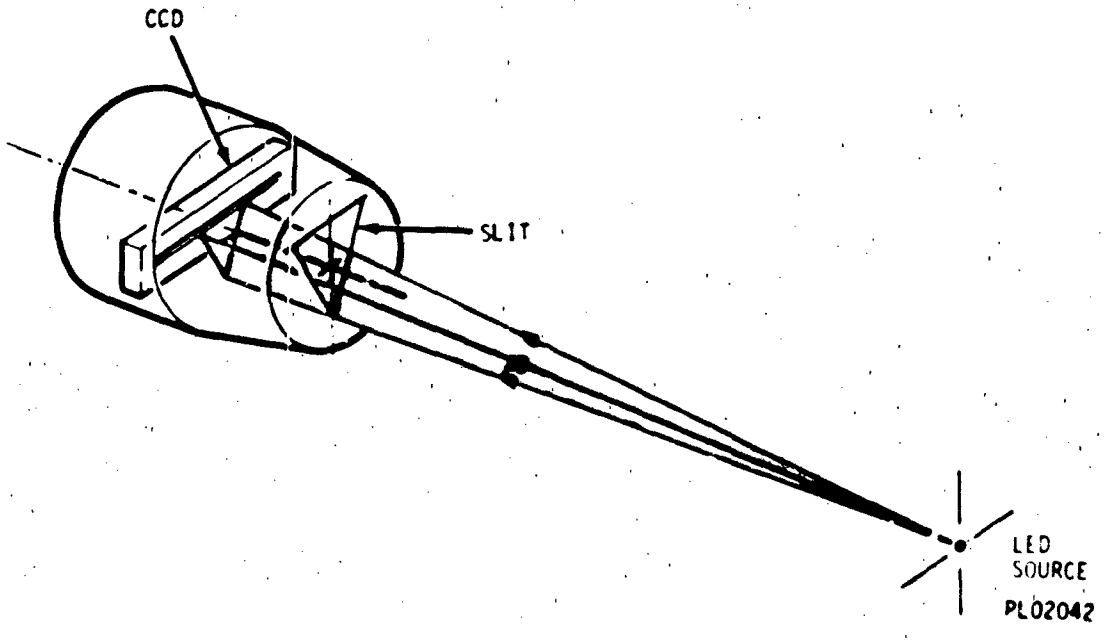

Figure 25. Schematic of V-Slit Camera.

data, in the form of two binary numbers per LED, are then transferred via the interface circuit to the system computer which performs the line-of-sight computation. With a modern 16-bit microprocessor, an iteration rate of 30 to 50 Hz is possible. Although a single camera provides sufficient information to give helmet orientation in roll, pitch, and yaw, a second camera and another set of LEDs are necessary to cover all the possible head positions.

This helmet-position sensing system is accurate to about 0.5 degree in most installations. This is more than adequate in helmet aiming systems where the pilot's ability to visually track a target is limited. The optical distortion caused by the canopy, compounded by the buffeting that occurs during high-speed flight, can induce errors of as much as 2 degrees.

This system will probably never attain the accuracy required in simulator applications. However, with further development, it could match the performance of System A. The main advantages of the System B are its insensitivity to noise and its ease of installation.

5.4 Mechanical Helmet-Position Sensing System. The design and analysis of a mechanical helmet-position sensing system developed for the breadboard FOHMD is described below. Although unacceptable for the combat mission trainer due to the mechanical drag and limited helmet freedom of motion, this system served a twofold purpose. It provided a means of establishing a firm set of performance criteria for the more complex, noncontact helmet-position sensing system. It also permitted a rigorous evaluation of the visor display early in the development project.

The mechanical system is basically a two-bar linkage. One bar is connected to the cockpit through joint 3, which has one degree of freedom. The second bar is coupled to the helmet via joint 1 and to the first bar via joint 2. Joints 1 and 2 have three and two degrees of freedom, respectively. Figure 26 gives a schematic representation of the mechanical helmet-position sensing system, which shows the fixed and movable coordinate systems.

The analysis that follows relates the general displacement of the helmet to the six measurable angles of the linkage.

5.4.1 Translation Measurement. The translation of the helmet is defined by the vector joining point A with the origin of the fixed coordinate system. This vector, denoted by V_{OA}, is the resultant of vectors V_{OC}, V_{CB}, and V_{BA}.

V_{OC} is a vector constant used to relocate the origin of the fixed coordinate system to the nominal helmet position.

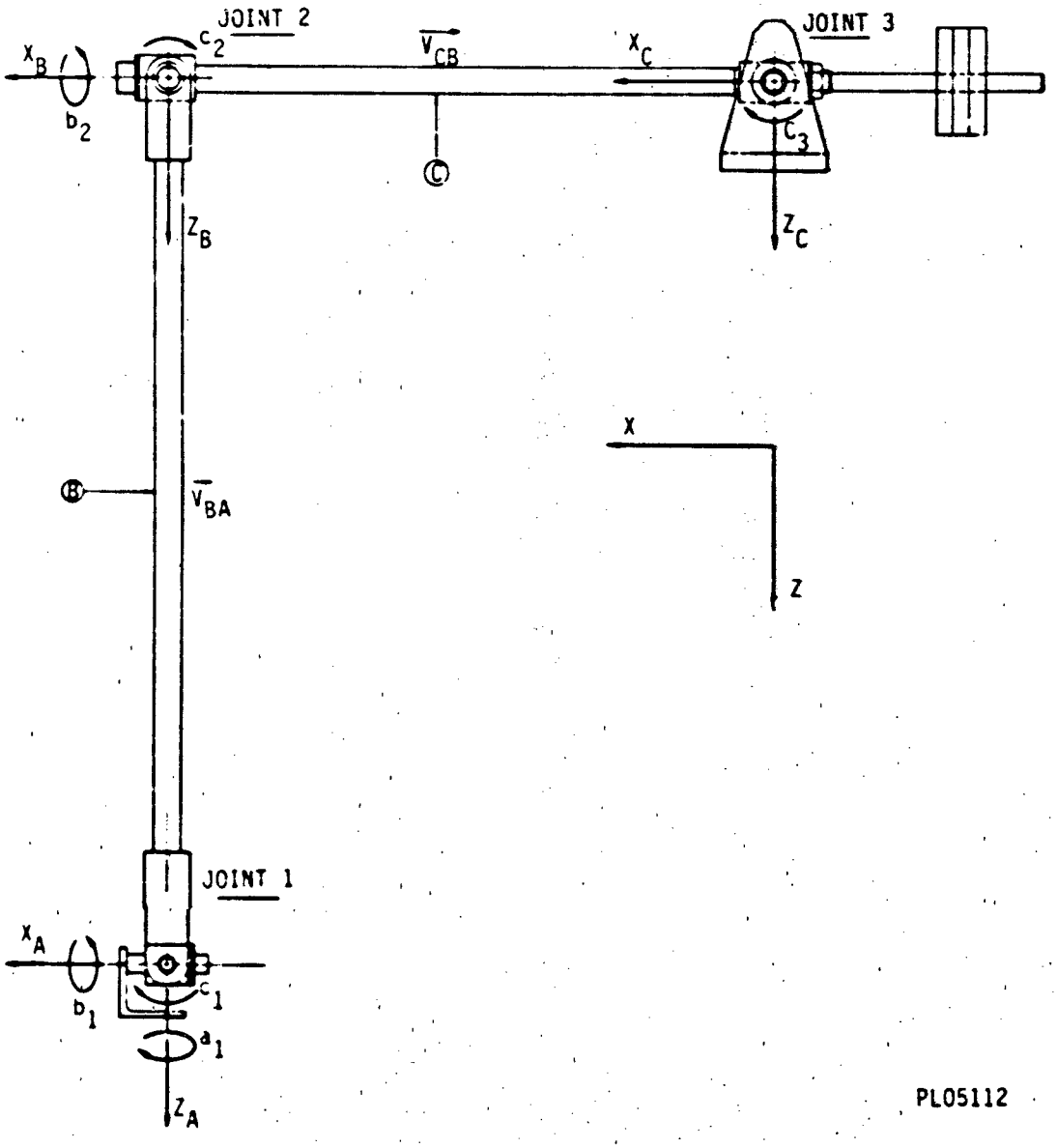

Figure 26. Mechanical Helmet-Position Sensing System Schematic Representation.

5.4.1 Translation Measurement (Cont'd)

$$\bar{V}_{OC} = \begin{bmatrix} -17.25 \\ 0. \\ -25. \end{bmatrix}^T \begin{bmatrix} \bar{i} \\ \bar{j} \\ \bar{k} \end{bmatrix} \qquad \text{(EQ 1)}$$

$\bar{V}_{OC}$ can be adjusted to suit the installation.

$\bar{V}_{CB}$ is the vector representing element C of the linkage. Since joint 3 has only one degree of freedom, element C is constrained to move in the X-Z plane. A single angle, c_3, defines the position of element C. V_{CB}, which is of length 17.25 inches (0.43815m), is given by:

$$\bar{V}_{CB} = (17.25) \begin{bmatrix} \cos(c_3) \\ 0. \\ -\sin(c_3) \end{bmatrix}^T \begin{bmatrix} \bar{i} \\ \bar{j} \\ \bar{k} \end{bmatrix} \qquad \text{(EQ 2)}$$

$\bar{V}_{BA}$ is the vector representing element B of the linkage. Joint 2 has two degrees of freedom; hence, two angles, b_2 and c_2, are required to define the position of element B with respect to element C. The orthogonal axes fixed to element C are denoted by X_C, Y_C, Z_C. As shown in Figure 27, a right-handed rotation about X_C in the amount b_2 defines Y'_C and Z'_C. With respect to these axes, vector V_{BA} can be expressed as:

$$\bar{V}_{BA} = (25.) \begin{bmatrix} \sin(c_2) \\ 0. \\ -\cos(c_2) \end{bmatrix}^T \begin{bmatrix} \bar{i}'_C \\ \bar{j}'_C \\ \bar{k}'_C \end{bmatrix} \qquad \text{(EQ 3)}$$

The unit vectors $\bar{i}'_C$, $\bar{j}'_C$, $\bar{k}'_C$ can be written in terms of $\bar{i}_C$, $\bar{j}_C$, $\bar{k}_C$ as follows:

$$\bar{i}'_C = (1.)i_C + (0.)j_C + (0.)k_C$$

$$\bar{j}'_C = (0.)i_C + \cos(b_2)j_C + \sin(b_2)k_C$$

$$\bar{k}'_C = (0.)i_C - \sin(b_2)j_C + \cos(b_2)k_C$$

$$\begin{bmatrix} \bar{i}' \\ \bar{j}' \\ \bar{k}' \end{bmatrix} = \begin{bmatrix} 1. & 0. & 0. \\ 0. & \cos(b_2) & \sin(b_2) \\ 0. & -\sin(b_2) & \cos(b_2) \end{bmatrix} \begin{bmatrix} \bar{i} \\ \bar{j} \\ \bar{k} \end{bmatrix} \qquad \text{(EQ 4)}$$

5.4.1 Translation Measurement (Cont'd)

The components of vector $\bar{V}_{BA}$ with respect to the X_C , Y_C , Z_C coordinate system can be found by combining equations 3 and 4:

$$\bar{V}_{BA} = (25.) \begin{bmatrix} \sin(c_2) \\ 0. \\ -\cos(c_2) \end{bmatrix}^T \begin{bmatrix} 1. & 0. & 0. \\ 0. & \cos(b2) & \sin(b2) \\ 0. & -\sin(b_2) & \cos(b_2) \end{bmatrix} \begin{bmatrix} \bar{i}_C \\ \bar{j}C \\ \bar{k}_C \end{bmatrix}$$

$$\bar{V}_{BA} = (25.) \begin{bmatrix} \sin(c_2) \\ -\cos(c_2)\sin(b_2) \\ \cos(c_2)\cos(b_2) \end{bmatrix}^T \begin{bmatrix} \bar{i}'_C \\ \bar{j}'_C \\ k'_C \end{bmatrix} \qquad \text{(EQ 5)}$$

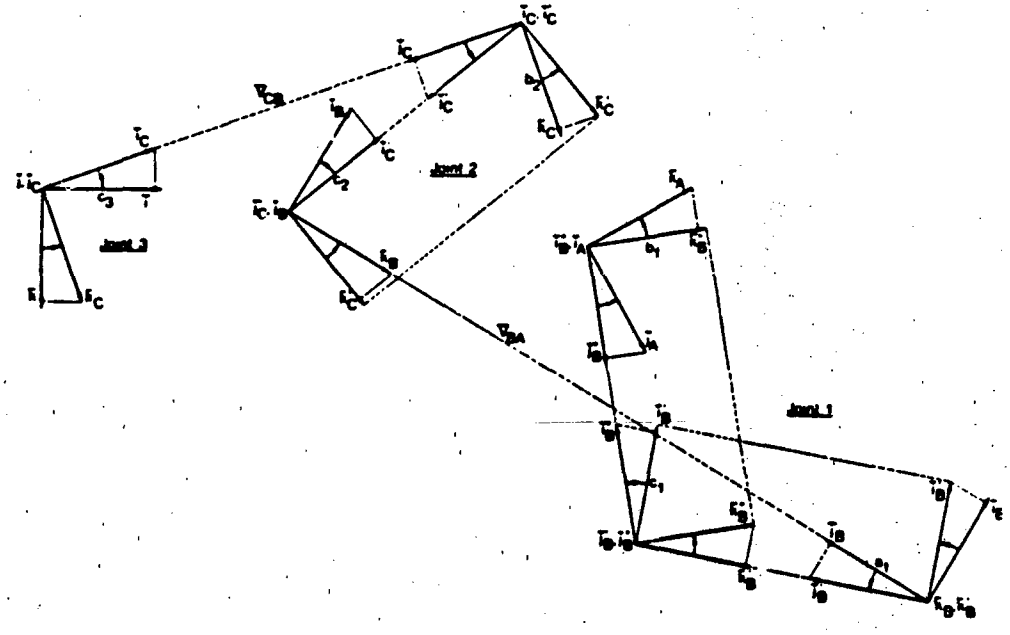

PL05113

Figure 27. Schematic Representation of Coordinate Transformations at Joints 1, 2 and 3.

5.4.1 Translation Measurement (Cont'd)

An additional transformation matrix is needed to carry vector $\bar{V}_{BA}$ into the fixed-cockpit coordinate system. This matrix, denoted by [C], relates the orthogonal unit vectors of element C to those of the fixed coordinate system; that is:

$$\bar{i}_C = \cos(c_3)i + (0.)j - \sin(c_3)\bar{k}$$

$$\bar{j}_C = (0.)i + (1.)j + (0.)\bar{k}$$

$$\bar{k}_C = \sin(c_3)i + (0.)j + \cos(c_3)\bar{k}$$

$$\begin{bmatrix} \bar{i}_C \\ \bar{j}_C \\ \bar{k}_C \end{bmatrix} = \begin{bmatrix} \cos(c_3) & 0. & -\sin(c_3) \\ 0. & 1. & 0. \\ \sin(c_3) & 0. & \cos(c_3 \end{bmatrix} \begin{bmatrix} \bar{i} \\ \bar{j} \\ \bar{k} \end{bmatrix} \qquad \text{(EQ 6)}$$

By combining equations 5 and 6, vector $\bar{V}_{BA}$ can be written in terms of the fixed unit vectors i, j, k.

$$\bar{V}_{BA} = (25.) \begin{bmatrix} \sin(c_2) \\ -\cos(c_2)\sin(b_2) \\ \cos(c_2)\cos(b_2) \end{bmatrix}^T \begin{bmatrix} \cos(c_3) & 0. & -\sin(c_3) \\ 0. & 1. & 0 \\ \sin(c_3) & 0. & \cos(c_3) \end{bmatrix} \begin{bmatrix} \bar{i} \\ \bar{j} \\ \bar{k} \end{bmatrix}$$

$$\bar{V}_{BA} = (25.) \begin{bmatrix} \sin(c_2)\cos(c_3) + \cos(c_2)\cos(b_2)\sin(c_3) \\ -\cos(c_2)\sin(b_2) \\ -\sin(c_2)\cos(c_3) + \cos(c_2)\cos(b_2)\cos(c_3) \end{bmatrix}^T \begin{bmatrix} \bar{i} \\ \bar{j} \\ \bar{k} \end{bmatrix} \qquad \text{(EQ 7)}$$

$\bar{V}_{OA}$, the vector defining the X, Y, Z position of the pilot's helmet is defined by:

$$\bar{V}_{OA} = \bar{V}_{OC} = \bar{V}_{CB}\ \bar{V}_{BA} \qquad \text{(EQ 8)}$$

where $\bar{V}_{OC}$, $\bar{V}_{CB}$, and $\bar{V}_{BA}$ are defined by equations 1, 2, and 7, respectively.

5.4.2 Rotation Measurement. In paragraph 5.4.1, the origin of the helmet coordinate system was located within the cockpit. Since a rigid body with one point fixed has three degrees of freedom, three additional independent rotations are needed to describe the general displacement of the helmet. These rotations are defined by the Euler angles. The Euler angles can be obtained from the matrix of direction cosines [T] which relates the helmet coordinate system to the fixed-cockpit coordinate system.

$$[T] = [A][B][C] \qquad \text{(EQ 9)}$$

A, B, and C are the matrixes of direction cosines relating adjacent coordinate systems. For example, matrix C relates the orthogonal unit vectors of element C ($\bar{i}_C$, $\bar{j}_C$, $\bar{k}_C$) to those of the fixed-cockpit coordinate system.

$$\begin{bmatrix} \bar{i}_A \\ \bar{j}_A \\ \bar{k}_A \end{bmatrix} = [A] \begin{bmatrix} \bar{i}_B \\ \bar{j}_B \\ \bar{k}_B \end{bmatrix}$$

$$\begin{bmatrix} \bar{i}_B \\ \bar{j}_B \\ \bar{k}_B \end{bmatrix} = [B] \begin{bmatrix} \bar{i}_C \\ \bar{j}_C \\ \bar{k}_C \end{bmatrix}$$

$$\begin{bmatrix} \bar{i}_C \\ \bar{j}_C \\ \bar{k}_C \end{bmatrix} = [C] \begin{bmatrix} \bar{i} \\ \bar{j} \\ \bar{k} \end{bmatrix} \qquad \text{(EQ 10)}$$

Matrix C appears in the derivation of vector $\bar{V}_{BA}$ and is given by equation 6.

$$[C] = \begin{bmatrix} \cos(c_3) & 0. & -\sin(c_3) \\ 0. & 1. & 0. \\ \sin(c_3) & 0. & \cos(c_3) \end{bmatrix} \qquad \text{(EQ 11)}$$

5.4.2 Rotation Measurement (Cont'd)

Figure 27 graphically illustrates the coordinate transformations at joint 2. Since joint 2 has two degrees of freedom, two angles are required to define the orthogonal unit vectors of element B in terms of those on element C. A right-handed rotation about X_C in the amount b_2 defines Y'_C and Z'_C. With respect to these axes, the orthogonal unit vectors of element B can be expressed as:

$$\bar{i}_B = \cos(c_2)\bar{i}'_C + (0.)\bar{j}'_C - \sin(c_2)\bar{k}'_C$$

$$\bar{j}_B = (0.)\bar{i}'_C + (1.)\bar{j}'_C + (0.)\bar{k}'_C$$

$$\bar{k}_B = \sin(c_2)\bar{i}'_C + (0.)\bar{j}'_C + \cos(c_2)\bar{k}'_C$$

$$\begin{bmatrix} \bar{i}_B \\ \bar{j}_B \\ \bar{k}_B \end{bmatrix} = \begin{bmatrix} \cos(c_2) & 0. & \sin(c_2) \\ 0. & 1. & 0. \\ \sin(c_2) & 0. & \cos(c_2) \end{bmatrix} \begin{bmatrix} \bar{i}'_C \\ \bar{j}'_C \\ \bar{k}'_C \end{bmatrix} \quad \text{(EQ 12)}$$

Equation 4 relates the unit vectors $\bar{i}'_C$, $\bar{j}'_C$, $\bar{k}'_C$ to those of element C.

$$\begin{bmatrix} \bar{i}_C \\ \bar{j}_C \\ \bar{k}_C \end{bmatrix} = \begin{bmatrix} 1. & 0. & 0. \\ 0. & \cos(b_2) & \sin(b_2) \\ 0. & \sin(b_2) & \cos(c_2) \end{bmatrix} \begin{bmatrix} \bar{i}_C \\ \bar{j}_C \\ \bar{k}_C \end{bmatrix} \quad \text{(EQ 13)}$$

Matrix B , the matrix relating the orthogonal unit vectors on element B to those of element C, can be found by substituting equation 13 into equation 12.

$$[B] = \begin{bmatrix} \cos(c_2) & 0. & -\sin(c_2) \\ 0. & 1. & 0 \\ \sin(c_2) & 0. & \cos(c_2) \end{bmatrix} \begin{bmatrix} 1. & 0. & 0. \\ 0. & \cos(b_2) & \sin(b_2) \\ 0. & -\sin(b_2) & \cos(b_2) \end{bmatrix}$$

$$[B] = \begin{bmatrix} \cos(c_2) & \sin(c_2)\sin(b_2) & -\sin(c_2)\cos(b_2) \\ 0. & \cos(b_2) & \sin(b_2) \\ \sin(c_2) & -\cos(c_2)\sin(b_2) & \cos(c_2)\cos(b_2) \end{bmatrix} \quad \text{(EQ 14)}$$

5.4.2 Rotation Measurement (Cont'd)

Matrix [A] relates the helmet coordinate system to the orthogonal unit vectors on element B. Since joint 1 has three degrees of freedom, matrix [A] is a function of three angles. As shown in Figure 27, a right-handed rotation about Z_B in the amount a_1 defines X'_B and Y'_B. A second rotation about Y'_B in the amount c_1 defines Z''_B and X''_B. A final rotation about X''_B in the amount b_1 yields the helmet coordinate axes X_A, Y_A, Z_A.

$$\bar{i}_A = (1.)\bar{i}''_B + (0.)\bar{j}''_B + (0.)\bar{k}''_B$$

$$\bar{j}_A = (0.)\bar{i}''_B + \cos(b_1)\bar{j}''_B + \sin(b_1)\bar{k}''_B$$

$$\bar{k}_A = (0.)\bar{i}''_B - \sin(b_1)\bar{j}''_B + \cos(b_1)\bar{k}''_B$$

$$\begin{bmatrix} \bar{i}_A \\ \bar{j}_A \\ \bar{k}_A \end{bmatrix} = \begin{bmatrix} 1. & 0. & 0. \\ 0. & \cos(b_1) & \sin(b_1) \\ 0. & \sin(b_1) & \cos(b_1) \end{bmatrix} \begin{bmatrix} \bar{i}''_B \\ \bar{j}''_B \\ \bar{k}''_B \end{bmatrix} \qquad \text{(EQ 15)}$$

$$\bar{i}''_B = \cos(c_1)\bar{i}'_B + (0.)\bar{j}'_B - \sin(c_1)\bar{k}'_B$$

$$\bar{j}''_B = (0.)\bar{i}'_B + (1.)\bar{j}'_B + (0.)\bar{k}'_B$$

$$\bar{k}''_B = \sin(c_1)\bar{i}'_B + (0.)\bar{j}'_B + \cos(c_1)\bar{k}'_B$$

$$\begin{bmatrix} \bar{i}''_B \\ \bar{j}''_B \\ \bar{k}''_B \end{bmatrix} = \begin{bmatrix} \cos(c_2) & 0. & -\sin(c_1) \\ 0. & 1. & 0. \\ \sin(c_1) & 0. & -\cos(c_1) \end{bmatrix} \begin{bmatrix} \bar{i}'_B \\ \bar{j}'_B \\ \bar{k}'_B \end{bmatrix} \qquad \text{(EQ 16)}$$

$$\bar{i}'_B = \cos(a_1)\bar{i}_B + \sin(a_1)\bar{j}_B + (0.)\bar{k}_B$$

$$\bar{j}'_B = -\sin(a_1)\bar{i}_B + \cos(a_1)\bar{j}_B + (0.)\bar{k}_B$$

$$\bar{k}'_B = (0.)\bar{i}_B + (0.)\bar{j}_B + (0.)\bar{k}_B$$

$$\begin{bmatrix} \bar{i}'_B \\ \bar{j}'_B \\ \bar{k}'_B \end{bmatrix} = \begin{bmatrix} \cos(a_1) & \sin(a_1) & 0. \\ -\sin(a_1) & \cos(a_1) & 0. \\ 0 & 0 & 1. \end{bmatrix} \begin{bmatrix} \bar{i}_B \\ \bar{j}_B \\ \bar{k}_B \end{bmatrix} \qquad \text{(EQ 17)}$$

5.4.2 Rotation Measurement (Cont'd)

Matrix [A], the matrix relating the orthogonal unit vectors on the helmet to those of element B, can be found by combining equations 14, 15, and 16.

$$[A] = \begin{bmatrix} 1. & 0. & 0. \\ 0. & \cos(b_1) & \sin(b_1) \\ 0. & -\sin(b_1) & \cos(b_1) \end{bmatrix} \begin{bmatrix} \cos(c_1) & 0. & -\sin(c_1) \\ 0. & 1. & 0. \\ \sin(c_1) & 0. & \cos(c_1) \end{bmatrix} \begin{bmatrix} \cos(a_1) & \sin(a_1) & 0. \\ -\sin(a_1) & \cos(a_1) & 0. \\ 0. & 0. & 1. \end{bmatrix}$$

$$A_{11} = \cos(c_1)\cos(a_1)$$

$$A_{12} = \cos(c_1)\sin(a_1)$$

$$A_{13} = -\sin(c_1)$$

$$A_{21} = \sin(b_1)\sin(c_1)\cos(a_1) - \cos(b_1)\sin(a_1)$$

$$A_{22} = \sin(b_1)\sin(c_1)\sin(a_1) + \cos(b_1)\cos(a_1)$$

$$A_{23} = \sin(b_1)\cos(c_1)$$

$$A_{31} = \cos(b_1)\sin(c_1)\cos(a_1) + \sin(b_1)\sin(a_1)$$

$$A_{32} = \cos(b_1)\sin(c_1)\sin(a_1) - \sin(b_1)\cos(a_1)$$

$$A_{33} = \cos(b_1)\cos(c_1) \qquad \text{(EQ 18)}$$

Since Euler angles are defined by the same sequence of rotations as followed for joint 1, equation 18 is also the matrix of direction cosines expressed in terms of Euler angles. The absolute rotation of the helmet (i.e., with respect to the cockpit coordinate system) can be determined by equating matrix [T] with equation 18 and solving for angles a*, b*, c*. The asterisk is used to denote quantities that are measured with respect to the fixed cockpit coordinate system.

$$a^* = \text{ATAN2}(T_{12}, T_{11})$$

$$b^* = \text{ATAN2}(T_{23}, T_{33})$$

$$c^* = \text{ASIN}(-T_{13}) \qquad \text{(EQ 19)}$$

Angles a*, b*, c* are more commonly referred to as yaw, roll, and pitch respectively.

5.4.3 Data Acquisition and Processing. Data processing tasks for the mechanical helmet position sensing system are accomplished by an INTEL iSBC 86/12 single-board computer. This computer's capabilities are summarized following:

(a)	CPU:	8086
(b)	CPU SPEED:	5 MHz
(c)	RAM (BASE BOARD):	32K
(d)	RAM (W/FULL EXPANSION):	64K
(e)	EPROM:	16K
(f)	EPROM (W/FULL EXPANSION):	32K
(g)	SERIAL I/O:	1
(h)	PARALLEL I/O LINES:	24
(j)	TIMERS:	2
(k)	INTERRUPTS:	8.

To determine the helmet position and orientation, a number of matrix multiplications and trigonometric functions must be evaluated. This necessitates the use of the 8087 numeric processor. The 8087 has the ability to perform the highspeed floating-point mathematics required in complex control algorithms.

Helmet position and orientation data are transferred from the INTEL 86/12 to the SEL 32/55 host computer through a MULTIBUS-SELBUS controller (MBSEL). The MBSEL board is an intelligent DMA controller which communicates with the SELBUS via a high-speed data (HSD) interface board. In this application, the HSD is in external mode and the 8086 is in control of the transfers. During initialization, the 8086 creates a transfer block consisting of four 16-bit words for each 32-bit quantity to be transferred. The first two words specify the target address in SEL memory and the data direction. The third and fourth words contain the data to be input to or output from the SEL. The 8086 initiates the data transfer by writing the starting address of the transfer block and the word count into the MBSEL registers. Because of the 86/12 board's dual-port RAM, the MBSEL can access the transfer block directly via the MULTIBUS. Data transfers are transparent to both the SEL and 8086 processors.

Rotational voltage differential transducers (RVDTs) are used to instrument joints 2 and 3, while potentiometers are used on joint 1. The analog signals from these transducers are brought to a BLC 711 analog input board. This board is built around a 12-bit, 50-kHz A/D converter.

The analog signals needed to drive the optical steering mechanisms are provided by a BLC 724 analog output board. The 724 contains four independent 12-bit D/A converters.

The MBSEL board, the two analog I/O boards, and the single-board computer are housed in an iSBC 660 system chassis. This chassis is 7 inches high and mounts in a standard 19-inch rack. It can accommodate up to eight cards. DC power is provided at ±5 and ±12 volts.

The subroutine which calculates the helmet position and orientation from the six measurable angles of the linkage is written in FORTRAN-86. All of the other routines including the MBSEL and analog I/O board drivers, the interrupt handler, and the 86/12 initialization routines, are written in ASSEMBLER-86. The software is compiled, linked, and located using an INTEL Series III microprocessor development system and down-loaded into the target system serially via the iSBC 957 interface and execution package. The final, error-free software resides on four 2732 EPROMs and is executed automatically on RESET.

5.5 Optical Helmet-Position Sensing System. Due to the lack of an "off-the-shelf" noncontact position sensor suitable for use on the FOHMD, it was decided to develop a new system, based on optical techniques. The optical helmet-position sensing system is based on a commercially available position sensor head. This compact device is capable of detecting the position of an infrared LED in two dimensions. The sensor employs a newly developed silicon position-sensitive detector (PSD). The PSD is actually a planar photodiode with very uniform resistive layers formed over both the top and bottom surfaces (see Figure 28). A camera lens is used to focus the infrared light onto the active area of the detector. This results in the generation of electron-hole pairs in the depletion layer directly under the light spot. The electrons migrate to the N-layer where they are channeled between two electrodes. Since the N-layer has a uniform resistivity, the current flowing to a given electrode will depend on its distance from the point of incidence. The same basic principles apply to the P-layer. By processing the current signals with the analog circuitry shown in Figure 29, the X and Y coordinates of the LED image can be determined.

In many respects, the device is superior to conventional noncontact position detectors. CCD cameras and scanning-type image sensors are either not accurate enough because they consist of discrete elements or not fast enough because of the limited scan speed.

With filtering, the resolution of the position sensor head can be as high as 0.02 percent of full scale. The filtering is necessary because of the high-frequency jitter that is normally present. The dynamic performance of the device is impressive: it can be used for vibration measurements at frequencies of up to 50 kHz.

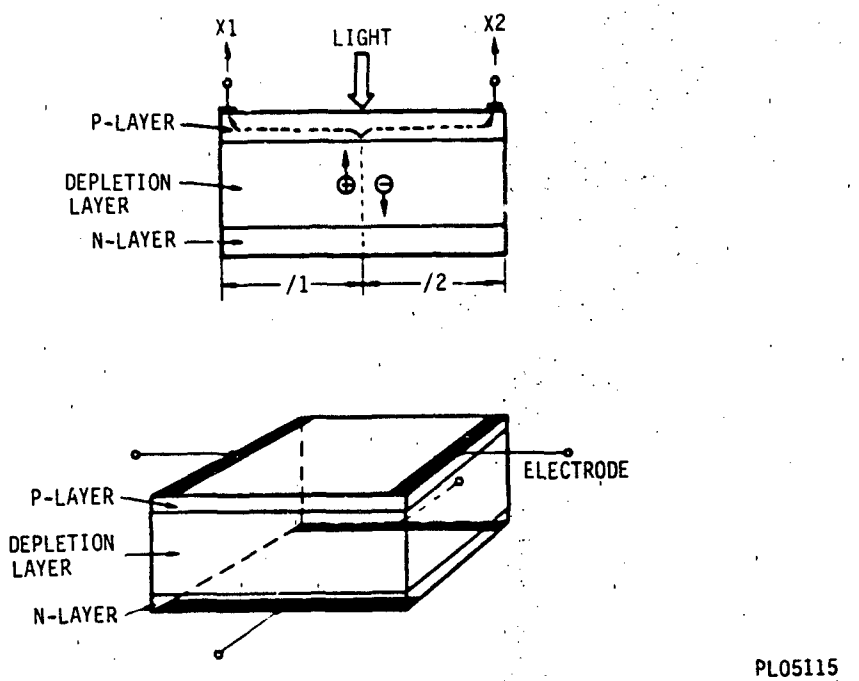

Figure 28. Schematic of Silicon Position-Sensitive Detector.

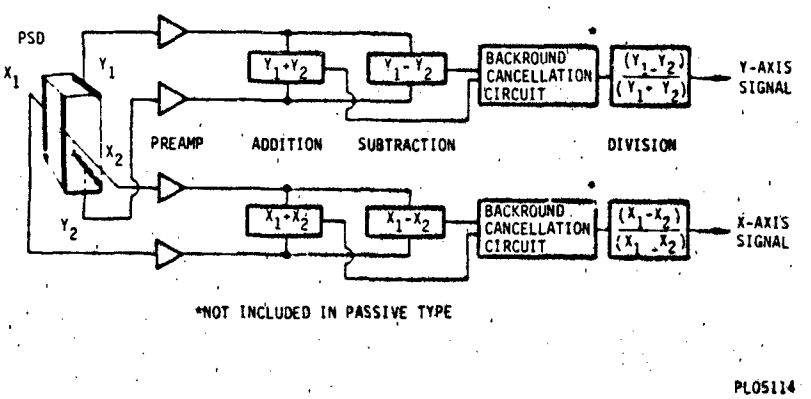

Figure 29. Analog Position Processing Circuit.

5.5 Optical Helmet-Position Sensing System (Cont'd)

The device can be applied to helmet-position sensing in a number of ways. The simplest approach involves two cockpit-mounted position sensor heads directed at a pattern of LEDs on the top of the pilot's helmet. As in System B described previously, the LEDs are flashed on in sequence. The helmet position and orientation are computed from the image coordinates of the LED pattern.

Two sensors viewing the same LED pattern are required to uniquely determine helmet position in six degrees of freedom. The image on the sensitive area of the detector is a two-dimensional perspective projection of an LED moving in three-dimensional space. Consequently, the three-dimensional position of the LED cannot be recovered from its image coordinates. At best, only the direction of the vector between the LED and the sensor can be determined. If the target LED is viewed from two locations, a triangulation scheme can be used to compute the LED position in three dimensions. Therefore, with a minimum of three LEDs and two sensors, the helmet position can be uniquely determined in all six degrees of freedom. The addition of more LEDs results in an overdetermined system of equations which can increase the accuracy of the measurement through the application of least-squares analysis.

Figure 30 is a schematic representation of the laboratory test-stand used in the development of the optical position sensing system. The two position sensor heads are mounted on inclination stages which provide a precisely controlled angular displacement of up to five degrees (see Figure 31). The inclination stages are fixed to movable carriages through a precision angle block. The carriages can be positioned anywhere along the horizontal rail. Their exact position can be determined from the vernier scale located on the guide rail. The vertical distance between the sensors and the helmet can be adjusted by raising or lowering the horizontal rail. The geometric layout of the position sensor heads and helmet is shown in Figure 32.

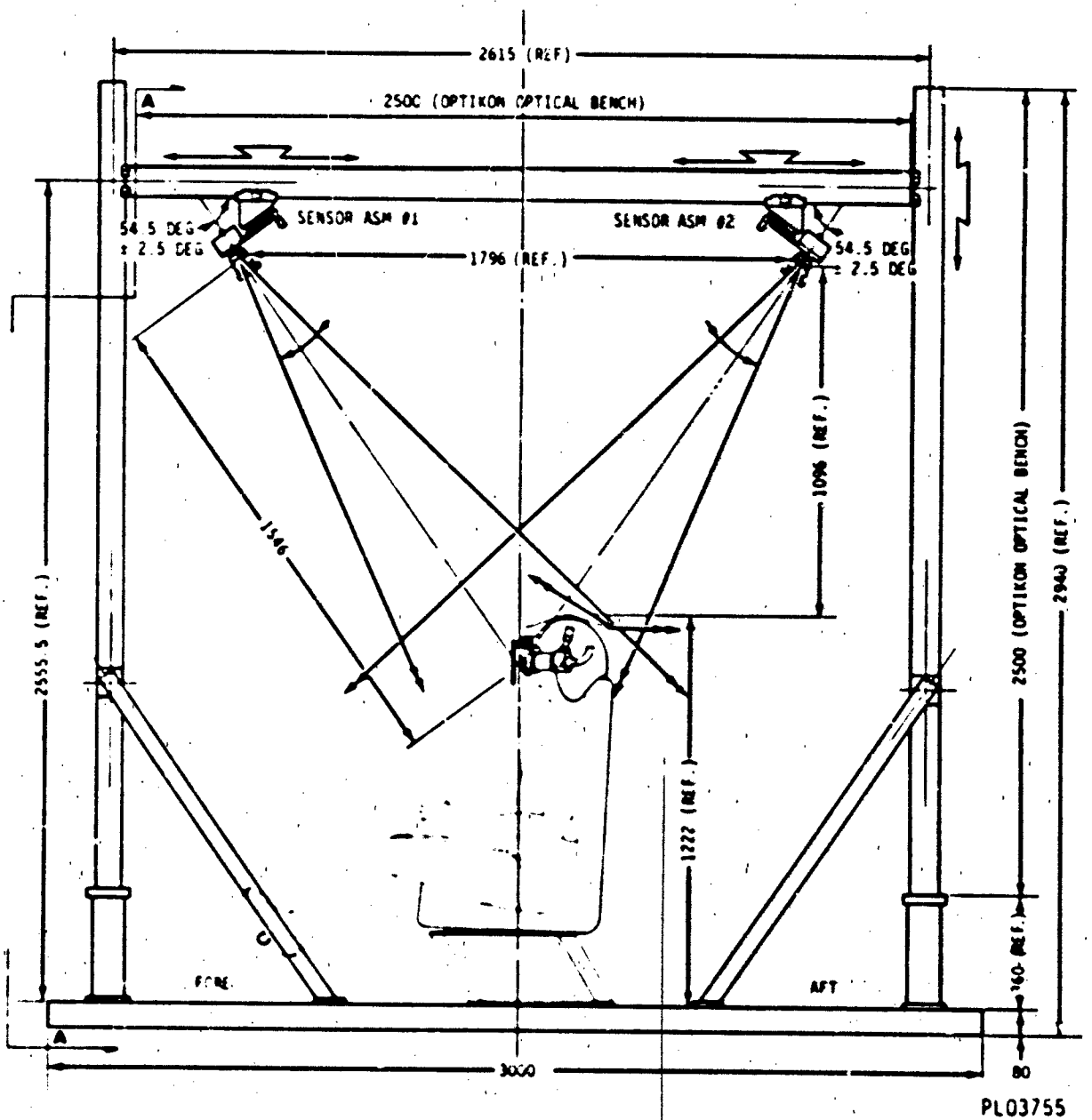

Figure 30. Test-Stand Layout for Optical Helmet-Position Sensing System.

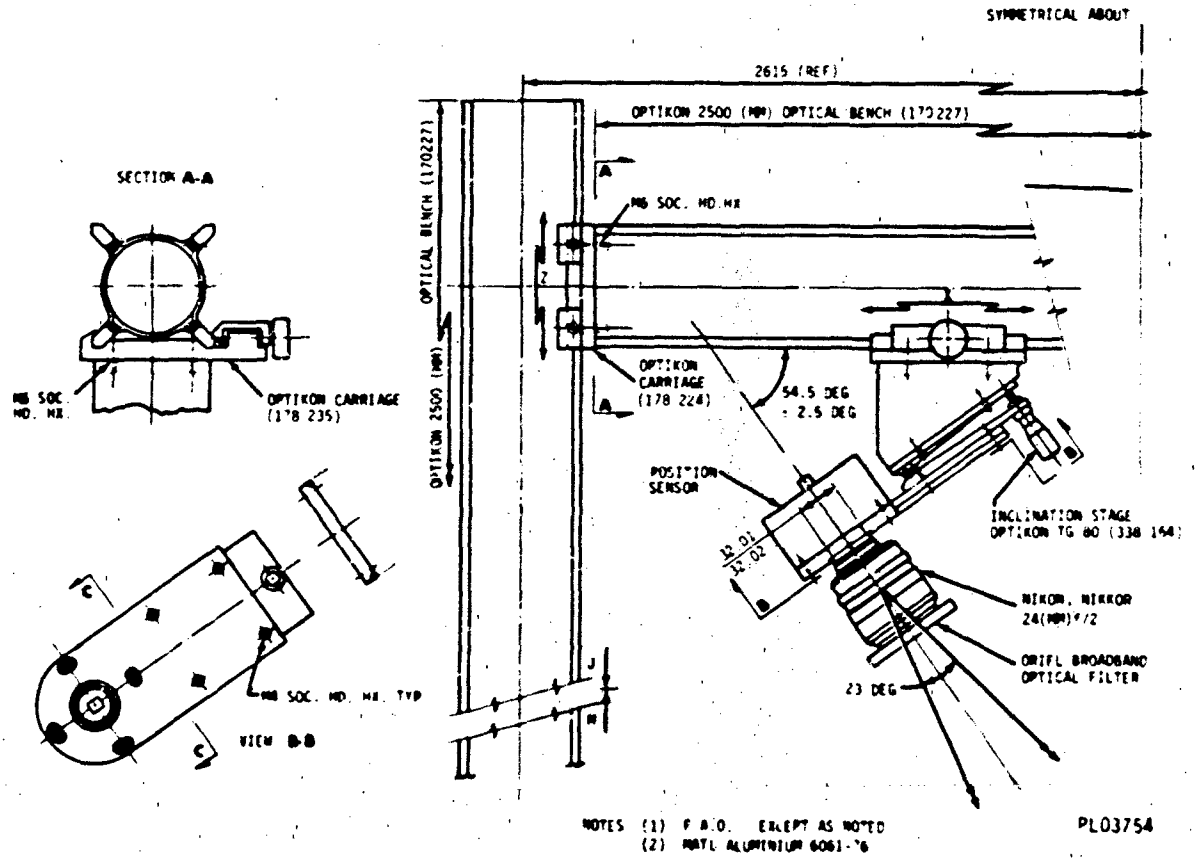

Figure 31. Assembly Detail for Position Sensor Head.

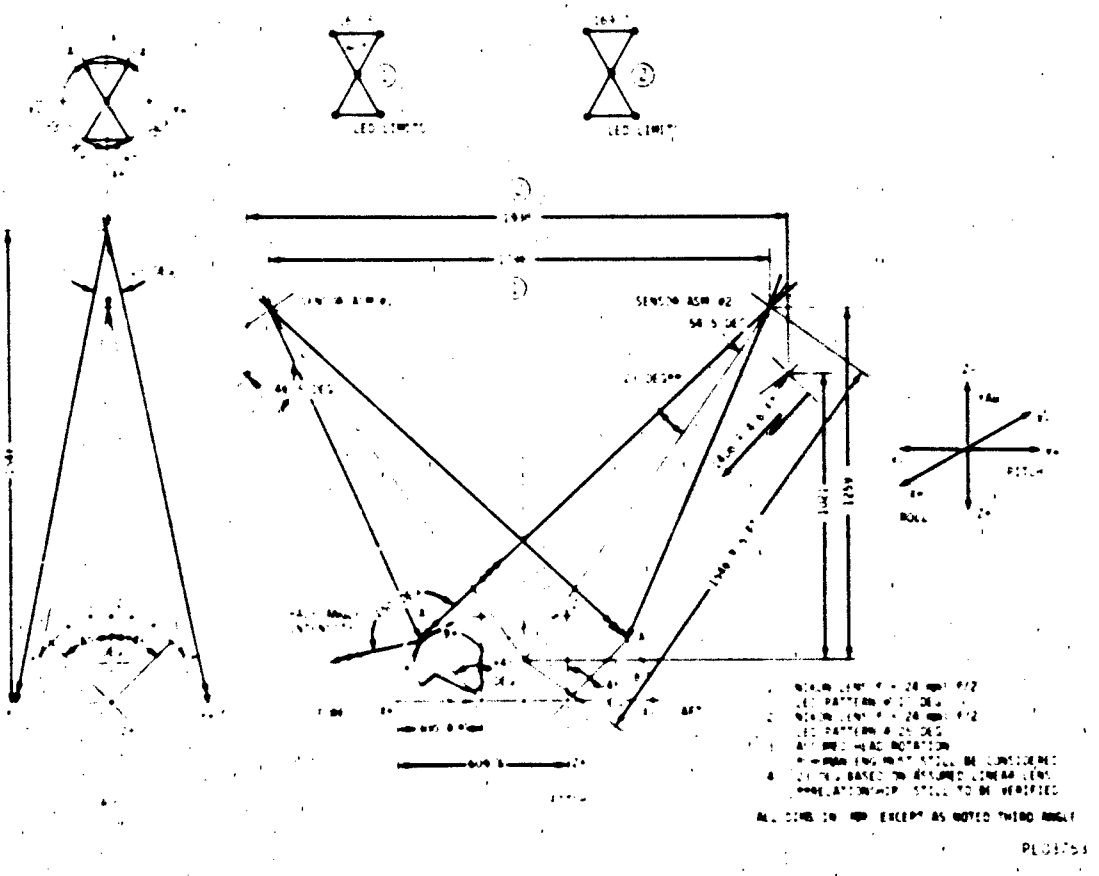

Figure 32. Geometric Layout of Position Sensor Heads and Helmet.

6. OPTICAL STEERING

6.1 Image Stability. One of the major concerns in the early stages of this project was whether or not a stable image could be obtained on a helmet-mounted display.

All computer-generated image systems have an inherent transport delay due to the amount of digital computation required for each displayed image. Consequently, during a head rotation, the displayed image will correspond to the head position existing at an earlier point in time. If no corrective action is taken, the image is displaced in the direction of head motion and only returns to the correct position in space when the head motion returns to zero.

6.2 Optical Steering Concept. The concept for stabilizing the image uses a mechanical device to steer the image in the opposite direction to head motion. A push-pull arrangement of linear motors moved the input of the fiber-optic bundle in the direction corresponding to yaw and pitch. Movements equivalent to ±4 degrees could be obtained with a response time of approximately 10 ms. Figure 33 shows a hypothetical head movement with corresponding image generator motion. The difference between these two motions is the required displayed image motion for obtaining a stable image.

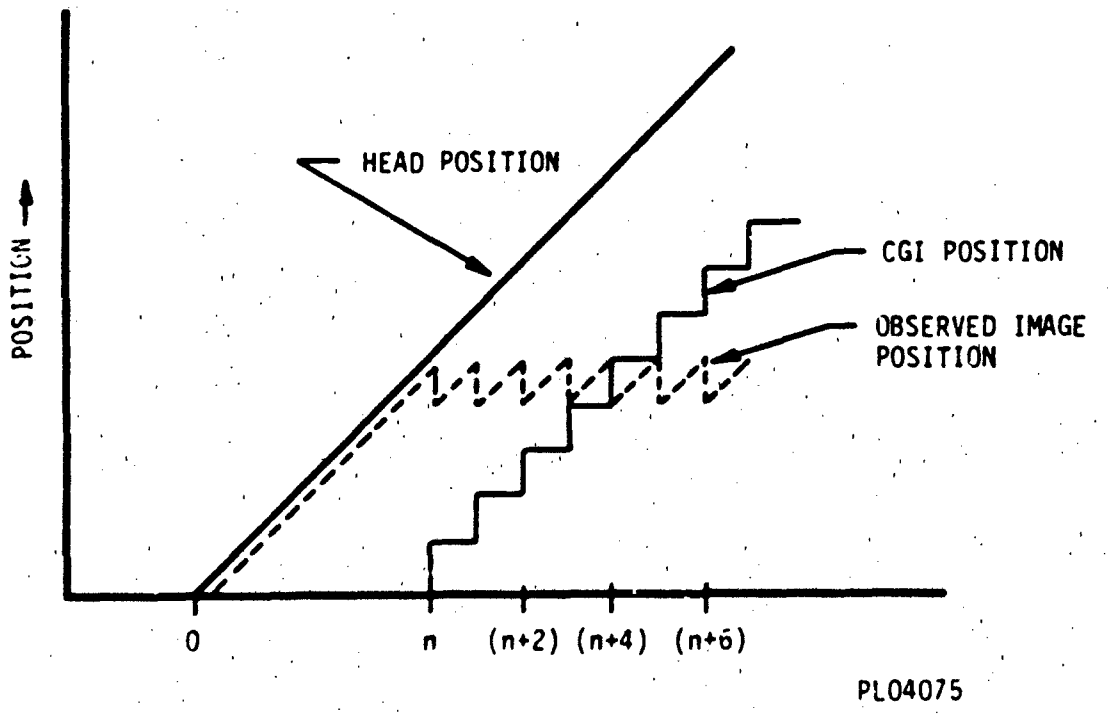

Figure 33. Effect of CGI Transport Delay on Image Stability.

There are some technical difficulties to the addition of the optical steering compensator. First, the compensator itself on a step position input will take a certain time to move to the desired position, as seen on Figure 34.

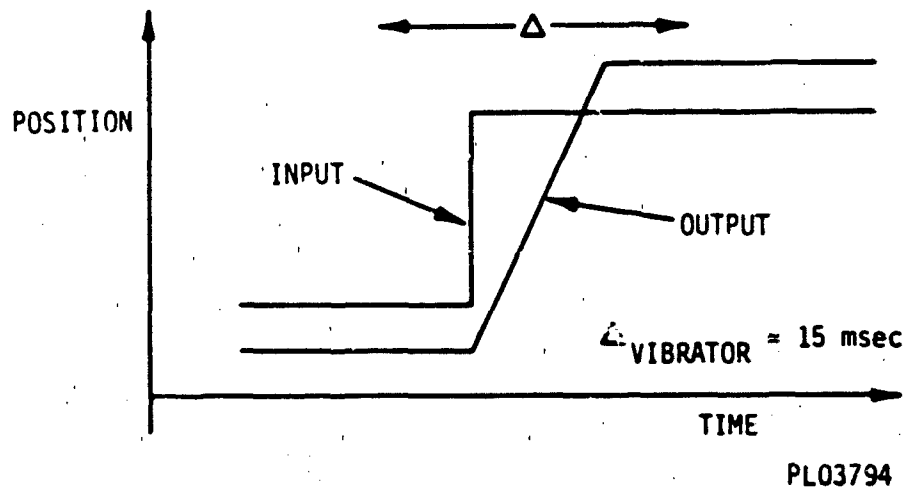

Figure 34. Typical Step Response of Any Mechanical System.

Any noise or small vibrations in the compensator tend to make the image shake and, ultimately, will decrease the resolution of the image.

Any offset in the circuit driving the motors will give an incorrect image on the helmet.

Each of these proolems can be minimized but only to the detriment of the others.

6.3 Design Criteria. In the system, the low-resolution and the high-resolution images are carried through different optical cables. Each eye has its own set of low- and high-resolution cables, making four optical cables. There are, consequently, four compensators. The displacements of optical cable with respect to the image generator are shown in Table 7.

Table 2 GCI Latency Compensator

DESIGN CRITERIA	INNER FIELD OF VIEW (High Resolution)	OUTER FIELD OF VIEW (Low Resolution)
MAXIMUM HEAD ROTATIONAL SPEED	40 deg/sec	40 deg/sec
LATENCY OF CGI COMPUTER	100 msec	100 msec
FIELD OF VIEW	40 deg x 40 deg	80 deg x 80 deg
FIBER CABLE BUNDLE	15 mm x 15 mm	10 mm x 10 mm
TOTAL TRAVEL	± 1.5 mm	± 0.5 mm

1. Two degrees of freedom: yaw and pitch
2. Step response time = 15 msec
   Frequency response = -3 dB at 50 Hz
3. No friction for accurate positioning (to ≈ 0.005 mm)
4. Servo-controlled system with velocity damping.

5.4 Physical Description. The system used to meet these requirements is shown in Figure 35. It consists of four vibrators (linear motors) arranged in a plus configuration. Each vibrator consists of a magnet with a coil around it arranged in very much the same configuration as in a speaker. The prototype actually used four speakers instead of vibrators. The motors are joined together with thin aluminum plates (1/16 inch) to allow for two degrees of freedom at the centerpiece (left and right, and up and down, see Figure 35). The following are main advantages over any other system:

(a) Very little moving mass, therefore allowing a very good response.

(b) No need for any hydraulic power, thus making it very practical and portable.

(c) Very little friction because there are no gears, pulleys, or bearings, thus providing good positioning.

6.4 Physical Description (Cont'd)

(d) The velocity damping may be taken from the induced electromagnetic force (EMF) in the vibrator coil.

(e) The displacement is a linear function of the current through the vibrators.

The optical cable goes through a hole in the bottom plate and is fixed on the centerpiece.

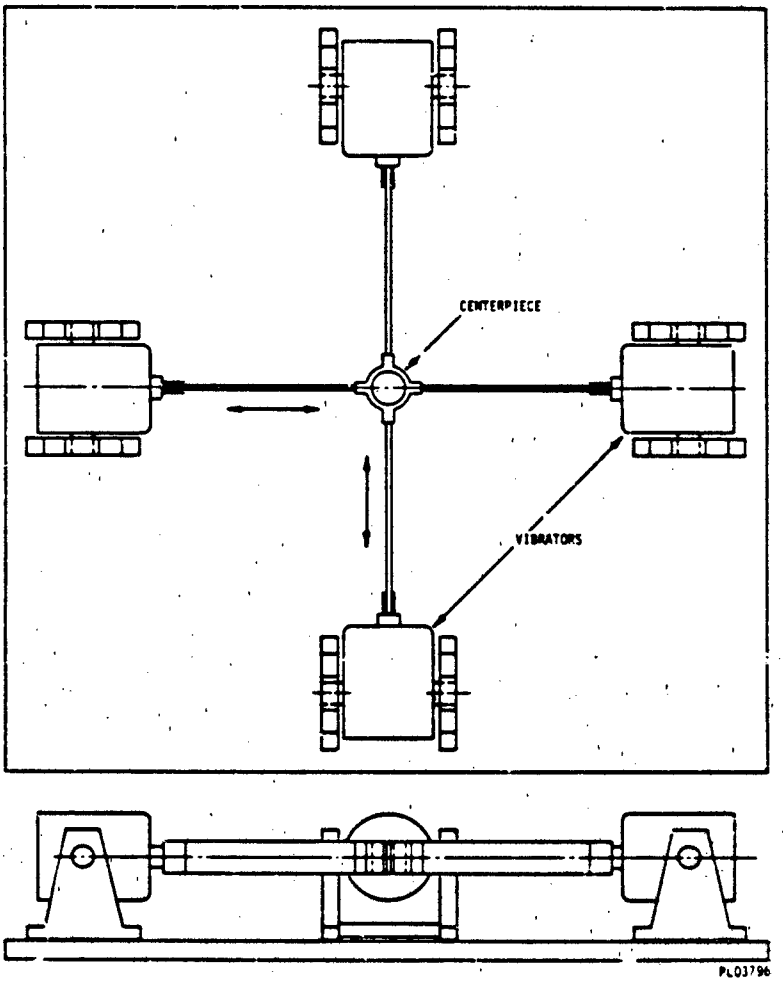

Figure 35. Mechanical Drawing of the Compensator.

6.5 Mathematical Description

6.5.1 Vibrator

6.5.1.1 Displacement vs Current. Figure 36 presents a cross-section of the vibrator.

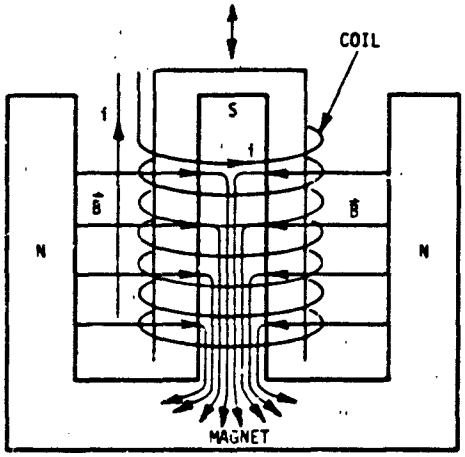

B: magnetic field

dl: element of length of coil

L: total length of coil

k: vibrator spring constant

x: displacement from neutral position

i: current through coil

Figure 36. Vibrator Cross-Section.

The force on the small element of length dl is given by:

$$\overline{dF} = \overline{dl} \times \overline{B} \qquad \text{(EQ 20)}$$

B is assumed uniform and orthogonal to dl so:

$$dF = Bi\ dl \qquad \text{(EQ 21)}$$

Integrating over the whole coil gives:

$$F = iBL \qquad \text{(EQ 22)}$$

The coil is kept centered horizontally and vertically by a spring for which:

$$F_S = kx \qquad \text{(EQ 23)}$$

These two forces are set equal, giving:

$$x = \frac{Bl}{k} i \qquad \text{(EQ 24)}$$

So, the displacement of the centerpiece will be proportional to the current through the vibrators.

6.5.1.2 Self-Inductance. Examine the coil of the vibrators in more detail. It can be represented by a pure resistor and a pure inductor as in Figure 37.

L: Inductance of coil

w: Angular frequency

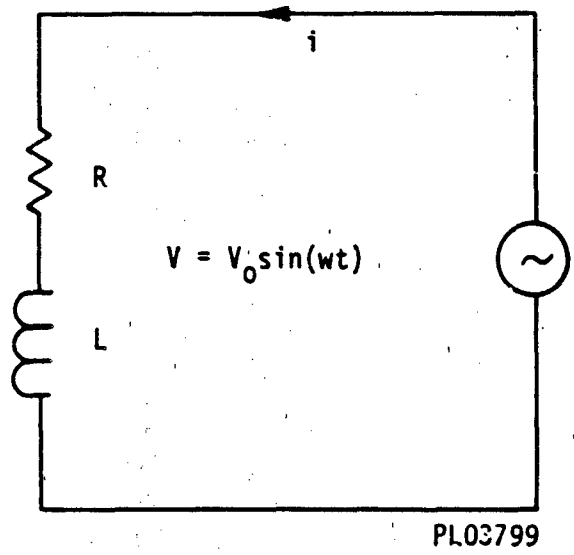

Figure 37. Mathematical Representation of Coil.

The current i will be $\frac{V}{Z}$

Where: $Z = R \quad jwL, \quad j = \quad -1$

giving: $i = \frac{V}{R + jwL}$

It follows that the current will lag the voltage by an angle ϕ

where: $\tan \phi = \frac{wL}{R}$ (EQ 25)

and that the magnitude of the current will be:

$$i = \frac{V}{R^2 + w^2L^2} \quad \text{(EQ 26)}$$

The self-inductance was measured to be very small due to the small number of turns in the coil. It is of the order of 1.0 mHz.

If this value is put into equations 25 and 26 along with w = 2π x 50 Hz (the maximum signal frequency), one gets:

(a) Current lag ≃ 8 deg or 0.5 msec

(b) Time constant = $\frac{L}{R}$ ≃ 0.2 msec

(c) Current magnitude = $\frac{V}{R}$ to 1 part in 5,000.

The effect of self-inductance is so small that it can be ignored.

6.5.1.3 Induced EMF. Looking back at Figure 36, the magnetic flux ζm will change with the position of the coil and, assuming a uniform magnetic field and small displacements, the relation between the two should be linear:

$$\phi m = kx \qquad k = \text{constant} \qquad \text{(EQ 27)}$$

Differentiating with respect to time gives:

$$\frac{d\,\phi m}{dt} = k\,\frac{dx}{dt} = kx \qquad \text{(EQ 28)}$$

From Faraday's law: a change in magentic flux with time through a coil will induce an EMF across the terminals:

$$\varepsilon = \frac{-d\,\phi\,m}{dt} \qquad \text{(EQ 29)}$$

So, equating equations 28 and 29 gives:

$$\varepsilon = -kx \qquad \text{(EQ 30)}$$

The induced EMF is therefore proportional to the velocity of the coil and, therefore, of the optical cable. The induced EMF on the vibrator can be measured from:

$$\varepsilon = V_v - iR_v,$$

V_v = Voltage across the vibrator terminals

R_v = Resistance of vibrator coil (EQ 31)

6.5.2 Control System. The circuit used to control the motion of the vibrators is shown in Figure 38. It has two inputs. The CGI position input is the angular position of the center of the image on the CGI with respect to the straightahead image (i.e., how far from the straight-ahead image is the present CGI image). The second input is the angular position of the head in yaw and pitch). The difference between these two inputs is the amount the

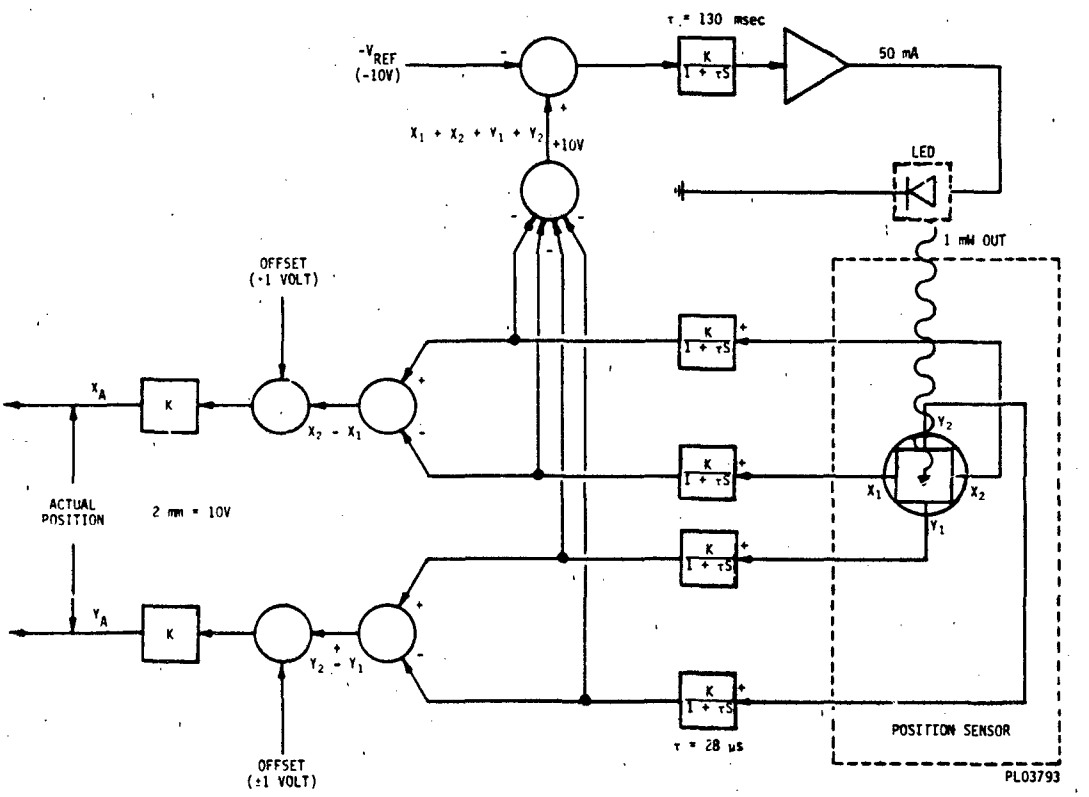

DUAL AXIS POSITION SENSING
CGI LATENCY COMPENSATOR

Figure 38. Control System Block Diagram.

6.5.2 Control System (Cont'd)

compensator has to move. This amount is compared with the amount that the compensator has moved. Any difference will be amplified with a gain K_{LG} to become a force term. It is then added to a velocity damping force term. The resulting force term goes to the servo amplifier to drive the motors to move the optical cable according to equations 24, 25 and 26.

The mechanical analogy to this compensator is shown in Figure 39.

The difference between the compensator position and what it should be will create a force $F = \Delta x k_{LG}$ which will be added by the damping force $F_D = -k_D x_A$ to the force on mass M. M will move until this force equals the spring force $F_s = -k_V x_A$ of the vibrator.

Summarizing, in mathematical form:

$$M \frac{d^2 x_A}{dt^2} = -k_V x_A - k_{LG} (x_A - (x_C - x_H)) - k_D x_A \qquad \text{(EQ 32)}$$

where x_A is taken from equations 30 and 31.

There are two of those circuits, one to drive each axis. There is also a circuit to determine the position of the optical cable. This is shown in Figure 40. It consists of an infrared LED fixed on the moving centerpiece, and of a PIN photodetector fixed on the bottom plate. The LED has a very small cone of radiation (≈4 deg). It is oriented toward the detector to create a spot of infrared light on the detector. The spot will create currents through all four outputs. The sum of all currents is proportional to the total amount of light falling on the surface of the detector. If this amount is kept constant, the following equations apply:

$$X_A = K (I_{X2} - I_{X1}) \qquad \text{(EQ 33)}$$

$$Y_A = K (I_{Y2} - I_{Y1}) \qquad \text{(EQ 34)}$$

where: I_{X1}, I_{X2}, I_{Y1}, I_{Y2} are the currents through the detector terminals as shown in Figure 41.

X_A, Y_A define the actual position of the spot in X and Y.

The detector supplies differential currents through X_1 and X_2 depending on the X position of the spot. Similarly for the Y axis.

Equations 33 and 34 were used and the total amount of light falling on the detector was kept constant by means of a feedback on the current through the LED.

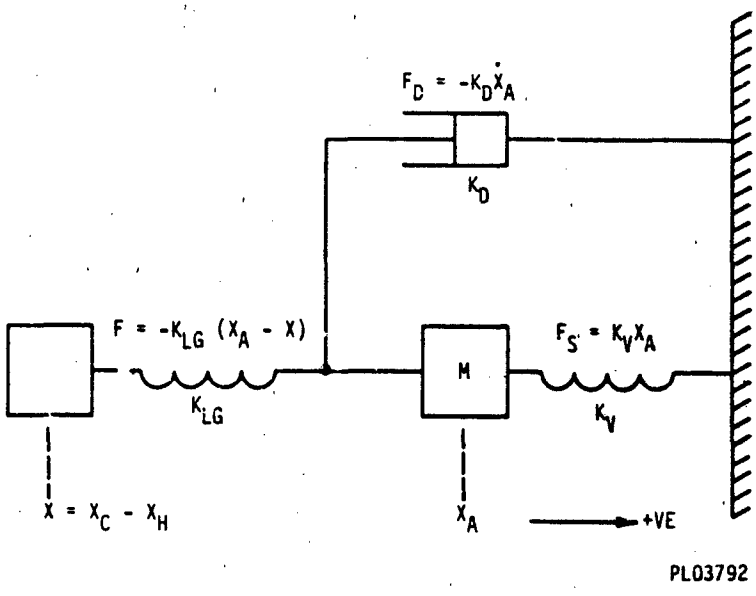

Figure 39. Control System Mechanical Analogy.

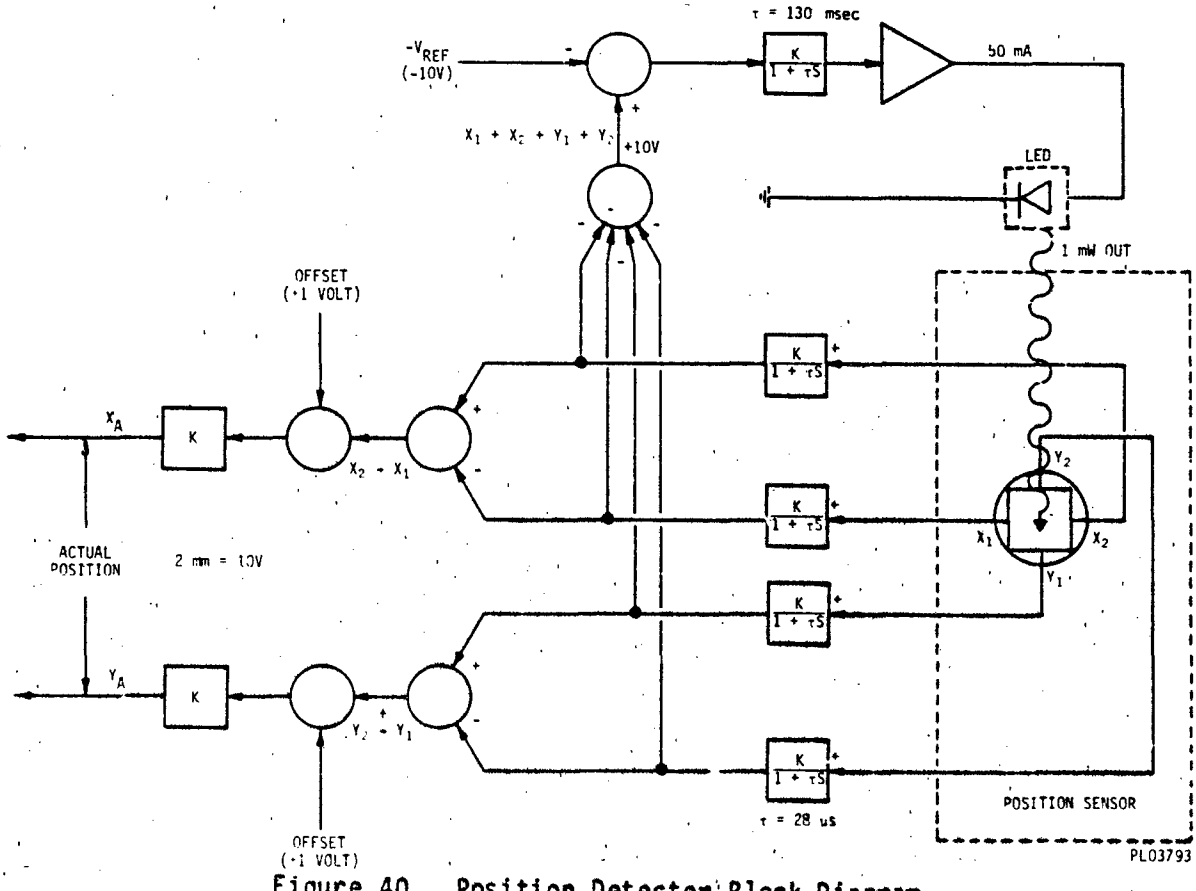

Figure 40. Position Detector Block Diagram.

6.6 Latency Compensation Unit for Breadboard System. There are four optical steering (O/S) tables for low- and high-resolution images on both eyes. The tables are equipped with vibrator motors at the corners which produce up to 102g. Guides and linear bearings on the motor shafts prevent axis-to-axis coupling from damaging the motors. The motors are driven using Inland servo amps which deliver displacements of approximately 1 mm/A. A displacement of -1.5 mm was eventually settled upon.

Positioning of the optical cable was determined using a light detector tracking unit with an LED attached to the centerpiece which links the motor shaft arms. The LED was infrared and the detector was wide spectrum, thus necessitating light shielding for the detector and also for the back face of the LED.

Buffer cards on the O/S table provide amplification of the detector signals before trarsmission to the optical steering card in the control cabinet. The O/S tables are mourted vertically on the light valve modules. The vertical axis proved to be more difficult to tune than the horizontal axis.

The optical steering cards offer test drive and error drive capacity as well as many tuning possibilities. Changing drive theories have made elliptic filters on the card unnecessary, but they are available for future development.

The control cabinet provides +28V power to the O/S servos, ±15V to O/S steering cards, the head tracker, and the accelerometer package. It also houses an Intel chassis for processing head tracker data. Though only four systems (O/S steering cards) are now in use, wiring is provided for six systems in case there is an expansion using eye-tracking. Test points for various drives, positions, and velocities are provided for all six systems.

6.7 Performance. The optical steering basically has a 10- to 12-msec delay to a step input (see Figures 41 to 43). In the field, the delay in the microprocessor software was matched to a measured video display in the digital image generator system.

The error drive thus created clearly stabilized images, and the effect was noticeable if the optical steering was switched in and out. With a video delay of 80 msec, the lag of the O/S itself was not significant.

Nevertheless, in order to create large displacements during the update time, the O/S was obliged to operate at a high gain (50 in its initial stages) and problems arose particularly in situations with little or no head movement where the least-significant bit toggling in the digital-to-analog signal could create 1-degree jumps in the image. The installation of an accelerometer which more accurately predicts the displayed head position (see section 7) clearly improved matters, so that the O/S will not have to function at such a high gain.

6.7 Performance (Cont'd)

Using the mechanical head tracker without using roll and translation in the drive scheme posed problems when the pilot's head was still. What was observed was coupling between rotational pots and translational RVDTs. Since the latter were not included in the drive, an error drive was present as noise in the no-movement position. The optical head tracker should solve this problem, but it must process the data quickly enough that some actual position data are available for drive purposes.

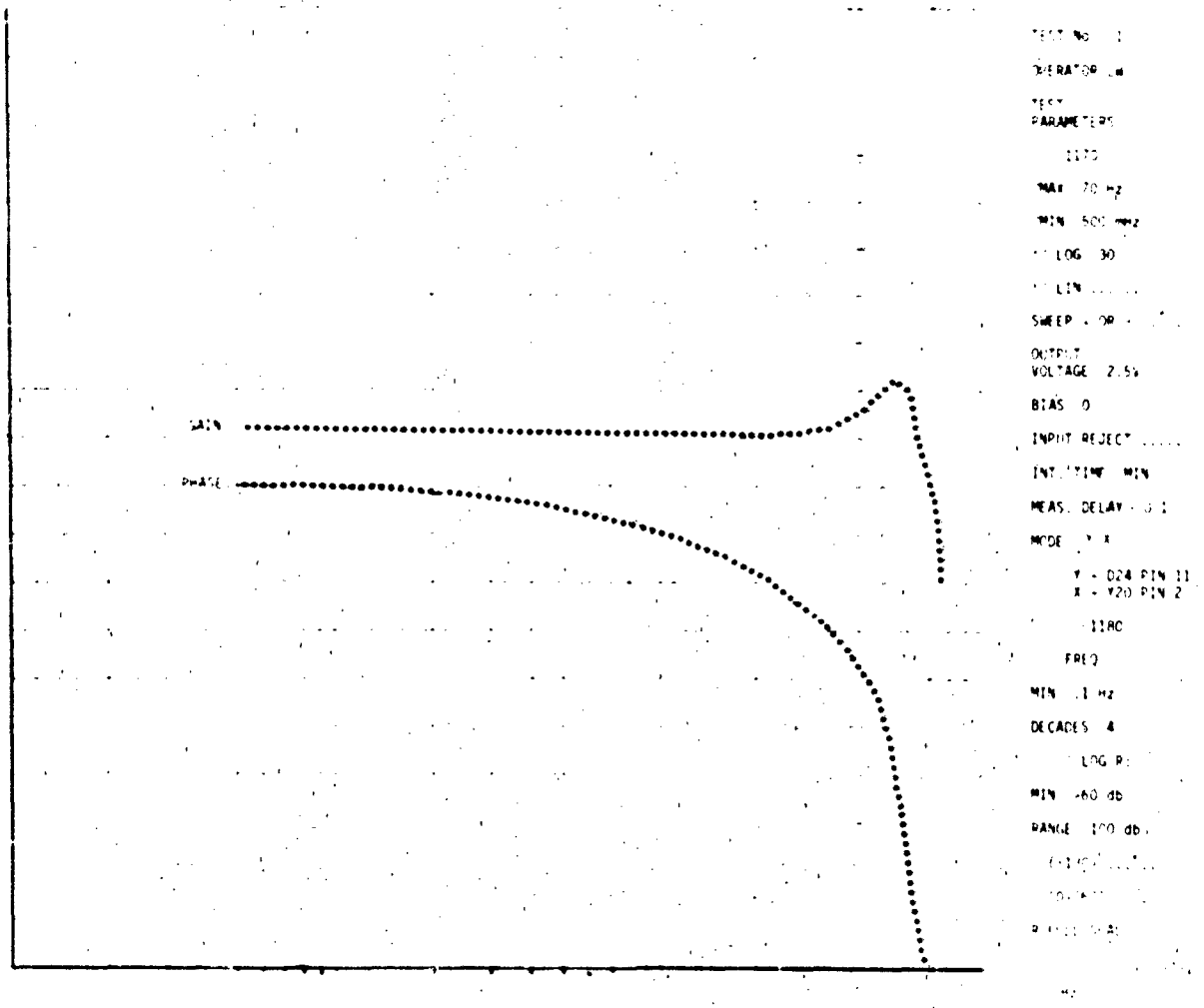

Figure 41. Y-Axis Displacement Reponse.

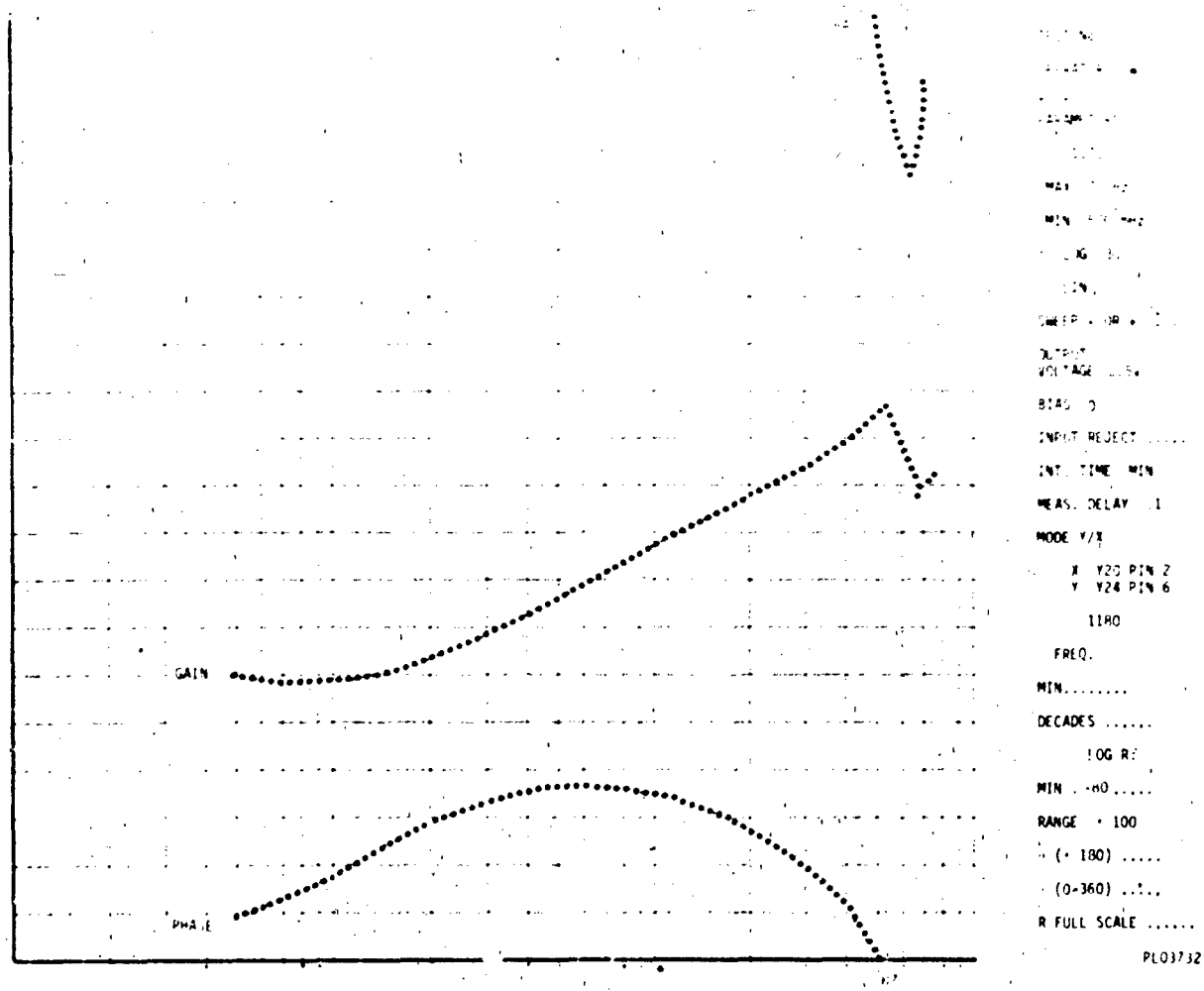

Figure 42. Y-Axis Velocity Response.

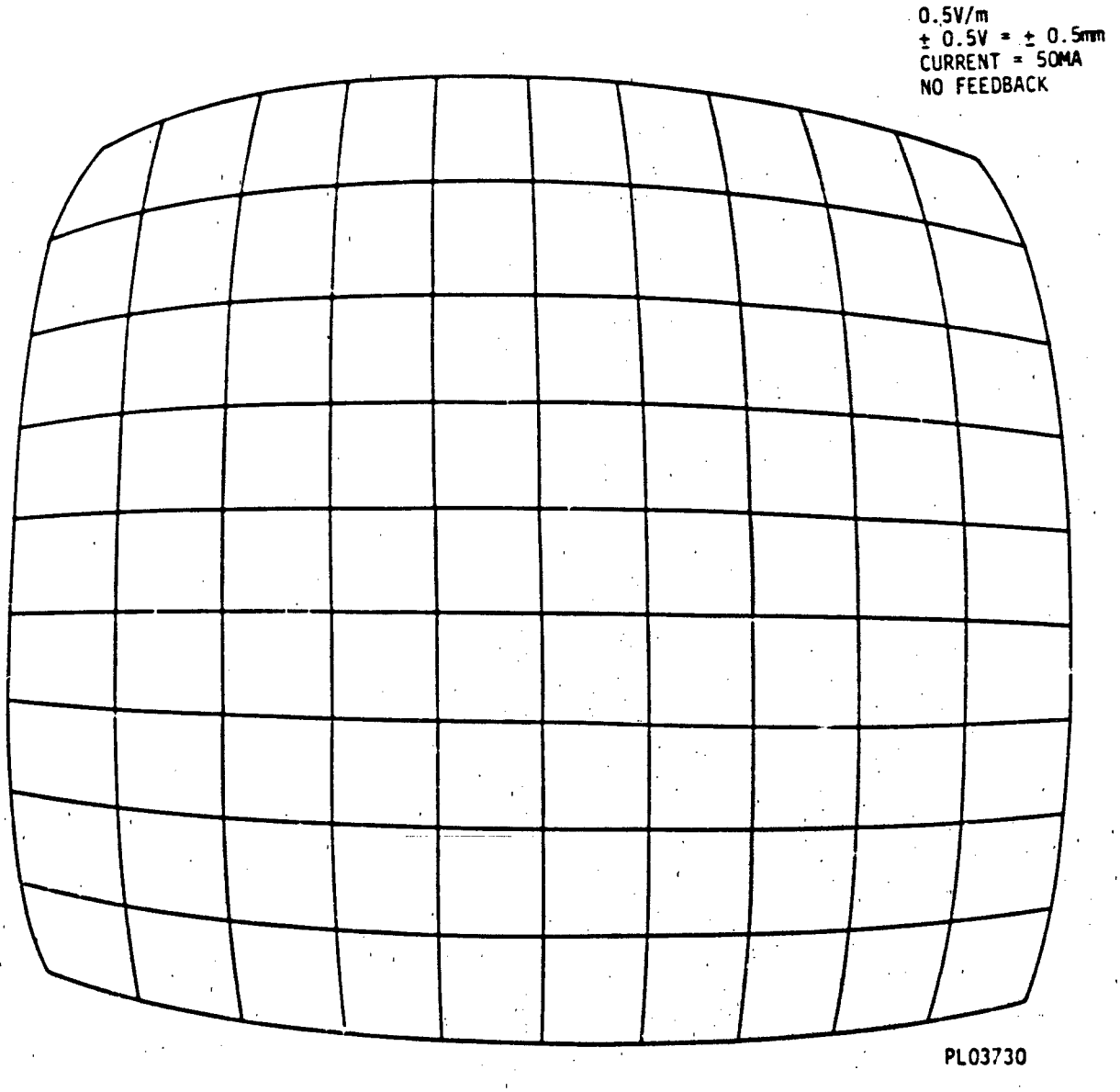

Figure 43. Detector Mapping Characteristics.

7. ACCELEROMETER PREDICTION OF HEAD POSITION

7.1 Delay Compensation. In order to reduce the image response time on the HMD, it was thought necessary to predict the position of the head movement. AFHRL attempted to extrapolate position data to do this but was unsuccessful due to the noise on the position signals. Their next approach was to integrate an acceleration signal in order to predict position. To this end, an angular accelerometer was installed on the yaw axis and sampled by the head-tracking computer. A predictor scheme based on an AFHRL analysis was used[3]. This calculated the extrapolated head position based on the present position plus the estimated velocity. The estimated velocity was derived from the actual velocity plus an acceleration term. To eliminate overshoots, the estimated velocity was limited to a reasonable value.

The following algorithm was programmed in the head-tracking computer:

$$v = (x - x\_) / tau$$

$$v^1 = \min(\max(v+a*tau\_1 ,-vlim),vlim)$$

$$x^1 = x + v^1*tau\_2$$

Where:

v	actual velocity
x	actual position
x_	last value of position
tau	iteration time
v^1	estimated velocity
a	measured acceleration
tau_1	acceleration coefficient
vlim	velocity limit
x^1	estimated position
tau_2	velocity coefficient

---

[3] List, U.H. Nonlinear Prediction of Head Movements for Helmet-Mounted Displays (AFHRL-TP-83-45, AD-A/36 590). Williams AFB, AZ: Air Force Human Resources Laboratory, Operations Training Division, December 1983.

7.2 Results. The experiment gave very realistic tracking of the visual scene. In fact, with the low-resolution scene, it was found that the mechanical delay compensation could be removed without adversely affecting the response of the CGI.

7.3 Conclusions. It is proposed to add accelerometers to the pitch and roll axes to complete the evaluation of the accelerometer-based prediction scheme. At the same time, the dual high-/low-resolution images will be integrated and the effect of acceleration-based prediction will be further investigated.

It is hoped that the mechanical delay compensator will become redundant. Further experiments will be done to use the mechanical delay compensator to obscure the effects of the discrete fiber bundle on the final image seen by the pilot.

8. HELMET DESIGN

8.1 Description of Current System. In the present design, the two Pancake Windows™ with display optics are mounted on a rigid tube. This assembly is then mounted on the front of the helmet. The helmet itself is of standard design having chin and nape straps for attachment. Two fiber-optic cables are connected to each Pancake Window Display™ optics assembly. Also connected to the helmet is a mechanical head tracker.

Fairly exacting adjustments are needed to set up the display for any given pilot in terms of interpupillary distance, shape of the pilot's head, and relative position of the exit pupil to the eye. Present design allows only for interpupillary distance adjustment which is achieved by the lead-screw displacing the two Pancake Window™ assemblies. The height and depth of exit pupil relative to the eye may be adjusted by padding the inside of the helmet as required, but this is a lengthy procedure.

Rigidity is required so that the position of the exit pupil does not change relative to the eye. The helmet itself is not rigid and may flex. The two Pancake Window™ optics assemblies are therefore mounted on a rigid frame and not on the helmet directly. Firmly attaching the frame to the helmet makes the helmet rigid as far as the optical design is concerned. It could be argued, however, that once the helmet is tightly placed on the pilot's head, it can no longer deflect substantially, thus eliminating the need for the frame and resulting in reduction of weight.

8.2 System Limitations. The weight of the breadboard display optics is approximately 7 pounds and the configuration with the helmet weighs approximately 13 pounds. Since the display optics are mounted at the front of the helmet, the center of gravity is very far forward from the pitch centerline of the helmet. As a result, the helmet has a tendency to pitch forward. A negator mechanism was designed to alleviate this problem, but it may, in some cases, impede the pilot's head motion.

Increased rotational inertia of the HMD has a definite effect on the head movement control system. Inertia may impede rotation when it is initiated and may retard braking action when the direction of rotation is to be reversed. As a result of this action, the helmet has a tendency to rotate relative to the pilot's head. The resultant change in the position of the exit pupil relative to the eye may cause an apparent loss of image.

The fiber-optic cables also increase the weight and inertia of the HMD system. Being fairly inflexible and having finite length, the fiber-optic cables may in some cases impede the motion of the pilot. The negator mechanism was designed to negate the weight of the cables, but the stiffness of the cables remains a problem. The torque exerted by the cables on the helmet causes the helmet to rotate from desired position, resulting in the loss of image to the pilot.

The mechanical head tracker is also connected to the helmet. It is mechanically balanced and therefore does not add weight to the system. However, the mechanical head tracker has a limited range of travel and limits the pilot's movements. The mechanical head tracker will be replaced by an optical one in the near future and is not considered here as a problem.

In summary, the weight of the HMD optics and the fiber-optic cables cause general discomfort when the helmet is worn, if the negator mechanism is not employed. The inflexibility of the fiber-optic cables and the inertia of the system impede the pilot's motion and cause the helmet to rotate relative to the pilot's head, thus causing the pilot, in some instances, to lose the field of view.

8.3 Helmet Design for HMD System. The helmet presently used has no mechanical fitting adjustments. This is not adequate. To minimize the helmet displacement problem, each pilot will have to be fitted with a modified helmet which best fits him. This will necessitate the use of at least three different-size helmets: small, medium and large. These helmets will have two independent straps. A conventional chin strap will be used in the customary fashion. A nape strap, fitted to the back of the helmet, will be used to prevent the helmet from pitching forward. This is necessary since most of the weight is concentrated at the front of the helmet. Also added to the inside back of the helmet will be a tension-adjustable pad. The tension adjustment knob will be provided on the side of the helmet.

The use of different-size helmets implies that the helmet display optics will have to be removable and be fitted from helmet to helmet quickly and accurately. This requires the addition of two more mechanical adjustments for optics: eight and depth of view. To speed up the adjustment procedure, a dummy display system will be fitted to the pilot first while the real display system is used elsewhere. With the adjustments set, the display optics can be readily mounted on the helmet. This will necessitate the use of at least six different helmets.

8.4 Helmet Displacement Experimental Results. Experiments were conducted to determine the relative displacement between the helmet and the head in single-axis (yaw) smooth pursuit head motion tasks. A potentiometer was mounted on the helmet and attached to the mouthpiece. An accelerometer was placed on the mouthpiece to record the rate of head rotation.

The head rotation for all the experiments in yaw was approximately ±45 degrees. The data on helmet displacements were taken for slow, medium, and fast rotations with helmet back padding tensioned and untensioned. It was found that the displacement measurements were affected by helmet fit and varied from subject to subject. However, a definite pattern emerged for all the data being collected, and the results here are presented for one subject only.

Figure 44(a) shows a plot of helmet/head displacement for slow (normal) rate of head rotation with back padding untensioned. The relative helmet displacement is approximately ±0.14 inch, which translates to ±1.3-degree helmet rotation. For the same rate of rotation and with back padding tensioned, the helmet displacement decreased to ±0.08 inch, which translates to ±0.75-degree helmet rotation (Figure 44(b)). For increased rates of rotation (Figure 44(c)), the relative displacement of the helmet increases substantially.

There are basically two reasons why the helmet displacement relative to the head should be kept to a minimum. First, the helmet displacement causes a change of position of exit pupil; thus, loss of image can occur. Second, if an eye tracker is used, the eye position measured will not be the actual one against which the eye tracker was calibrated. In eye-tracked displays, the eye-pointing direction of the pilot is monitored continuously and the CIG generates the visual information such that it is always concentrated in the eye-pointing direction. When the helmet rotates relative to the head, this direction is altered and is no longer correct.

8.5 Conclusion. For HMD purposes, the primary function of the helmet is to support the display optics so that the image generated by the CGI is visible to the pilot at all times. Furthermore, the pilot's head movements should not be hindered by the system design. The present system configuration does not completely meet the above requirement.

The weight of the display optics is taken up by the mechanical negator system but the increased inertia due to the optics mass is not compensated for. The combined stiffness of the four fiber-optic cables impedes the pilot's head motion and causes a relative displacement between the helmet and the pilot's head.

In the second phase of the development, the weight of the helmet-displayed optics will be substantially reduced. Two fiber-optic cables will be used instead of the present four. This will greatly reduce the stiffness problems associated with fiber-optic cables and will improve the overall system design. Lighter, smaller, better-fitting helmets equipped with tension-adjustable padding and attachment straps will reduce helmet/head displacement problems. With the stated improvements, the overall helmet-mounted system design will come close to meeting the stated requirements.

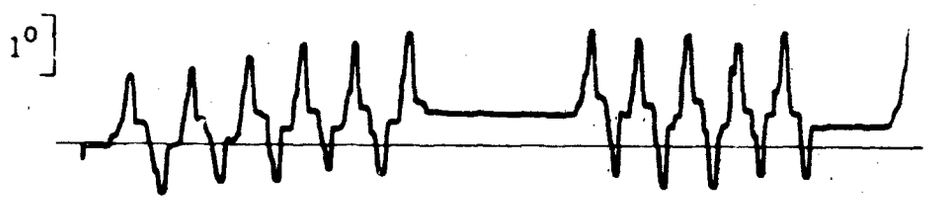

(a) SLOW YAW ROTATION
BACKPADDING UNTENSIONED

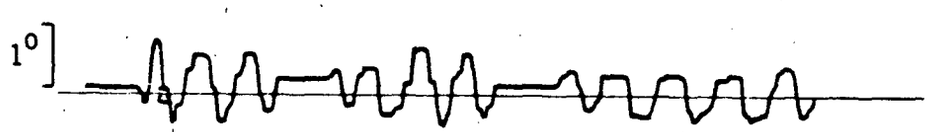

(b) SLOW YAW ROTATION
BACKPADDING TENSIONED

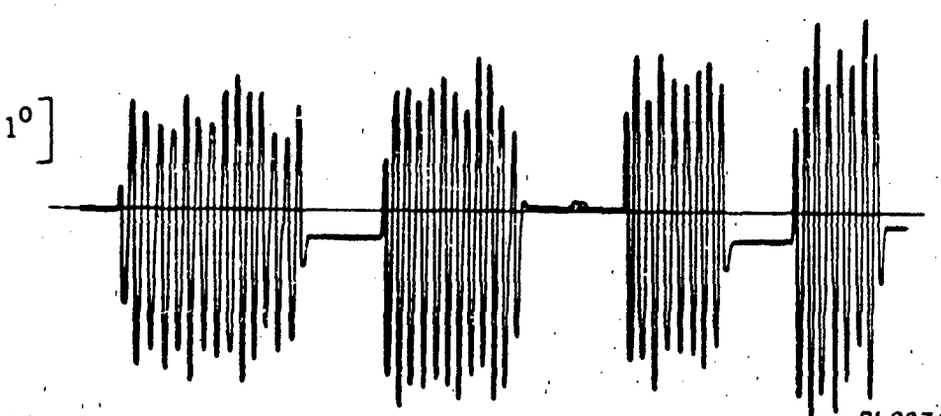

(c) RAPID YAW ROTATION
BACKPADDING UNTENSIONED

PL03744

SAMPLE TIME HISTORIES OF RELATIVE HELMET-HEAD DISPLACEMENT FOR YAW STIMULUS. EACH DEVISION ON TIME SCALE REPRESENTS 1.0s.

Figure 44. Sample time histories of relative helmet/head displacement for yaw stimulus. Each division on time scale represents 1 sec.

9. MODULATION TRANSFER FUNCTION

9.1 General. The modulation transfer function (MTF) of a visual system is the only known metric for reliable measurement of resolution. If the MTF of each component in the system is known, the overall system MTF can be calculated by simple multiplication of the individual MTFs. A typical MTF measurement on an optical system consists of viewing a sinusoidally modulated test pattern having a variable spatial frequency. The modulation of the image is measured at appropriate frequencies, and the MTF (as defined in Figure 45) is plotted against spatial frequency. The modulation of the test pattern is usually assumed to be 100 percent. If it is significantly lower than 100 percent, a correction factor should be applied. In the case of a television display, such as the light valve, a signal with 100 percent modulation is used to create an image test pattern.

9.2 System MTF. Figure 46 shows the MTFs supplied by the manufacturers of the main system components and the expected MTF of the overall system. No MTF measurements have been taken on the equipment to date. The group of bars on the USAF three-bar test pattern corresponding to 2.5 arc min per line pair could just be seen through the helmet optics and fiber-optic cable. This indicates that the MTF is lower than expected. Farrand Optical Co. plans to make a set of MTF measurements on the system. In particular, the effects of the coupling between fiber-optic expanders and fiber-optic cables and the effect of grinding the end of fiber-optic components to increase numerical aperture will be investigated.

9.3 Background MTF. Figure 47 gives the expected MTFs for the background field. The demand function of the eye has been extrapolated from multiplying the normal demand function by a factor of 0.2 which is the acuity of the eye at 10-degree eccentricity.

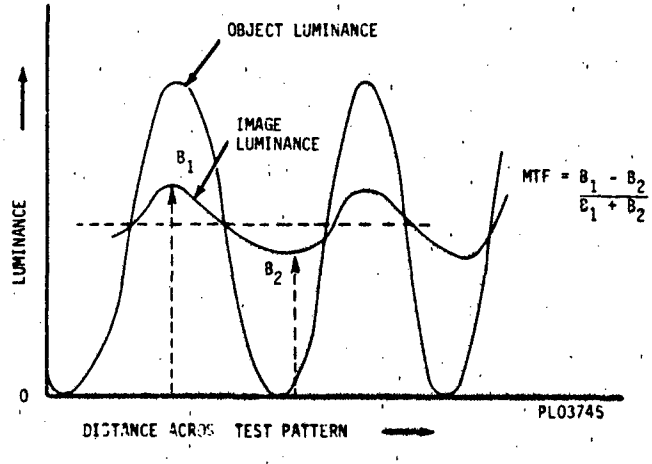

Figure 45. MTF Measurement.

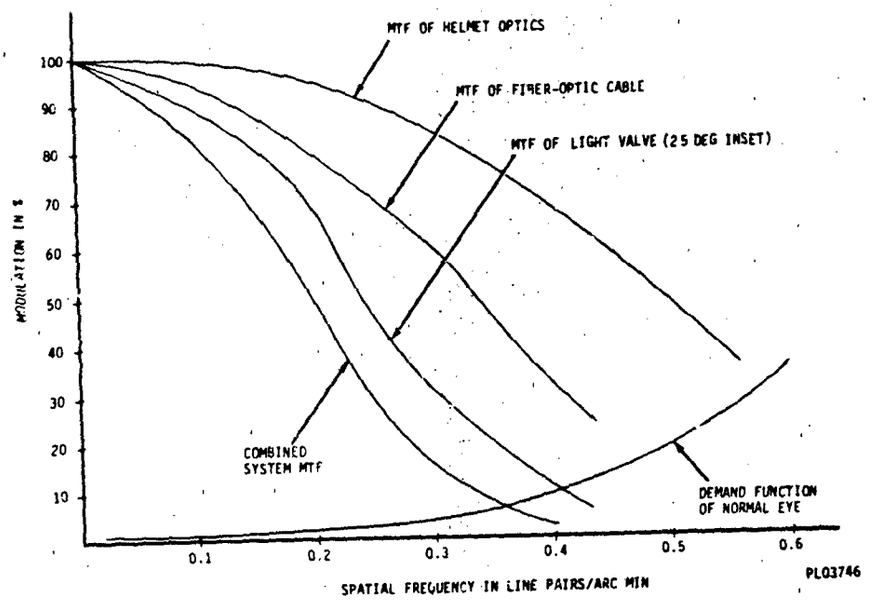

Figure 46. MTF of Inset Field.

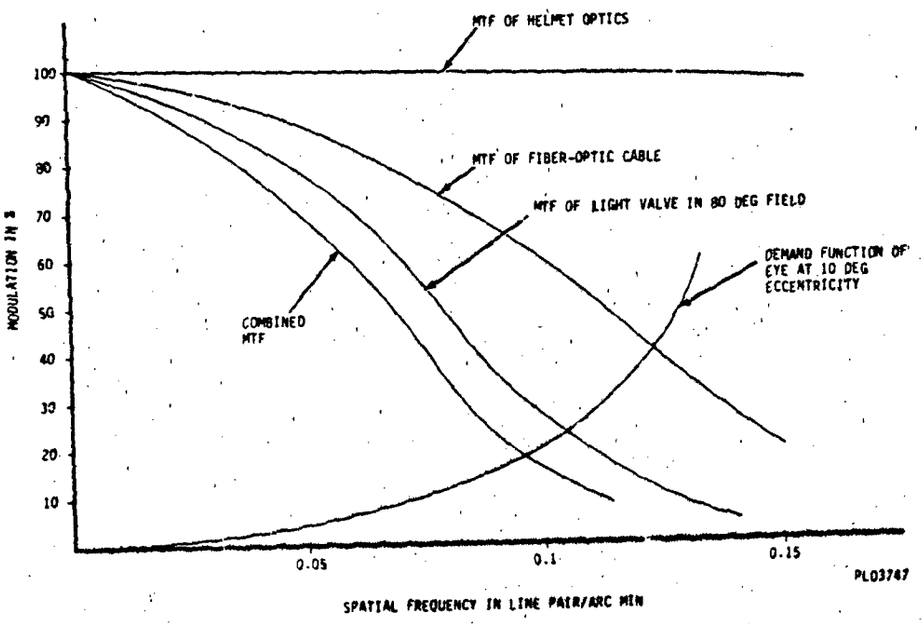

Figure 47. MTF of Background Field.

10. BLENDING OF HIGH-RESOLUTION AREA INTO BACKGROUND

10.1 Introduction. The blending of high-resolution insets into low-resolution background imagery has always been a major problem in visual simulation. Systems that used such insets to portray targets, particularly ground targets, did not achieve the goal of real-world performance because the high-resolution area was too visible. No matter how well the areas were blended together in terms of luminance and color, the higher spatial frequencies and greater level of detail in the inset area seemed to attract the attention of the eye.

The breadboard HMD has a different problem because the high-resolution inset is always in the same central area of the visual field. The boundary between the two fields will be 12.5 degrees away from the center of the field if a 25-degree inset is used. The possibility that this boundary may be a serious distraction is a major cause of concern.

The experience of AFHRL with scanned insets on a previous project indicated that the blending should take place over a 5-degree area on the vertical edges of the inset and a 3-degree area at the top and bottom.

Figure 48 shows the desired shape of the neutral density optical filter for blending the inset into the background, and Figure 49 shows the filter transmission characteristics.

A major complication in this task was in the optical steering technique for stabilizing the image during head movements. The input ends of the fiber-optic cables are moved to compensate for the CGI transport delay (see section 6). The masks, therefore, could not be placed in the helmet optics because head movements would cause movement of the image relative to the masks. They had to be placed at an image plane, however, and the only other accessible image plane was at the input end of the fiber optics. This was not an ideal location because the color multiplexing prisms would cause a coloring effect in the boundary area. However, the effect would be slight and would tend to cancel between inset and background because the shift in color would be in opposite directions.

10.2 Initial Experiments. Initial experiments were carried out with thin metal masks placed slightly in front of the image plane at the fiber-optic cable to produce a defocused edge spread over several degrees. This defocused edge would cause vignetting of the image and should have caused the luminance of the image to change in an almost linear fashion across the boundary. Unfortunately, the non-uniform characteristics of the exit pupil in the light valve caused considerable color variations across the boundary, indicating that any mask must be placed either at or very close to an image plane.

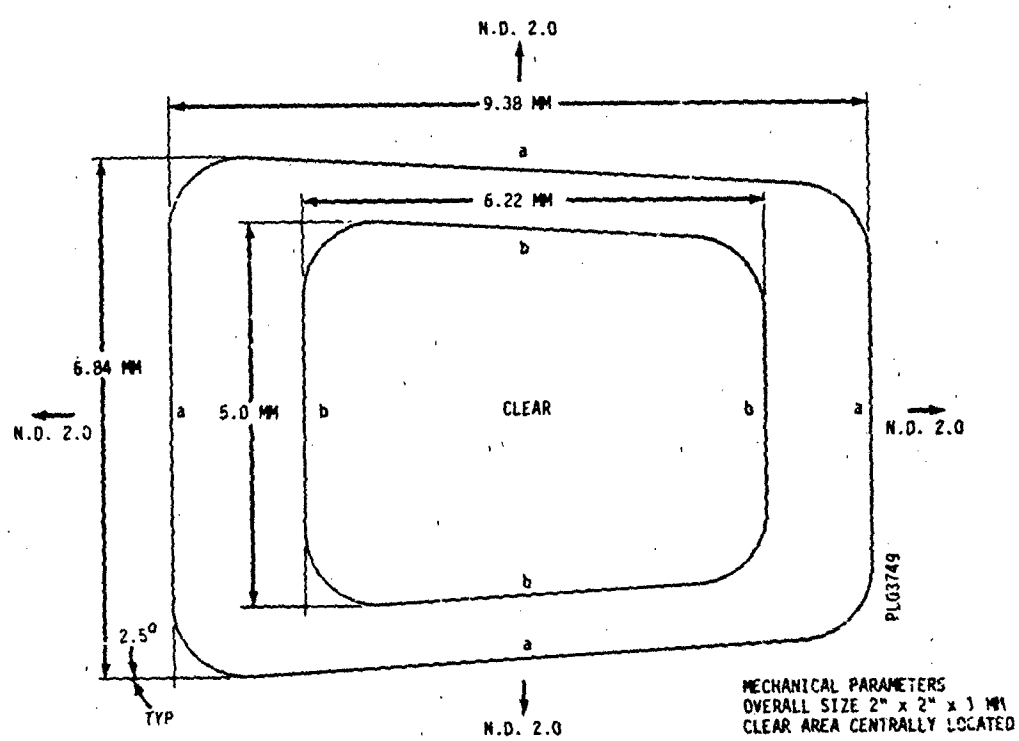

Figure 48. Neutral Density Filter Shape.

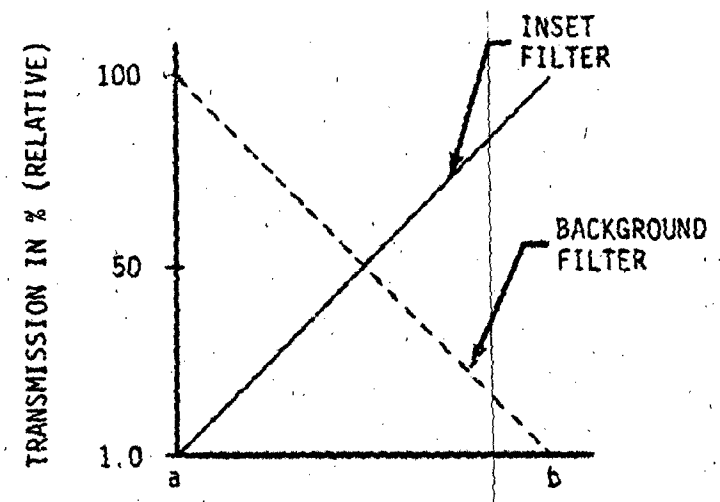

Figure 49. Filter Transmission Characteristics.

10.2 Initial Experiments (Cont'd)

Several companies were approached to make filters with the characteristics shown in Figures 48 and 49. A manufacturer in New York agreed to make a complete set. There was no assurance, however, that the two filters would match each other due to the difficulties involved in manufacturing such filters.

Optical filters will probably be adequate to enable the breadboard HMD to be evaluated. Further research, particularly in the alternative technique of electronic blending, will be required before a satisfactory solution is found for the engineering prototype. From the work that has been carried out so far, the most logical place for the blending to be implemented is the digital image generator itself. This possibility will be investigated thoroughly during the breadboard evaluation.

11. LUNING EFFECT

11.1 Introduction. The first time the breadboard helmet display was tested using two uniform light sources to illuminate each eyepiece, an unusual effect was noticed. The central overlapping area was bounded by two dark bands forming a distinct line in an otherwise uniform field (see Figure 50). The line was still present when the light valves were connected and test patterns such as color bars and resolution charts were displayed The visibility of the bands forming the line was not constant but varied as one stared at different parts of the image. The most likely reason for this phenomenon can be attributed to binocular rivalry and, fortunately, existing knowledge of this effect suggests a solution. Binocular rivalry occurs when one eye becomes dominant, preventing imagery in the other eye from being processed. The effect usually occurs when dissimilar information is presented to the two eyes; and it may affect the entire field seen by the non-dominant eye, or parts of that field. Usually, the dominant eye alternates at intervals of a few seconds. In this particular case, the inboard, or nasal, information for each eye ends in a sharply defined curve. Bright imagery is present on one side and almost total darkness on the other side. In the test situations described, the other eye was presented with a uniformly bright image in this part of the visual field. Conditions exist, therefore, to cause rivalry and each eye remains dominant on the far side of each inboard field for a few degrees, thereby giving an illusion of a dark band. This effect has been termed "luning".

10.2 Field Stops. It is known that long lines with high contrast are a major factor in causing rivalry and it was postulated that the solution might be to reduce the contrast across the boundary by providing gradual transition from full luminance to zero luminance. A simple way of proving this idea was to insert a field stop, between the eye and the Pancake Window", shaped to match the inboard boundary of each field. The proximity of the stop to the eye caused vignetting at the inboard boundary. Adjustment of the lateral and longitudinal position of the stop caused a gradual reduction in luminance which was sufficient to completely suppress the luning effect. Neutral-density filters, which will be placed at the output of the fiber-optic cables and which should duplicate the effect of the field stop, are currently being made. The transmittance curve for the filters is shown in Figure 51. The optimum shape for this curve will be determined during the evaluation period.

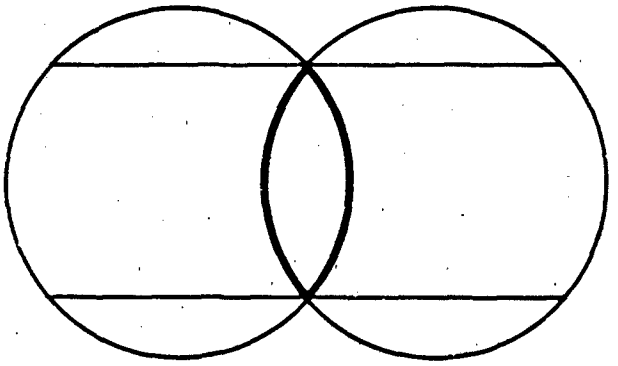

PL05116

Figure 50. Luning Effect.

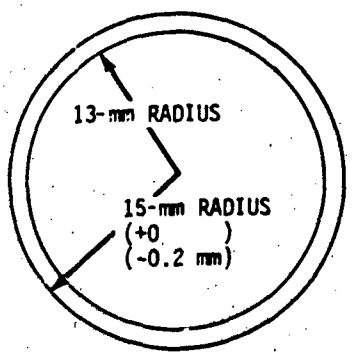

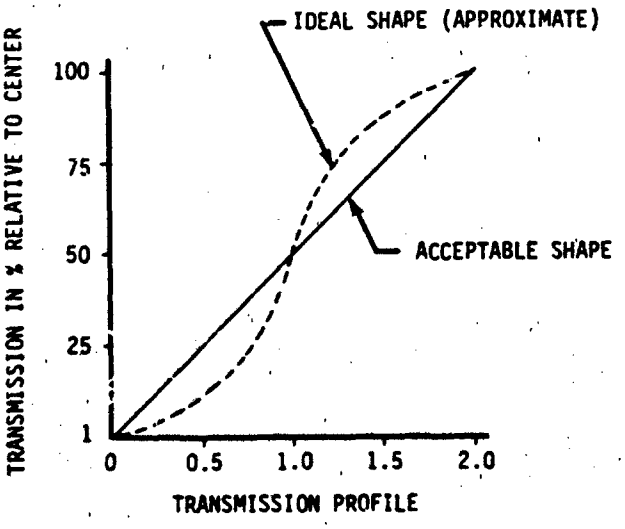

THICKNESS - 0.02 IN ± 0.01
MATERIAL - OPTICAL-QUALITY GLASS
METALLIC ALLOY COATING IS TO BE APPLIED TO THE OUTER 2 mm OF THE GLASS DISC WITH A TRANSMISSION PROFILE AS SHOWN.

PL03743

Figure 51. Radial Wedge Neutral-Density Filter.

12. EFFECT OF LIGHT VALVE PERSISTENCE

12.1 General. Apart from the non-uniform distribution of color in its exit pupil, the light valve is an ideal image source for the HMD. The design of the optics and the small size of the image on the oil layer enable almost 100 percent of the light output to be channeled into the fiber-optic cables. However, the temporal characteristics of the oil layer will cause a loss in resolution for moving imagery in a manner similar to that of television camera. Because the head will be in motion for much of the time during target acquisition tasks, this is a major cause of concern.

12.2 Light Valve Modification. The decay characteristics of the light valve are shown in Figure 52. The electron beam deposits a charge on the oil layer, causing it to deform fairly rapidly and resulting in the step rise in the luminance curve. As the electrical charge is dissipated, surface tension restores the oil layer to a flat surface, giving the exponential decay in luminance. The decay time is determined by the viscosity of the oil which, in turn, is controlled by the temperature of the oil. It is normally set to allow the luminance to decay to 17 percent of its peak value by the end of one field; i.e., 16.7-msec. This value has been determined empirically to give the best compromise between light output and image lag in normal commercial use. Lag, or image persistence, has considerably greater importance in the HMD, and the oil temperature should probably be set to reduce the luminance-decay time constant to as low a value as possible. This is believed to be feasible at the expense of reduced light output and possibly reduced light valve life. This will be investigated during the evaluation period.

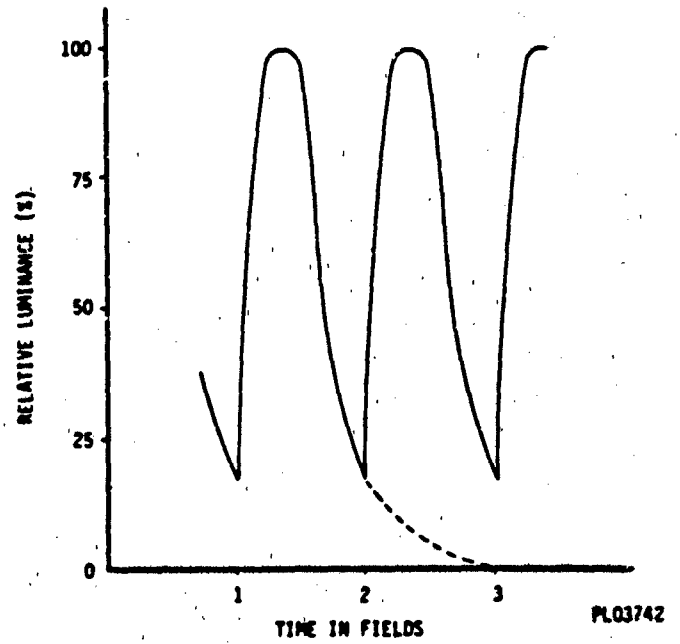

Figure 52. Temporal Response of Light Valve.

12.3 Rotating Shutter. Another technique for reducing image persistence is with a rotating shutter as shown in Figure 53. The wheel is similar in construction to the color wheels used in field-sequential color television. The wheel is synchronized to the field rate of the light valve and is positioned close to an image plane in such a way that the spokes of the wheel follow the scanning beam down the picture. By increasing the width of the spokes relative to the width of the clear aperture and adjusting the phase of the wheel relative to the vertical synchronization of the projector, the shutter will blank out the trailing edge of the luminance curve, as shown in Figure 54.

The clear position of the shutter can be made equivalent to as little as 3 msec. A 5-msec shutter was made and installed close to the input end of the fiber-optic cable on one of the background channels. However, the portion of the light remaining in the second field created a double image and prevented a true evaluation of the decrease in persistence. If the oil temperature can be increased sufficiently to reduce the amount of light spilling over into the second field to a negligible amount, the rotating shutter will be investigated further.

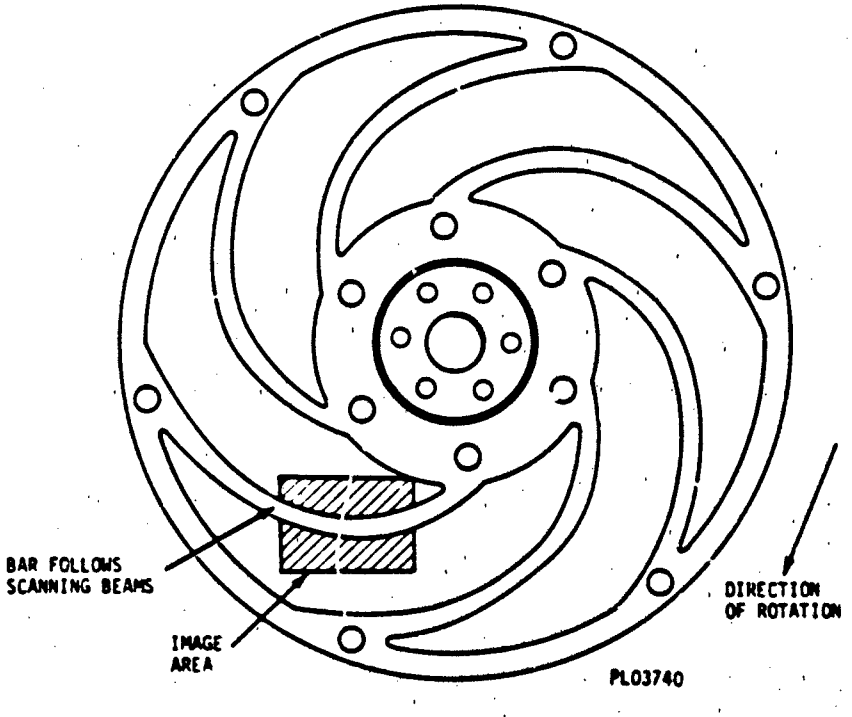

Figure 53. Rotating Shutter.

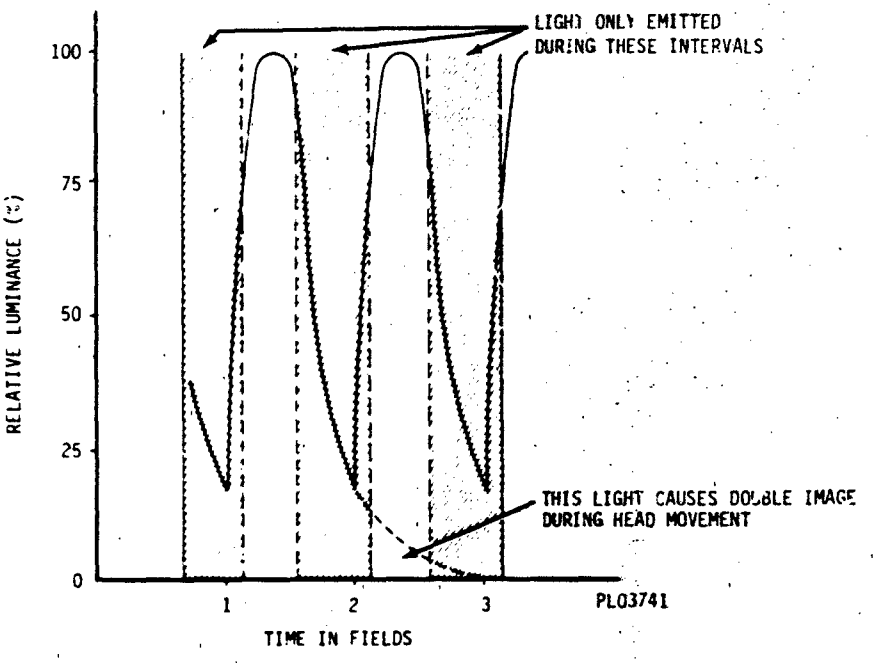

Figure 54. Use of Rotating Shutter Wheel to Reduce Image Lag.

12.4 Optical Steering Mechanism. A third technique for reducing the lag effect is with the optical steering mechanism (see section 6) which is primarily used for compensating the CGI transport delay. The drive algorithm for the optical steering subtracts the potentiometer position delayed by a discrete number of fields from the current potentiometer position (either pitch or heading) and uses the result to drive the image in the appropriate direction. A typical motion sequence is shown in Figure 55. It can be seen that the optical steering tries to follow the actual image motion during the steady-state condition but is limited by its own response. It has been observed that the lag effect is less noticeable when the optical steering is used to compensate for CGI transport delay than when using the alternative method involving use of an acceleration-based prediction algorithm. To obtain a perfectly stable image with no smearing, however, would require the optical steering to follow the head motion during a complete field together with a portion of the second field while the end of the first field is still decaying. The only way this could be achieved is if alternate fields to each eye were blanked out to allow the steering mechanism to recover between active fields. Figure 56 shows the timing of the steering relative to the projector field rate. The response of the optical steering is 6 dB down at 60 Hz, which should allow good image stabilization over the entire image. The resulting dichotic display will be acceptable only if flicker remains

12.4 Optical Steering Mechanism (Cont'd)

below threshold and if the psychophysical aspects of dichotic viewing do not affect pilot performance. Preliminary experiments have shown that flicker will not be seen in the 25-degree inset at luminance levels of about 10 ftL, but would be very noticeable in the 80-degree background field. This indicates, therefore, that almost perfect stabilization of the image could be obtained in the central region of the visual field. Further experimentation will be carried out once all four channels of the HMD can be viewed simultaneously.

Although the theoretical reduction in MTF at head velocities of about 100 deg/sec is considerable and small objects are smeared in the direction of motion as shown in Figure 57, the observed effect on picture quality is not as severe as might be expected. The vestibular ocular reflex, which maintains the eye in a stable position during head motion, is a form of smooth pursuit. Although the response of this reflex is maintained up to about 10 Hz, it is likely that at head velocities greater than 20 or 30 deg/second, which is the normal limit for smooth pursuit, saccadic movements must also be used to maintain fixation. Under these conditions, the acuity of the eye would be reduced by as much as five times and, hence, any degradation in picture quality would be less noticeable. Experiments to quantify both the loss in MTF and the loss in observer performance will be carried out during the evaluation period.

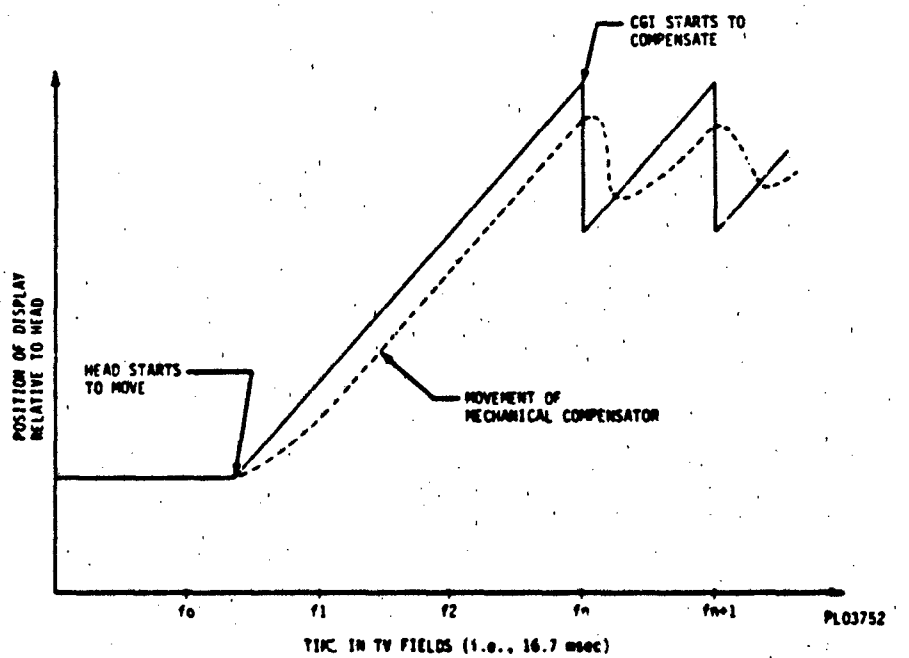

Figure 55. Motion of Optical Steering Showing Partial Compensation for Light Valve Persistence.

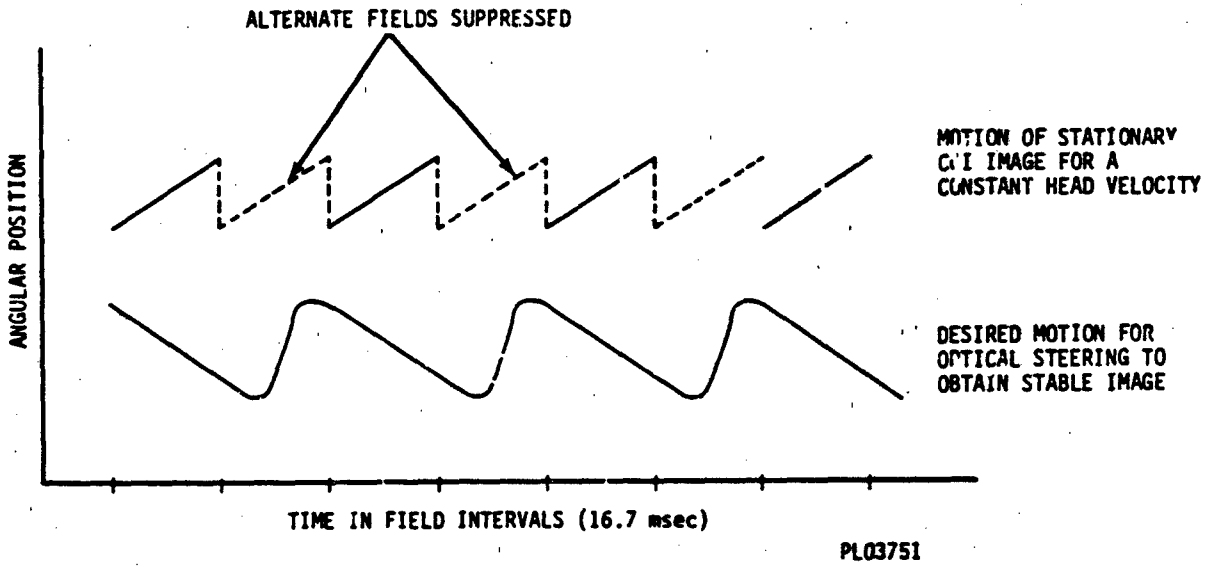

Figure 56. Image Stabilization Using Optical Steering and Dichotic Viewing.

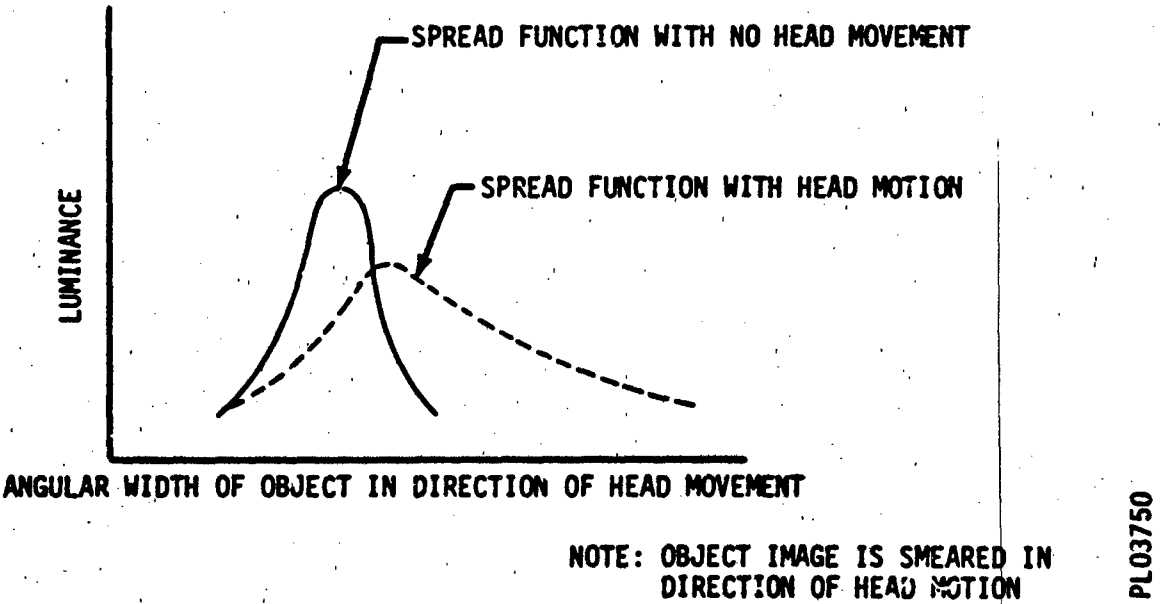

Figure 57. Light Valve Persistence Effect on Spread Function of a Small Bright Object.

13. EYE-SLAVED PROJECTOR

13.1 Overview. The goal of the area-of-interest (AOI) visual system is to produce a high-resolution display which is indistinguishable from the real world in terms of pilot performance for a required task. To approach this goal, parameters for an AOI display such as inset size, inset shape, resolution differential (between AOI inset and periphery) and a method of edge blending must be first determined.

These parameters could be investigated in experiments using the final prototype HMD. However, investigating these parameters would require modifications in the optical system and/or CGI, which would not only be a difficult task but would be time-consuming and expensive.

13.2 Eye-Slaved Projector Development. In an attempt to investigate how variations in AOI parameters affect the observer's performance, an eye-slaved projector (ESP) system has been developed at CAE. A preliminary model was developed during the early stages of the project. It consisted of a three-channel slide projection system in which a high-resolution image, slaved to the observer's eye movements, moved within a low-resolution field. A block diagram of the optical system is shown in Figure 58.

The 35-mm slides used in the three channels are identical except in resolution. At the viewing distances used in the experiment, the resolutions corresponded to visual acuities (VAs) of 1.0, 0.3, and 0.1. The mark shown in Figure 59 was placed close to the plane of the slides and could move in X and Y axes in response to eye movements. A composite image was thus obtained in which the area located by the observer's eye had high resolution and was surrounded by progressively lower resolution fields. The slides were also capable of being moved in X and Y in response to head movements. This would allow the interactions between head and eye movements to be investigated once the ESP was coupled to the HMD.

It became apparent after preliminary testing and a review meeting held in November, 1982, that the inherent 50-msec delay between eye movements and actuation of the eye-slaved masks was not only perceptible but distracting to the viewer. As a result, an accurate assessment of the AOI display was not possible with this system. At the review meeting, it was decided that a faster, hydraulically actuated ESP system was needed. It was also decided that connecting the ESP to the HMD was impractical and that a rear projection screen presentation would be sufficient. It would, in fact, be preferable for most of the eye-slaved experiments envisaged at that time because it would allow the beamsplitters to be removed. (They were causing a certain amount of chrominance variation between channels.) Once the basic evaluation of the breadboard HMD had been completed, it was expected that a limited form of eye slaving could be introduced into the digital imagery generator (DIG) to allow investigations of a different nature, including head and eye interactions.

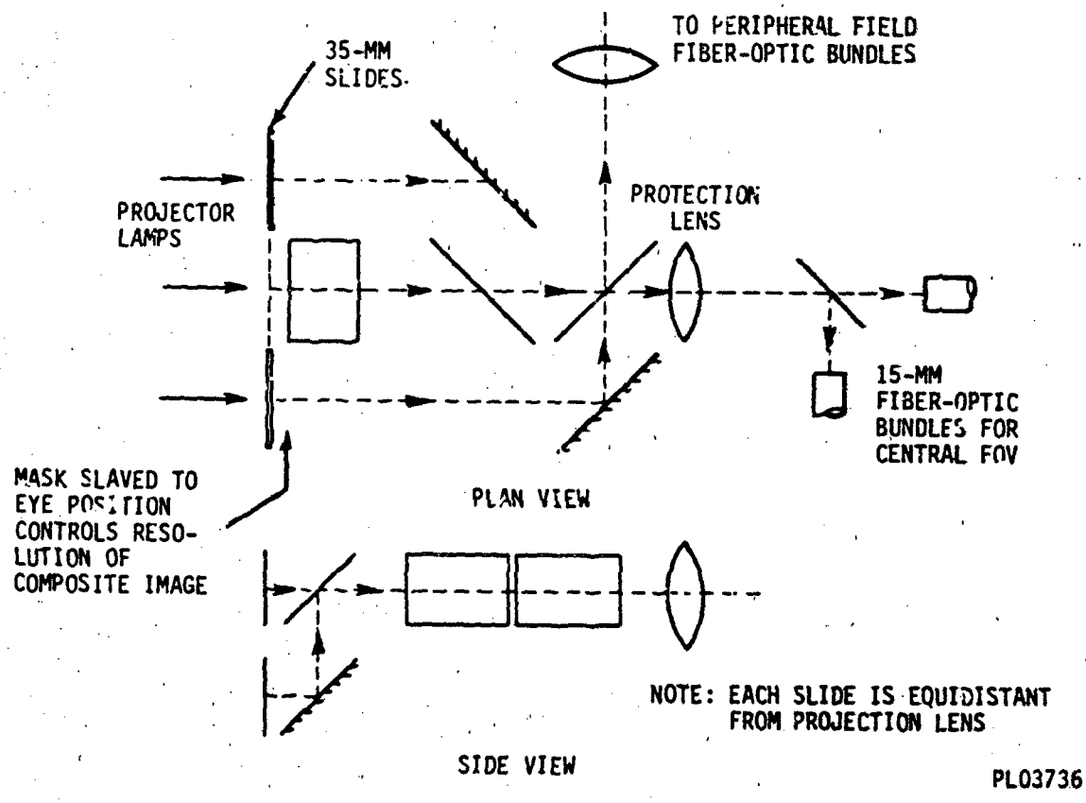

Figure 58. Optical Layout of Eye-Slaved Projector.

13.2 Eye-Slaved Projector Development (Cont'd)

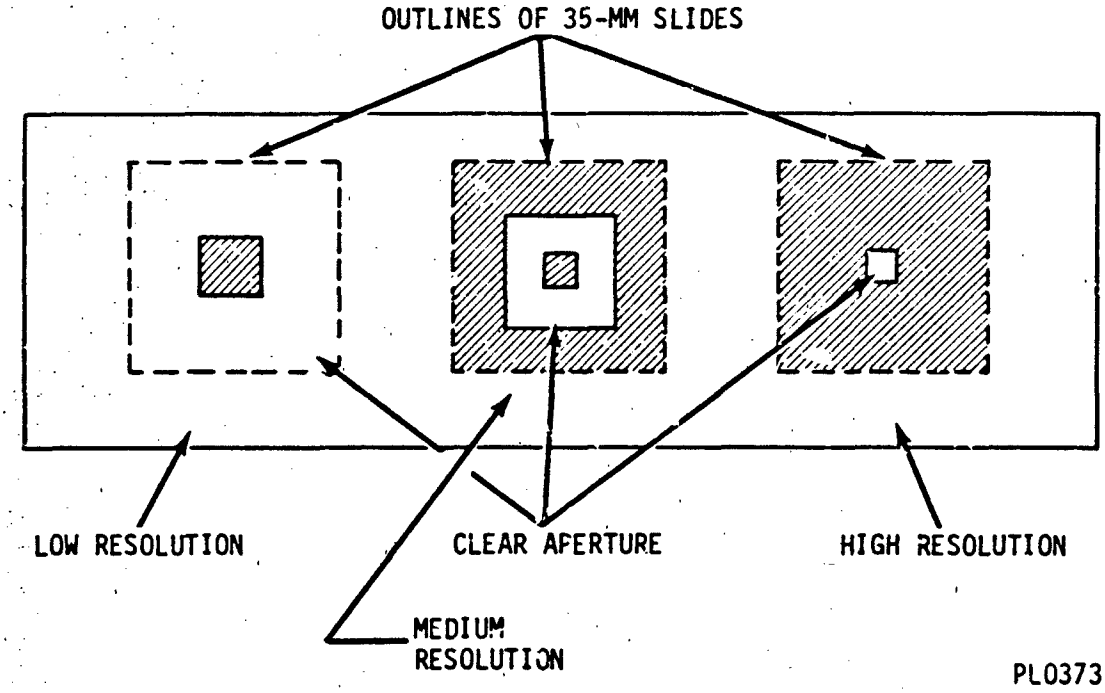

Figure 59. Eye-Slaved Mask Used To Produce Composite Image.

From November 1982 to April 1983, an hydraulically actuated ESP system was conceived and built. Schematic diagrams of this system are presented in Figures 60 and 61.

The hydraulically actuated system (Figure 60) consists of three projector lamps, optics and projection lenses mounted on an optical bench such that the images from the three channels may be superimposed on a rear projection screen. Stimulus slides may be placed in each of the three holders situated between the projection and condenser lenses. The mask holders located in front of the stimuli are mounted on an aluminum plate (Figure 61) that moves horizontally along linear bearings. The mask plate is fixed onto another aluminum plate that moves vertically. In this way, the movement of the two plates allows the mask to travel in two dimensions. Light passing through the slides and masks produces a projected image of a high-resolution area inset into a low-resolution field.

The motion of the plates is controlled by hydraulic actuators which receive input from the CAE-designed control circuitry. The circuitry accepts signals having a magnitude of approximately 300 mV/deg from the eyetracker. The slightly underdamped system results in the mask holder travelling 1 inch in 10 msec (with a 5-percent overshoot). This travel is equivalent to the

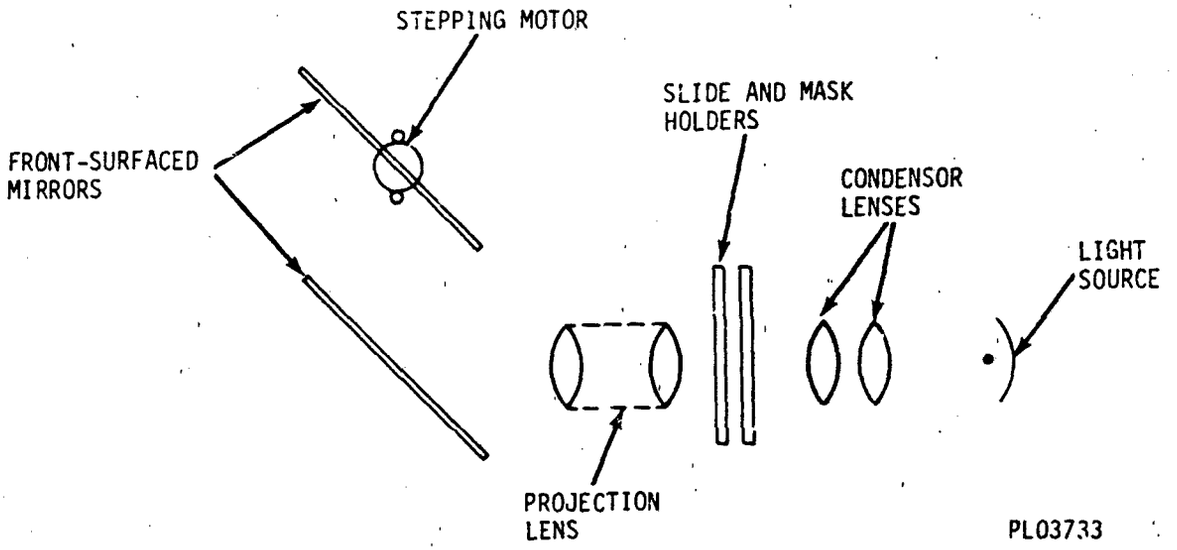

Figure 60. Eye-Slaved Projection Optics.

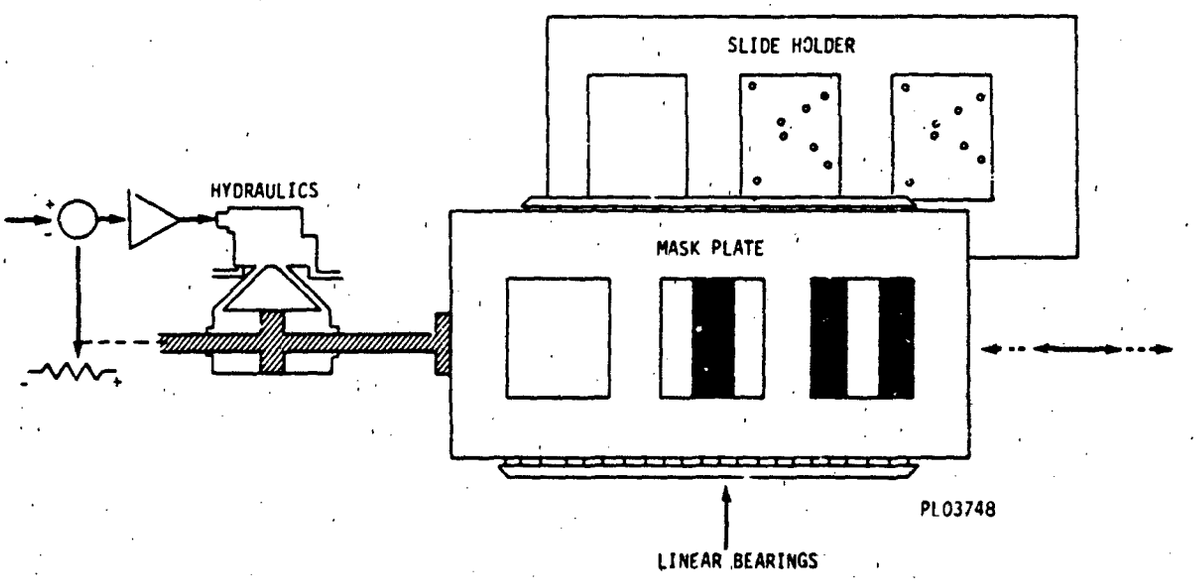

Figure 61. Hydraulic Actuator Controlling Mask Plate in X Dimension.

projected image moving approximately 6000 deg/sec, which exceeds the maximum acceleration of a saccadic eye movement. Preliminary inspection of the eye-tracking display seems to indicate that the 10-msec delay between eye movements and movements of the masking plate is not noticeable.

13.3 Psychophysical Experiment. In the proposed set of experiments, an observer's performance based on detection and recognition tasks will be assessed for varying parameters of an AOI display. The study will initially be investigating eye-slaved movements in the horizontal dimension. A rear projection screen will display a single horizontal line to the observer. Due to the limited range of the eyetracker (+20 deg), the field will subtend 50 degrees in length by approximately 1.5 degrees in height. As shown in Figure 60, two parallel front surface mirrors have been placed in front of the projection lenses. Light passing through the two mirrors is reflected onto the rear projection screen. One of the mirrors rotates along its horizontal axis such that the projected image may be vertically displaced. A computer-controlled stepping motor located at the axis of rotation actuates the motion of the mirror.

The stimuli are constructed by photographing arrays of dot-matrix Landolt "C" characters, producing positive slides. Slides of identical character arrays will be placed in two channels of the ESP such that their images are superimposed at the rear projection screen. The low-resolution slides are created by defocusing the camera, and changes in character size resulting from this procedure are compensated for in the photographic process. Different low-resolution slides will be produced, ranging in resolution from 6 to 20 arc minutes per line pair, while the high-resolution slides will have a resolution of 2 arc minutes. In addition to varying the resolution relationship between the AOI and peripheral field, various AOI sizes and shapes will be used.

For approximately 50 spatial locations across the FOV, Landolt C's oriented in both directions will be available for presentation. The computer will actuate the stepper motor so that, on each trial, the location and orientation of the character will be randomly determined. The observer will be required to detect, with an appropriate lever press, the orientation of the gap in the Landolt C. Reaction time to accomplish the task, frequency of saccades and average fixation duration will be compared across conditions.

13.4 Status of Eye-Slaved Projection Experiment

13.4.1 Hardware. In April 1983, the hydraulically actuated ESP was completed. An Apple IIe microcomputer was purchased to control the experimental variables, as well as monitor the observer's responses.

13.4.2 Summary. The software and hardware development for the ESP psychophysical experiment are complete. Data collection is now in progress.

14. CONTINUING PROGRAM

14.1 Prototype System. The breadboard HMD system has been demonstrated in a flying simulation system to AFHRL personnel, using an AFHRL cockpit, computer system and CIG visual system. The design of the prototype HMD will be completed in 1984, with delivery of the prototype system planned for January 1985. The prototype system will consist of the following:

(a) Improved helmet

(b) Improved HMD helmet and relay optics

(c) Improved fiber-optic cables (2)

(d) Optical head tracking system

(e) Accelerometers for head motion prediction

(f) Support structure for system components

(g) Instructor display system

(h) Light valve (LV) projectors (4) supplied by AFHRL.

The integrated breadboard demonstration showed the capability of the helmet-mounted display with fixed high-resolution insets to provide the full color, high brightness, and unrestricted field of view (FOV) necessary for air-to-air and air-to-ground combat simulation. The prototype design will require only two fiberoptic cables for reduced weight and freer head movement; it has improved helmet optics and mounting, improved relay optics, and an optical head tracker (noncontact) with accelerometer lead prediction for faster, more accurate head-position sensing.

14.2 Inset FOV Size. A concurrent research effort is studying the optimal inset FOV size using a computer-controlled eye-tracking/slaved projection system developed as part of the current program.

14.3 Instructor/Operator Station Requirements. A separate study of instructor/operator station (IOS) requirements for air combat simulation using the HMD has progressed to the point of defining and purchasing the necessary display hardware. An operating IOS will be delivered with the prototype HMD.

14.4 Further Activities. Further activities covered by the current program are the integration of the equipment at the AFHRL, support of the system during AFHRL demonstration evaluation activities, and the carrying out of experiments (in conjunction with the AFHRL) to determine parameters for the refined engineering prototype system.

★U.S. GOVERNMENT PRINTING OFFICE 1984-569-053/454